TU Delft

Delft University of Technology

# Reconfigurable Range-Doppler Processing and Interference Mitigation for FMCW Radars

Neemat, Sharef

**DOI**
10.4233/uuid:75c2b62b-d8c0-481e-b5d4-63cdbfcf1a80

**Publication date**
2020

**Document Version**
Final published version

**Citation (APA)**
Neemat, S. (2020). *Reconfigurable Range-Doppler Processing and Interference Mitigation for FMCW Radars*. [Dissertation (TU Delft), Delft University of Technology]. https://doi.org/10.4233/uuid:75c2b62b-d8c0-481e-b5d4-63cdbfcf1a80

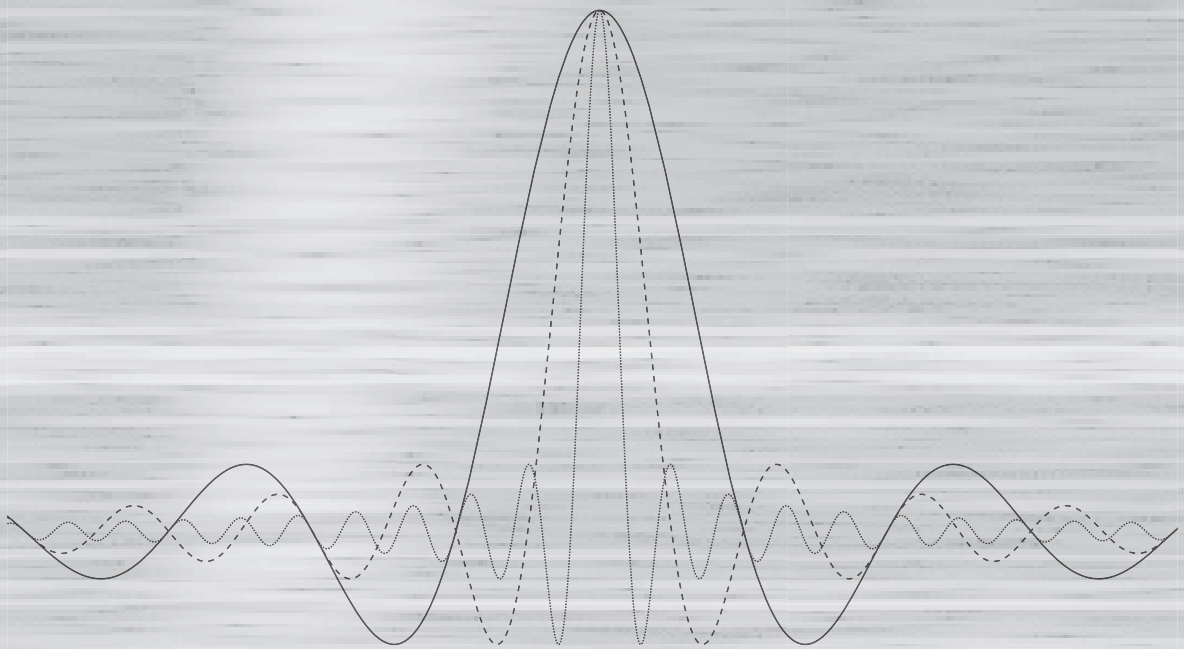
**Important note**
To cite this publication, please use the final published version (if applicable).
Please check the document version above.

**Copyright**
Other than for strictly personal use, it is not permitted to download, forward or distribute the text or part of it, without the consent of the author(s) and/or copyright holder(s), unless the work is under an open content license such as Creative Commons.

**Takedown policy**
Please contact us and provide details if you believe this document breaches copyrights.
We will remove access to the work immediately and investigate your claim.

*This work is downloaded from Delft University of Technology.*
*For technical reasons the number of authors shown on this cover page is limited to a maximum of 10.*

# Reconfigurable Range-Doppler Processing and Interference Mitigation for FMCW Radars



Sharef Neemat

# Propositions

accompanying the dissertation

**RECONFIGURABLE RANGE-DOPPLER PROCESSING AND INTERFERENCE MITIGATION FOR FMCW RADARS**

by

**Sharef NEEMAT**

1. A deramping FMCW radar can observe targets with multiple target response function widths, and in multiple Doppler ambiguity intervals, from one coherent processing interval – using one chirp burst with a fixed PRF.
2. It is simple to detect FMCW-to-FMCW radar interference using a single-side-band receiver.
3. The SNR is the most important parameter when using interpolation for reconstructing beat frequencies for the purpose of interference mitigation.
4. It is counterintuitive in a PhD that finding problems is part of the problem.
5. A PhD is a trap worth falling into.
6. Submitting papers to IEEE transactions is a good and bad idea for a PhD candidate.
7. Meditation works against a practicer's quality-of-life in the long term.
8. Those trapped in the challenge-accomplishment-reward loop are in a – invisible to them – psychological prison not recognized by today's world-order, and they are not looking forward to escape.
9. "Don't give me life's water in humiliation, but give me in pride a glass of wild-gourd"— Antarah ibn Shaddad.
10. "Brevity is the soul of wit"— William Shakespeare.

These propositions are regarded as opposable and defendable, and have been approved as such by the promotor Prof. DSc. A.G. Yarovoy.

# Reconfigurable Range-Doppler Processing and Interference Mitigation for FMCW Radars

# Reconfigurable Range-Doppler Processing and Interference Mitigation for FMCW Radars

## Dissertation

for the purpose of obtaining the degree of doctor
at Delft University of Technology
by the authority of the Rector Magnificus prof.dr.ir. T.H.J.J. van der Hagen
chair of the Board for Doctorates
to be defended publicly on
Wednesday 1 April 2020 at 15:00 o'clock

by

**Sharef Ahmed Neemat**

Master of Science in Electrical Engineering
University of Cape Town, Cape Town, South Africa,
born in Riyadh, Saudi Arabia.

This dissertation has been approved by the promotor.

Composition of the doctoral committee:

| | |
|---|---|
| Rector Magnificus, | chairperson |
| Prof. dr. A.G. Yarovoy | Delft University of Technology, promotor |
| Dr. O.A. Krasnov | Delft University of Technology, copromotor |
| | |
| *Independent members:* | |
| Prof. dr. M.R. Inggs | University of Cape Town |
| Prof. dr. K. Kulpa | Warsaw University of Technology |
| Prof. dr. C.S. Vaucher | Delft University of Technology |
| Prof. dr. ir. G.J.T. Leus | Delft University of Technology |
| Prof. dr. ir. H.W.J. Russchenberg | Delft University of Technology |

TU Delft Delft University of Technology

مدينة الملك عبدالعزيز للعلوم والتقنية KACST

King Abdulaziz City for Science and Technology

ISBN 978-94-028-1977-9

Copyright © 2020 by Sharef Ahmed Neemat
All right reserved. No part of this material protected by this copyright notice may be reproduced or utilized in any form or by any means, electronic or mechanical, including photocopying, recording or by any information storage and retrieval system, without the prior permission of the author.

An electronic version of this dissertation is available at
http://repository.tudelft.nl/.

*To my family*

# CONTENTS

**List of Figures** **x**

**List of Tables** **xii**

**1 Introduction** **1**
1.1 Why FMCW Radar? . . . 1
1.2 FMCW Radar Operational Background . . . 2
1.3 FMCW Radar Theory Review . . . 5
1.4 FMCW Radar Operational Challenges . . . 8
1.5 Research Objectives and Questions . . . 9
1.6 Novelty and Main Results . . . 11
1.7 Dissertation Outline and Chapters' Abstracts . . . 13
References . . . 16

**2 An Interference Mitigation Technique for FMCW Radar Using Beat-Frequencies Interpolation in the STFT Domain** **17**
2.1 Introduction . . . 18
2.2 Theory . . . 22
2.2.1 Deramp Linear FMCW Receivers . . . 22
2.2.2 FMCW Interference . . . 24
2.2.3 Linear Prediction of FMCW Beat-Frequencies . . . 25
2.2.4 Beat-Frequencies in the STFT Domain . . . 28
2.2.5 Beat-Frequency Fluctuation Model . . . 29
2.3 Method . . . 29
2.3.1 Beat Signal Reconstruction Steps . . . 29
2.3.2 Reconstruction Parameters Selection Trade-offs . . . 32
2.4 Simulations . . . 32
2.5 Experimental Verification . . . 35
2.5.1 Experimental Setup . . . 35
2.5.2 Experiment 1: Interference Mitigation for a Single Sweep (Range-Profile) . . . 38
2.5.3 Experiment 2: Interference Mitigation in a Range-Doppler CPI . . . 40
2.5.4 Results and Discussion . . . 41

2.6 Conclusion . . . 49
References . . . 50

**3 Decoupling the Doppler Ambiguity Interval from the Maximum Operational Range and Range Resolution in FMCW Radars 53**
3.1 Introduction . . . 54
3.2 Theory. . . . 57
3.2.1 Related FMCW Radar background . . . 57
3.2.2 Operational parameters trade-offs, and Parameters Decoupling . . . 57
3.3 Method . . . 60
3.4 Implementation Feasibility . . . 61
3.4.1 Receiver channels calibration . . . 61
3.4.2 Maximum chirps' center-frequency difference. . . . 61
3.4.3 Limitations . . . 61
3.5 Simulations and Experimental Verification . . . 63
3.5.1 Simulations . . . 63
3.5.2 Experimental Setup . . . 64
3.5.3 Experiments Description. . . . 66
3.5.4 Experiments Results and Discussion . . . 68
3.6 Conclusion . . . 73
References . . . 75

**4 Reconfigurable Range-Doppler Processing and Target Response Function Width Improvement for FMCW Radar 77**
4.1 Introduction . . . 78
4.2 Theory. . . . 81
4.2.1 FMCW Radar Background . . . 81
4.2.2 Beat Frequency Spectral Width and Processing Gain Improvement . . . 81
4.2.3 Reconfigurable Range-Doppler Processing. . . . 82
4.3 Method . . . 84
4.4 Simulations for Sweeps Concatenation for Different Values of $d$ . . . 89
4.5 Possible Range-Resolution Improvement Investigation. . . . 89
4.5.1 Possible Range-Resolution Improvement for Different Values of $d$ . . . 89
4.5.2 Possible Range-Resolution Improvement for Different Values of $M$ . . . 93
4.5.3 Simulations for Sweeps Concatenation for $M_{\max}$ . . . 94
4.5.4 Reconfigurable Range-Doppler Processing Limitations . . . 94

4.6 Experimental Verification . . . . . 96
4.6.1 PARSAX Experimental Setup . . . . . 96
4.6.2 PARSAX Experiment 1: A Stable Target . . . . . 96
4.6.3 PARSAX Experiment 2: A Moving Target . . . . . 98
4.6.4 TI Experimental Setup . . . . . 99
4.6.5 TI Experiment 1: Corner Reflectors . . . . . 101
4.6.6 Results and Discussion . . . . . 102
4.7 Conclusion . . . . . 103
References . . . . . 105

**5 Conclusions and Recommendations** **108**
5.1 Conclusions . . . . . 108
5.2 Societal, Scientific and Technical Implications . . . . . 110
5.3 Recommendations for Future Work . . . . . 111
References . . . . . 112

**Summary** **113**

**Samenvatting** **115**

**Acknowledgements** **117**

**ABOUT THE AUTHOR** **119**

**List of Publications** **121**

# List of Figures


1.1 Simplified deramping FMCW radar block diagram. . . . . 3
1.2 Deramping FMCW terminology, concepts and operational overview. 4
1.3 FMCW up-chirp waveform with depicted symbology. . . . . 5
1.4 Example sketch for trade-off trends for relations between classical-processing FMCW performance parameters. . . . . 10

2.1 STFT for a single interference contaminated sweep as received using the FMCW radar's Double-Side-Band (DSB) receiver. . . . . 21
2.2 Deramping linear FMCW operational overview. . . . . 23
2.3 Recipe for the proposed interference mitigation technique; and the setup for the first experiment. . . . . 27
2.4 Optional reconfigurable LP coefficients scheme for CPI processing. 28
2.5 Plots for simulation is Section 2.4. . . . . 33
2.6 Signal spectrum related to Fig. 2.5(h) after restoration. . . . . 35
2.7 RSNR for simulations in Section 2.4. . . . . 36
2.8 Experimental setup. . . . . 37
2.9 Simplified simultaneous polarimetric PARSAX radar block diagram. 38
2.10 Filter order selection based of average interpolation errors. . . . . 39
2.11 Setup for the second experiment in Section 2.5.3. . . . . 40
2.12 Range-Doppler maps used in the second experiment (Section 2.5.3). 43
2.13 Range profile for the sweep in Fig. 2.1 . . . . . 44
2.14 A cut through the range-Doppler maps in Fig. 2.12. . . . . 44
2.15 A cut through the range-Doppler maps before thresholding. . . . . 45

3.1 Concept sketch of the solution waveform presented in this chapter 56
3.2 Graphical illustration of the proposed processing technique described in Section 3.3. . . . . 62
3.3 Simulation results for the different waveforms in Table 3.1 and Table 3.2. . . . . 64
3.4 Simulation results for the different waveforms in Table 3.1 and Table 3.2. . . . . 65
3.5 The experimental PARSAX radar mounted on the roof, and targets used for experiments in Section 3.5.2. . . . . 66

3.6 Simplified radar block diagram. . . . . 67
3.7 Photographs of the experimental setup. . . . . 68
3.8 Range-Velocity maps presenting results for the chimney. . . . . 69
3.9 Range-Velocity maps presenting results for the car. . . . . 71
3.10 Range-Velocity maps presenting results for the extended target. . . 72

4.1 Deramping operational overview, highlighting beat-frequency signals and the transient region. . . . . 79
4.2 Simplified sinc function spectral bandwidth illustration for signals with different durations. . . . . 83
4.3 Reconfigurable range-Doppler processing permutations of fast-time slow-time received sweeps. . . . . 86
4.4 Examples for reconfigurable CPI processing with transient region frames extrapolation. . . . . 87
4.5 Depiction of phase matching in the STFT domain after transient region frames extrapolation . . . . . 88
4.6 Simulation setup for the results presented in Fig. 4.7, where cases (a) to (e) correspond to Fig. 4.7 sub-figure labels. . . . . 91
4.7 Simulation Results for the scenario setup using the parameters in Table 4.2 and illustrated in Fig. 4.6. . . . . 92
4.8 A repetition of the simulation results presented in Fig. 3.3, but with the addition of results for waveform (W.e) . . . . . 98
4.9 Simulation photographs. . . . . 99
4.10 Simplified PARSAX radar block diagram with the configuration used for experiments discussed is Section 2.5. . . . . 100
4.11 Experiment setup using the TI mmWave IWR1443 radar, as described in Section 4.6.4. . . . . 101
4.12 Zero-padded Zero-Doppler cut zoom-in on the Chimney shown in Fig. 4.9 (a) and (b). . . . . 102
4.13 Range-Velocity results maps for the automobile in the experiment described in Section. 4.6.3. . . . . 104
4.14 Range profiles for the result of the experiment described in Section 4.6.5. . . . . 105

# LIST OF TABLES


2.1 Interpolation Parameters Trade-offs . . . . . 30
2.2 Results related to Fig. 2.6 for the strongest target. . . . . 34
2.3 Results of the second experiment. . . . . 46
2.4 Setup parameters for experiments in Section 2.5 . . . . . 48

3.1 Worked-out trade-offs for waveforms discussed in the theory Section 3.2.2. . . . . 58
3.2 (Continued) Worked-out trade-offs for waveforms discussed in the theory Section 3.2.2. . . . . 59
3.3 Simulation and processing parameters. . . . . 63
3.4 Results related to the target range cuts for the first and second experiments (Fig.3.8(e) and Fig. 3.9(d)). . . . . 70

4.1 Flexible CPI processing gain vs Maximum Unambiguous Doppler Velocity tradeoff example. . . . . 84
4.2 Simulation setup parameters. . . . . 90
4.3 Worked-out example for the discussion in Section 4.5.2 of $M$ chirps. 95
4.4 PARSAX experiment setup parameters. . . . . 97

# 1

# INTRODUCTION

*This chapter presents motivations for research on FMCW radars, deramping FMCW radar background, theory and operational challenges. Those are then followed by this dissertation's research objective and research questions, then a showcasing of this dissertation's novelty and main research results. Finally a dissertation outline is presented.*

## 1.1. WHY FMCW RADAR?

Deramping (stretch) Frequency Modulated Continuous Wave (FMCW) [1], [2] radars with chirp-sequence waveforms are widely used in numerous fields and applications. They are also known for their ability to deal with short-range applications as opposed to high peak power systems with dead time. They are identified as a simple low-cost solution in contemporary literature for their low sampling-rate requirements, and therefore are attractive to commercial applications. They are further identified by their low peak power characteristic, and hence have a lower probability of intercept property, making them a tempting solution in military applications. Example fields and applications are automotive (cruise control, parking assist, collision avoidance, blind-spot detection and self-driving), medical (tumour detection and monitoring, cardiorespiratory activity monitoring, sleep quality monitoring), Human-Computer-interaction (micro gestures tracking and recognition and tangible painting applications), weather

Parts of this chapter are based on:
**S. Neemat**, O. Krasnov, and A. Yarovoy, "Waveform and Receiver Parameters Design Choices for a Reconfigurable Digital FMCW Radar," 2016 *17th International Radar Symposium (IRS).* © 2019 IEEE with permission.

and geophysical phenomena, and much more. Some of these applications are predicted to grow to a point of having a world-wide impact, with major market players showing interest in – and already manufacturing – this radar class like the Google Soli project. With Soli, Google is planning to integrate FMCW radars in wearables, phones, computers, cars and Internet of things (IoT) devices. Because of the wide-range of possible applications, Google has developed software development kits which enables developers to build customise their own processing methods. With this being said, it becomes a challenging task to even try and estimate a future market value for this type of radar.

The aforementioned applications all share the need to detect, track and classify targets with different Pulse Repetition Frequencies (PRFs) for velocity estimation in different Doppler ambiguity intervals or for providing different inputs to target classification algorithms. On the other-hand, this predicted increase in the number of radars will require means and techniques to avoid or mitigate radar-to-radar interferences, which is an issue not thought of by the scientific community during the early days of radar.

The aforementioned interesting situation has triggered a need to look for advanced waveforms and signal processing methods which are simple to implement, and have motivated the research presented in this dissertation.

## 1.2. FMCW RADAR OPERATIONAL BACKGROUND

Deramping FMCW radars operate by mixing the transmitted chirp with the received echoes, producing what are known as beat signals – after filtration and digitization. A simplified block diagram of an FMCW radar is presented in Fig. 1.1. The main concepts discussed hereafter are illustrated in Fig. 1.2.

After deramping – for a single point-target, the time delay between the probing signal transmission and the scattered signal reception will result in a single-tone signal, known as a beat-frequency, whose frequency is proportional to that target's range. Range is therefore defined by frequency.

To elaborate, this single-tone beat-signal for that point-target is observed during a certain time interval within the radar's sweep time. Classical signal compression is then done by converting this single-tone signal to the spectral domain. As a result, the point-target is represented as a sinc-function-shaped spectral line which has a bandwidth that is inversely proportional to the duration of the signal observation time interval. The conversion of this compressed signal from the spectral domain to the range domain (to produce a range-profile) is done by rescaling the spectrum grid to a range grid using a scaling equation. As a result, the sinc-function-shaped spectral line – related to that point-target – is converted into what can be called a point target response function (analogous to the impulse response function in pulse-compression radar).

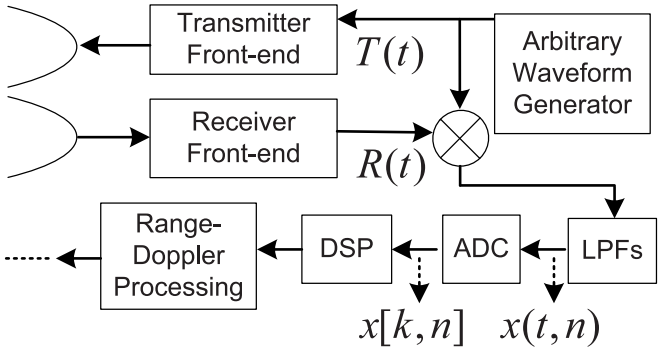



Figure 1.1: Simplified deramping FMCW radar block diagram. Transmitted and received signals are mixed to produce beat-frequencies, low pass filtered (LPF), digitized and handled by a Digital Signal Processor (DSP) for range-Doppler processing and beyond.

In classical FMCW processing, the width of this response function after scaling is inversely proportional to the transmitted bandwidth during the observation time interval. This width represents the actual radar range resolution, which is directly proportional to the target's range localization accuracy. The range-resolution granularity defines the width of what is known as targets' range bins. A radar's range-resolution is a criterion by which the radar's ability to separate targets that are close in range is evaluated. The Fourier Transform (FT) is typically used to convert beat signals to the spectral domain. The FT frequency spectral width is defined by the signal observation time, or by the combination of the observed samples number and the sampling frequency [3].

Legacy computer architectures used in FMCW radars are highly compatible with the FT for its reduced computational requirements and predictable latency.

Target velocities are calculated from Doppler processing – also typically using the FT – across targets' range bins from multiple sweeps. The radar's Pulse/sweep Repetition Frequency (PRF) is therefore the Doppler sampling frequency, and in consequence defines the radar's maximum unambitious Doppler velocity.

The time spent to gather multiple sweep returns for range and Doppler processing is typically known as a Coherent Processing Interval (CPI). Sweeps in a CPI are typically arranged in a fast-time slow-time matrix, where fast-time is the time within a sweep, and slow-time is the time across multiple sweeps. The total processing gain in the CPI is the pulse compression gain - also known as the time-bandwidth product (BT) - multiplied by the number of sweeps in the CPI. The total processing gain in a CPI is therefore contributed to the matrix's 2-D FT processing gain.

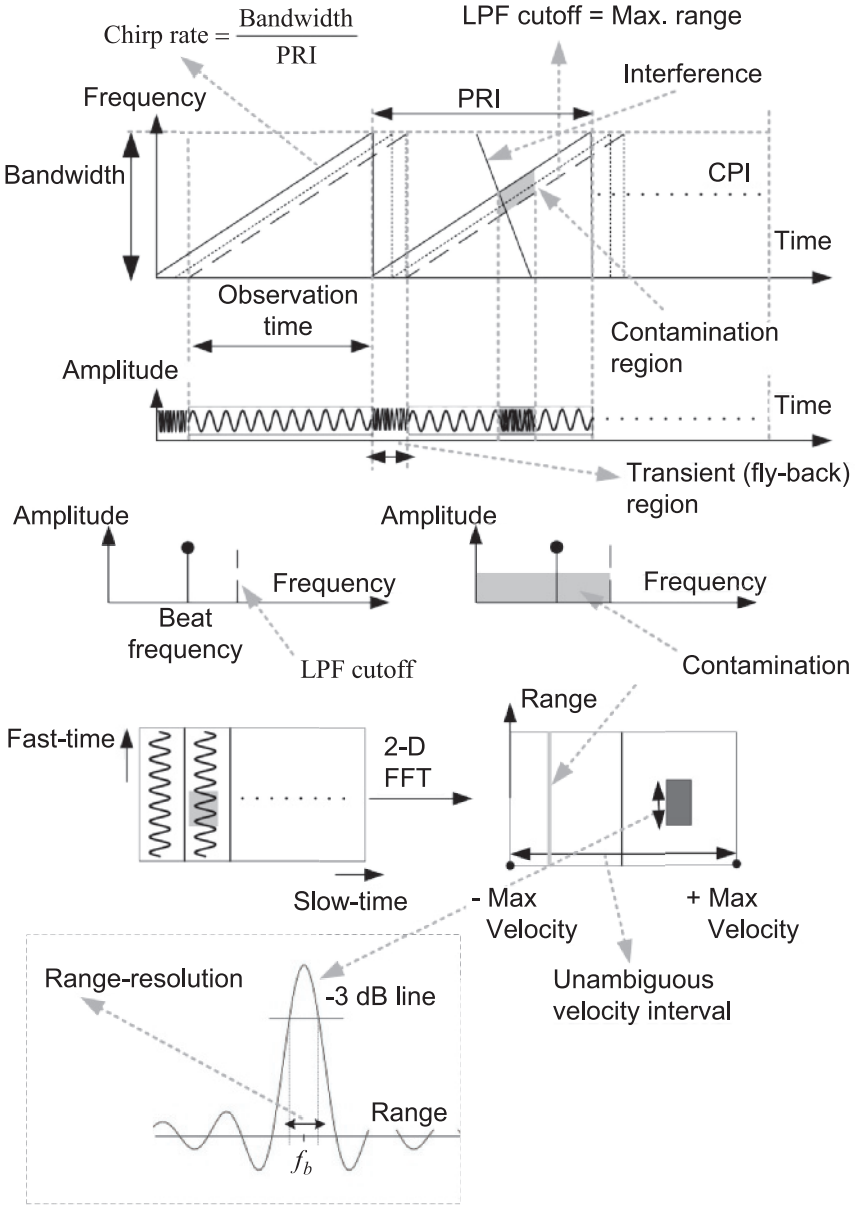



Figure 1.2: Deramping FMCW terminology, concepts and operational overview associated with Section. 1.2.

It is typical for radars to transmit at different PRF values, across multiple CPIs to unambiguously determine targets' ranges and velocities [5]. In FMCW, the aforementioned target observation time is limited by what is known as the "tran-

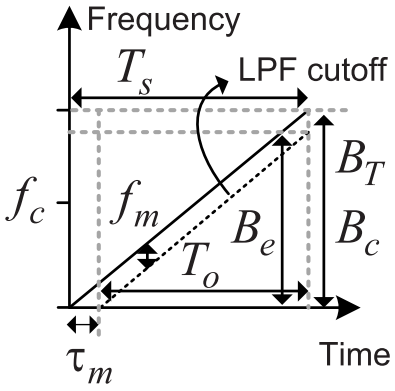



Figure 1.3: FMCW up-chirp waveform with depicted symbology following the equations in Section. 1.3.

sient" or "fly-back" region between frequency sweeps [6]. The received signal is typically only sampled after the transient region.

The sweep's chirp-rate defines the ratio between the transmitted bandwidth and the sweep time (PRI). The radar's maximum operational range is defined by its maximum beat-frequency, which is typically set by a Low Pass Filter (LPF) placed subsequent to the mixing of the transmitted and received signals. Deramping receiver implementations can be I/Q Single-Side-Band (SSB) or Double-Side-Band (DSB). Using an SSB implementation allows the possibility to reject positive or negative frequencies as desired.

Since FMCW radars are widely used, they might suffer from interferences from other radars operating within their vicinity, as in Multiple-Input and Multiple-Output (MIMO) radar networks and in automotive scenarios, or from themselves as in the case of fully polarimetric radars with dual-orthogonal signals [7], where there is a leakage between two mutually orthogonal channels (cross-channel interference).

## 1.3. FMCW RADAR THEORY REVIEW

This subsection reviews basic FMCW theory [2], [9] as foreground, with a scope bound by commonality of the presented material in subsequent chapters in the thesis. Noting that cos notations instead of complex will be used hereafter to orient the theory with radar systems that mix transmitted and received signals in the digital domain (FPGA).

An FMCW radar like the one depicted in Fig. 1.1 typically transmits an up-

chirp like the ones depicted in Fig. 1.2 and Fig. 1.3, which can be expressed as:

$$T(t) = A_t \,\mathrm{rec}\left(\frac{t}{T_s}\right)\cos\left[2\pi(f_c t + \frac{1}{2}\alpha t^2)\right] \tag{1.1}$$

for $-T_s/2 < t < T_s/2$, where $T_s$ is the sweep time. In this thesis, for simplicity, we assume that $T_s$ equals to the Pulse Repetition Interval (PRI). $A_t$ is the amplitude, $f_c$ the carrier center frequency, and the chirp-rate $\alpha$ is:

$$\alpha = B_T / T_s \tag{1.2}$$

where $B_T$ is the total transmitted chirp bandwidth. In classical FMCW processing, the total bandwidth is the same as the chirp transmitted bandwidth $B_c$ in Fig.1.3. The chirp-rate preceding sign determines if it is an up-chirp or a down-chirp.

The radar receives an echo signal from a target after a time delay $\tau$, which can be expressed as:

$$R(t) = A_r \,\mathrm{rec}\left(\frac{t}{T_o}\right)\cos\left[2\pi(f_c(t-\tau) + \frac{1}{2}\alpha(t-\tau)^2)\right] \tag{1.3}$$

for $-T_o/2 < t < T_o/2$, where $A_r$ is the received amplitude. The observation time $T_o$ (ADC sampling interval. The duration over which samples are taken) is related to the sweep time as:

$$T_o = T_s - \tau_m \tag{1.4}$$

where $\tau_\mathrm{m}$ is the maximum system delay corresponding to the desired radar maximum range. A target's delay is therefore related to its range as:

$$\tau = 2(R_0 + vt)/c \tag{1.5}$$

where $R_0$ is its initial range and $v$ its relative velocity (line of sight velocity).

In deramp (de-chirp) processing, the transmitted signal is mixed with the received one to produce – after proper filtration – what is known as a beat signal. This signal is in baseband and can be expressed – after simplification and discarding of usual negligible terms in a narrow-band system with no accelerating targets – for the $n^{\mathrm{th}}$ sweep in a CPI, following [1] and [8], as:

$$x(t,n) = A_b \cos[2\pi(\frac{2\alpha R_0}{c}t + \frac{2f_c v}{c}t + \frac{2vB_c n}{c}t + \frac{2f_c vn}{c}T_s)] \tag{1.6}$$

where $t$ is fast-time within the sweep and $A_b$ is the beat signal amplitude. Estimating the frequency term $2\alpha R_0/c$ provides the target range. The second and third terms are the usual FMCW range-Doppler coupling terms. The target's

velocity $v$ is estimated from the phase evolution in the last phase term over multiple sweeps in a CPI ($nT_s$), hence the 2-D FT typically performed on beat-signals from multiple sweeps in a CPI to estimate range and velocity.

It then follows that the estimated frequency term – known as the beat-frequency – is related to the target's range, and that the maximum operational range $R_m$ is related to a maximum beat-frequency $f_m$ as:

$$f_b = \frac{2\alpha R_0}{c}, \quad f_m = \frac{2\alpha R_m}{c}. \tag{1.7}$$

The target range is then:

$$R_0 = \frac{c}{2\alpha} f_b. \tag{1.8}$$

Note that one can also observe the ($\tau_\mathrm{m}$, $f_m$) relation from the geometry in Fig. 1.3, in the sense that the LPF implementing the $f_m$ cutoff-frequency defines the maximum range $R_m$ in de facto.

The effective bandwidth is related to the transmitted on by:

$$B_e = \frac{B_T T_o}{T_s}, \tag{1.9}$$

which also expresses the degradation in the transmitted bandwidth due to the reduced observation time ($T_o < T_s$). The range-resolution is therefore:

$$\Delta R = \frac{c}{2B_e}. \tag{1.10}$$

The unambiguous Doppler-velocity interval $v_u$ is defined by the PRF as:

$$v_u = \pm \frac{\lambda \mathrm{PRF}}{4}, \tag{1.11}$$

where $\lambda$ is the wavelength. The dwell time in the CPI depends on the number of sweeps gathered in one CPI ($N_\mathrm{CPI}$), and on the sweep time. It is defined as:

$$T_d = N_\mathrm{CPI} T_s. \tag{1.12}$$

The Doppler frequency resolution is the dwell time's inverse and is defined as:

$$\Delta f_D = \frac{1}{T_d}. \tag{1.13}$$

The Doppler velocity resolution is:

$$\Delta v_D = \frac{\lambda}{2T_d}. \tag{1.14}$$

The sweep compression gain (also known as the BT time-bandwidth product) [9] is:

$$G_r = B_e T_o. \tag{1.15}$$

The total processing gain in a CPI is the BT product multiplied by the number of sweeps in the CPI ($N_{\text{CPI}}$):

$$G_{\text{CPI}} = G_r N_{\text{CPI}}. \tag{1.16}$$

## 1.4. FMCW RADAR OPERATIONAL CHALLENGES

Real-time reconfigurable digital FMCW radar systems offer degrees of flexibility in selecting operational parameters for the transmitted waveform and for the digital receiver signal processing chain. These parameters are tightly-coupled and a change in any of them will affect the rest, and subsequently the entire system. The more reconfigurability and flexibility a radar has, the more challenging its situation becomes. The discussion hereafter is a step in the road towards the development of methods and waveforms to operationally enhance the radar's performance and increase its resistance to interferences – with the purpose of taking it beyond its current state-of-the-art.

The first FMCW radar challenge is related to interference resistance. Processing interference-contaminated beat-frequencies with the FT yields poorer radar detection, due to undesired artifacts such as a noise-floor level increase in range-profiles, which is significantly higher than the system noise-floor, masking weak targets – and spurious vertical lines in range-Doppler – as illustrated in Fig. 1.2. While zeroing the contaminated part of the beat-frequency signal is the simplest interference suppression method, it causes signal phase discontinuity, which results in - after performing the range-compression FT - target-response broadening in range and high residual sidelobes. This in turn causes worse range resolution. Inverse-windowing compromises interferences complete elimination and smoothing the area between the signal and the interference. Both zeroing and windowing cause Signal to Noise Ratio (SNR) loss. Using other state-of-the-art mitigation methods are challenging because they require waveform or receiver architecture diversity, utilize signal processing techniques that are not real-time implementable or have unpredictable latencies, require detection or a priori target information, or are not suitable for the sensing of very extended targets (atmospheric observation).

The second FMCW radar performance challenge pertaining to the research presented in this dissertation is related to the fact that typical processing faces challenges related to the multi-dimensional coupling between the radar's PRF, maximum operational range, maximum unambiguous Doppler velocity, range-resolution, and the CPI processing gain (as can be surmised from the equations

in the previous subsection). This is in the sense that if there is an operational requirement for the observation of fast(er) moving targets, the radar requires the utilization of a higher PRF, which in turn reduces the range resolution and due to the reduced transmitted bandwidth and reduced observation time (assuming a fixed chirp-rate). But, if the transmitted bandwidth is to be maintained as it was before increasing the PRF – by increasing the chirp-rate, which is not always possible for legacy systems – the maximum operational range will be reduced due to the typically fixed LPF cutoff frequency, and a trade-off is then made between the maximum operational range and the unambiguous Doppler velocity interval. If the chirp-rate cannot be changed and there is a desire to increase the PRF, that would result in a range resolution degradation.

Since the processing gain is contributed to the 2-D FFT gain in a CPI – operationally, to maintain this gain, the total number of samples stored in a CPI is typically kept the same when changing the PRF. This is in the sense that more sweeps of shorter durations are required to be received when operating in a High PRF (HPRF) mode, and less sweeps of longer duration in a low PRF mode. If the radar operates in a HPRF mode, it is true that different unambiguous Doppler velocity intervals can be created by simply discarding every other sweep(s) in the fast-time slow-time matrix, but that would then result in a total processing gain loss – due to the discarded data. Examples of these performance parameters trade-off trends are illustrated in Fig. 1.4. Furthermore, in typical FMCW processing, the received signals are only sampled after the transient region (demarking the end of a received sweep) as seen in Fig. 1.2, causing discontinuities in received beat-frequencies – and putting a limit on the possibility of having a continuous observation time, as seen in the equations in Section. 1.3. This puts limitations on the radar's achievable performance, and victimizes it to operational parameters trade-offs. Note that the observation time is typically the same as the integration time – due to the transient-region – as seen in Fig. 1.2. It then becomes challenging from a design and cost point-of-view to improve the resolution without increasing the transmitted bandwidth. This is not always possible due to cost and bandwidth allocation restrictions.

## 1.5. RESEARCH OBJECTIVES AND QUESTIONS

This dissertation aims to investigate and develop methods and waveforms for the operational enhancement of deramping FMCW radars. This is in the sense that there is a desire for this research to take FMCW radars beyond their existing state-of-the-art performance limitations, and increase their resistance to interference. To achieve these objectives, the following Research Questions (**RQ**) will be addressed:

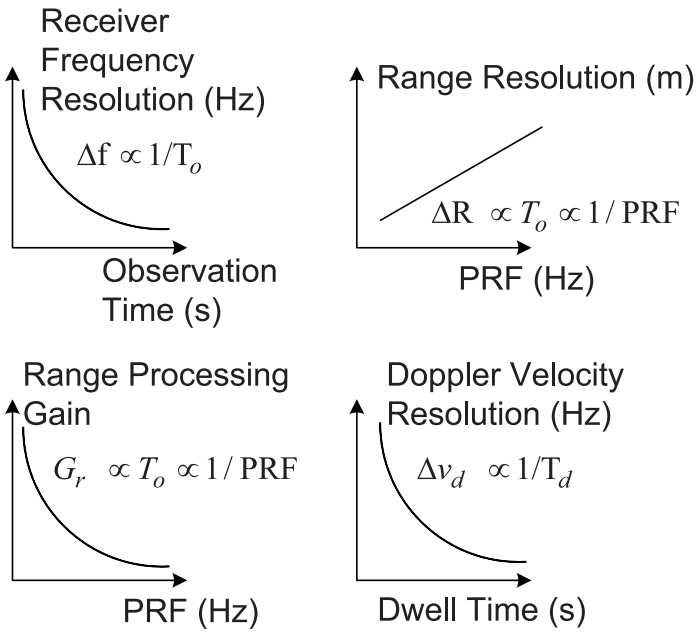



Figure 1.4: Example sketch for trade-off trends for relations between classical-processing FMCW performance parameters for a fixed chirp-rate and fixed LPF cutoff-frequency, as described in Section 1.4.

(**RQ.**1) Is there a way to mitigate FMCW radar interferences where the developed mitigation method restores any SNR loss due to the interference and/or the mitigation technique itself? Can the method be evaluatable in performance in the range-Doppler domain (as opposed to only in a range-profile)?

(**RQ.**2) Is there a way to decouple the Doppler velocity ambiguity interval – defined by the PRF – from parameters like the maximum operational range, range resolution, all while maintaining the same transmitted chirp-rate? Would it be possible to liberate the radar from the design/operational trade-offs associated with these parameters? Particularly in the scenario in which the PRF is to be increased for the observation of fast(er) moving targets.

(**RQ.**3) Is there a way to overcome the existence of the transient (fly-back) region in deramping FMCW radar beat-signals? This is in the sense that its existence limits the maximum observation time in a single sweep. Would manoeuvring it then allow the coherent chaining of beat-signals – from

multiple sweeps – in a way that could improve the target response function width? Could it also improve the SNR? And since the beginning of a sweep and the transient region are related – and therefore the Doppler velocity ambiguity interval is related too in de facto – could overcoming the presence of the transient region then allow for Doppler processing PRFs that are different from the transmitted PRF?

All developed methods for the aforementioned research questions aim to comply with the general requirements that they:

- Are applicable for the deramping class of FMCW radars.
- Rely only on the FT as the primary frequency estimation tool for range and Doppler processing.
- Be applicable to the sensing of very extended targets (atmospheric observation).
- Not require target detection or any a priori target information to begin with.
- Have a predictable execution latency.

The justifications for the FT reliance requirement are:

- Real-time implementation considerations and performance predictability.
- Compatibility with legacy receiver architectures and most available computing resources.
- Linearity of the FT in the sense that noise and clutter still maintain their statistical distribution further up the radar processing-chain, beyond range-Doppler maps.

Note that the aforementioned research questions (**RQ**1, **RQ**2 and **RQ**3) are mapped onto individual **chapters** in this dissertation.

## 1.6. NOVELTY AND MAIN RESULTS

The novelty and main results presented in this dissertation are as follows:

**Chapter 2** (**RQ**1): **An Interference Mitigation Technique for FMCW Radar Using Beat-Frequencies Interpolation in the STFT Domain**
A method was developed to mitigate FMCW radar interferences. The method restored any SNR loss due to the interference, and was evaluatable in performance

in the range-Doppler domain (as opposed to only in a range-profile). The novelty is highlighted in:

- The first ever interference mitigation method for deramping FMCW radar receivers via model-based beat-signals interpolation in the time-frequency domain.
- The introduction of an optional linear prediction interpolation coefficients reconfigurable estimation mode for CPI processing. Coefficients are estimated for the current observation scene using a known single interference-free sweep. These coefficients are then reused for the restoration of subsequent interference-contaminated sweeps in the CPI.
- An evaluation of the method's performance in the range-Doppler domain. The aim was to additionally showcase the maintenance of the radar's coherence over a CPI after interference mitigation.

**Chapter 3** (**RQ**2): **Decoupling the Doppler Ambiguity Interval from the Maximum Operational Range and Range Resolution in FMCW Radars**
A method was developed to decouple the Doppler ambiguity interval – defined by the PRF – from parameters like the maximum operational range and range resolution, all while maintaining the same transmitted chirp-rate. The novelty is highlighted in:

- The first ever processing method for the coherent integration of frequency multiplexed chirps within one sweep/PRI – for deramping FMCW radar in the time-frequency domain.
- The method constructed a single fast-time slow-time matrix – with an extended Doppler ambiguity interval, while maintaining the range resolution and CPI processing gain – in one go.

**Chapter 4** (**RQ**3): **Reconfigurable Range-Doppler Processing and Target Response Function Width Improvement for FMCW Radar**
A method was developed to overcome the existence of the transient (fly-back) region. The novelty is highlighted in:

- The first ever method for deramping FMCW radar sweeps coherent concatenation in the time-frequency domain.
- The method allowed for target response function width improvement without transmitting additional bandwidth.

- The method offered the ability to – in parallel – generate different size fast-time slow-time matrices, and allowed for Doppler processing PRFs that are different from the transmitted PRF, without compromising on the total CPI processing gain. This offered the ability to observer different unambiguous Doppler velocity intervals in one CPI.

Note that all the developed methods complied with the general requirements specified in the previous subsection. The research conclusions are presented in Chapter 5.

## 1.7. DISSERTATION OUTLINE AND CHAPTERS' ABSTRACTS

Chapters 2, 3 and 4 of this dissertation have their publication status in accordance with the copyright footnote at each chapter, and are related to research questions (**RQs**) as defined in Section 1.5. The chapters are as follows:

- **Chapter 2**: "An Interference Mitigation Technique for FMCW Radar Using Beat-Frequencies Interpolation in the STFT Domain". This is related to **RQ.**1.
  **Abstract**:
  *A Frequency Modulated Continuous Wave radar interference mitigation technique using the interpolation of beat-frequencies in the Short-time Fourier transform (STFT) domain, phase matching and reconfigurable linear prediction coefficients estimation for Coherent Processing Interval (CPI) processing is proposed. The technique is non-iterative and does not rely on algorithm convergence. It allows the usage of the (Fast Fourier Transform) FFT as the radar's beat-frequency estimation tool, for reasons like real-time implementation, noise linearity after the FFT and compatibility with legacy receiver architectures. Verification is done in range and in range-Doppler using radar experimental data in two ways: firstly by removing interferences from interference-contaminated data, and secondly by using interference-free data as reference-data, and processing it - as if it had interferences - using the proposed technique, inverse cosine windowing and zeroing for comparison. We found that processing with the proposed technique closely matches the reference-data, outperforms the inverse cosine windowing and zeroing techniques.*

- **Chapter 3**: "Decoupling the Doppler Ambiguity Interval from the Maximum Operational Range and Range Resolution in FMCW Radars". This is related to **RQ.**2.
  **Abstract**:
  *Classical sawtooth Frequency Modulated Continuous Wave (FMCW) radars*

*experience a coupling between the maximum unambiguous Doppler-velocity interval, maximum operational range, range resolution and processing gain. Operationally, a trade-off is often necessarily made between these parameters. In this chapter, we propose a waveform and a processing method that decouples the aforementioned parameter dependencies at the price of using multiple receiver channels within the radar. The proposed method exploits the fact that beat-frequency signals have the same baseband frequency, even if the transmitted and received chirps occupy different radio frequency bands, and have different center-frequencies. We concatenate those baseband signals in the time-frequency domain to restore the range resolution and processing gain. An overview of the FMCW parameters trade-off for different waveforms and a feasibility analysis of implementing the proposed processing method are presented. The proposed method is verified by simulations and experiments with an FMCW radar for stable, moving and extended-moving targets. We found that the proposed method indeed allows for the unambiguous Doppler-velocity interval extension, without compromising the operational maximum range, range resolution and processing gain. We furthermore discussed the method's limitations and imperfections.*

- **Chapter 4**: "Reconfigurable Range-Doppler Processing and Target Response Function Width Improvement for FMCW Radar". This is related to **RQ.**3.
  **Abstract**:
  *A reconfigurable range-Doppler processing method for FMCW radar is presented. By concatenating beat-frequency signals from more than one sweep, continuous targets' observation time is extended beyond that of a single chirp duration, leading to target response function width improvement. Multiple two-dimensional slow-time fast-time matrices can be created – in the digital domain – with the same number of elements as in the original matrix. This offers a realization of a software defined pulse/sweep repetition rate (PRF) for Range-Doppler processing. The signal concatenation is done in the Short-time Fourier Transform (STFT) domain, where beat-frequency slices are extrapolated to compensate for the observation time lost in the transient region between sweeps, then a phase correction is applied to each frequency-slice as appropriate, followed by an Inverse STFT (ISTFT). The proposed method is verified with simulation and experiments with two FMCW radars for stable and moving target scenarios. We found that the method allows for target response function width improvement. It additionally allows the decoupling of the transmitted PRF from the Doppler processing PRF, permitting the facility to observe different unambiguous Doppler velocity intervals from one CPI, without compromising on the total CPI processing gain.*

*Method limitations and shortcomings are additionally highlighted.*

- **Chapter 5**: Conclusions and Recommendations for Future Work.

## REFERENCES

[1] D. E. Barrick, "FMCW radar signals and digital processing," *NOAA Technical Report ERL 283-WPL 26*, 1973.

[2] A. G. Stove, "Linear FMCW radar techniques," *IEE Proc. or Radar and Signal Process.*, 1992. [Online]. Available: http://dx.doi.org/10.1002/andp.19063240204

[3] N. B. Jones and J. D. Watson, *Digital signal processing: principles, devices, and applications*. P. Peregrinus Ltd. on behalf of the Institution of Electrical Engineers, 1990.

[4] G. H. D. B. C. J. A. D. Stimson, George W., *Stimson's Introduction to Airborne Radar (3rd Edition)*. Institution of Engineering and Technology, 2014.

[5] M. A. Richards, *Fundamentals of Radar Signal Processing, Second Edition*. McGraw-Hill, 2014.

[6] E. D. Adler, E. A. Viveiros, T. Ton, J. L. Kurtz, and M. C. Bartlett, "Direct digital synthesis applications for radar development," in *Proc. Intern. Radar Conf.*, May 1995, pp. 224–226.

[7] D. Giuli, M. Fossi, and L. Facheris, "Radar target scattering matrix measurement through orthogonal signals," *IEE Proc. for Radar and Signal Process.*, 1993.

[8] M. Jankiraman, *Design of Multi-Frequency CW Radars*. SciTech, 2007.

[9] W. L. Melvin and J. A. Scheer, *Principles of Modern Radar: Volume 3 : Radar Applications*. SciTech Publishing Inc, 2014.

[10] T. Schipper, M. Harter, T. Mahler, O. Kern, and T. Zwick, "Discussion of the operating range of frequency modulated radars in the presence of interference," *Int. J. Microwave Wireless Technolog.*, 2014.

[11] J. Bechter and C. Waldschmidt, "Automotive radar interference mitigation by reconstruction and cancellation of interference component," *IEEE MTT-S Int. conf. on Microwaves for Intelligent Mobility (ICMIM)*, 2015.

[12] F. Uysal and S. Sanka, "Mitigation of automotive radar interference," *2018 IEEE Radar conf. (RadarConf18)*, 2018.

# 2

# An Interference Mitigation Technique for FMCW Radar Using Beat-Frequencies Interpolation in the STFT Domain

*A Frequency Modulated Continuous Wave radar interference mitigation technique using the interpolation of beat-frequencies in the Short-time Fourier transform (STFT) domain, phase matching and reconfigurable linear prediction coefficients estimation for Coherent Processing Interval (CPI) processing is proposed. The technique is non-iterative and does not rely on algorithm convergence. It allows the usage of the (Fast Fourier Transform) FFT as the radar's beat-frequency estimation tool, for reasons like real-time implementation, noise linearity after the FFT and compatibility with legacy receiver architectures. Verification is done in range and in range-Doppler using radar experimental data in two ways: firstly by removing interferences from interference-contaminated data, and secondly by using interference-free data as reference-data, and processing it - as if it had interferences - using the proposed technique, inverse cosine windowing and zeroing for comparison. We found that processing with the proposed technique closely*

This chapter is based on:
**S. Neemat**, O. Krasnov, and A. Yarovoy, "An interference mitigation technique for FMCW radar using beat-frequencies interpolation in the STFT domain," *IEEE Transactions on Microwave Theory and Techniques*, pp. 1–14, 2018. © 2019 IEEE with permission.

*matches the reference-data, outperforms the inverse cosine windowing and zeroing techniques*



## 2.1. INTRODUCTION

Frequency Modulated Continuous Wave (FMCW) radars might suffer from interferences from other radars operating within their vicinity, as in Multiple-Input and Multiple-Output (MIMO) radar networks and in automotive scenarios, or from themselves as in the case of fully polarimetric radars with dual-orthogonal signals [2], where there is a leakage between two mutually orthogonal channels (cross-channel interference).

In deramp FMCW radars (stretch-processing), targets' range is deduced from beat-frequency estimation. Processing interference-contaminated beat-frequencies with (Fast Fourier transform) FFTs yields poorer radar detection, due to undesired artifacts such as a noise-floor level increase in range-profiles, which is significantly higher than the system noise-floor, masking weak targets; and spurious vertical lines in range-Doppler. The nature and effects of these interferences on *range-profiles* have been widely studied in the last ten years as in [3] and [4]. The FMCW interference dwell time derivations and interference shapes in an FMCW receiver due to different waveforms can be found in [5]. Analytical formulas for calculating the probability of the occurrence of ghost targets and the interference power per range-bin was presented in [6]. Comprehensive studies of interferences for full polarimetric FMCW radars can be found in [7], and for FMCW radars in general in [8], where interference appearance in range-Doppler maps are illustrated. Interference detection was studied in [9] where image processing techniques were used to detect the interference in the Short-Time Fourier Transform (STFT) domain. In [10] the interference is detected by virtue of using a Single-Side-Band (SSB) I/Q receiver. In an SSB, there usually is only noise in the image-band of the radar, and therefore any interference will be clearly visible in the image-band and simple to detect using a threshold. Once the interference slope is known, its extension into the desired signal band can be deduced from the slope. To solve the interference problem, several approaches have been proposed, among them: 1) zeroing or inverse-windowing the interference-contaminated parts of the signal in the time domain as in [11] and [12]. Inverse-windowing the detected interference regions was proposed in [9]; 2) using waveform-diversity and receiver-architecture-diversity techniques to avoid the interference (e.g. frequency ramp modulation [13], frequency hopping [14] and [15], digital-beam-forming for interference suppression [16]; 3) interference reconstruction and cancellation techniques[17]; 4) sparse sampling techniques in [18] (where interference detection is done by monitoring target peak-power threshold levels against interference-induced noise, then mitigation

is done by reconstructing the interference-free signal using a sparse-signal recovery algorithm); and - most recently - in [19].

While zeroing a part of the beat-frequency signal is the simplest interference suppression method, it causes discontinuities in the periodicity of the tones in the signal, which results in - after performing the range-compression FFT - high residual sidelobes. This in turn causes worse range resolution and the masking of weak targets. Inverse-windowing compromises interferences complete elimination and smoothing the area between the signal and the interference. Both zeroing and windowing cause Signal to Noise Ratio (SNR) loss.



Despite of all aforementioned research on interference mitigation, there is still a need to develop an interference mitigation technique that: 1) relies on the FFT as the primary beat-frequency estimation tool in the radar system; 2) attempts to restore any SNR loss after mitigating the interference; 3) is usable for very extended-target scenarios (atmospheric observations for example) where a single target peak-power threshold level - or any form of target detection - cannot be set to begin with. The justification for the emphasis on using the FFT is: 1) real-time implementation considerations and performance predictability; 2) compatibility with legacy receiver architectures; 3) linearity of the FFT in the sense that noise and clutter still maintain their statistical distribution further up the radar processing-chain, beyond range-Doppler maps. This linearity is not guaranteed if parametric frequency estimation algorithms are used instead of the FFT. The maintenance of such a statistical distribution for noise and clutter is beneficial for many detection algorithms.

Looking at the zeroed parts of beat-frequencies as a missing data *frame* or segment has lead us to consider model-based interpolation as a possible solution, similarly to the problem in acoustics signal processing. In 1986, speech was proposed to be considered as a sum of sine waves with arbitrary amplitudes, frequencies and phases by McAulay (a member of the radar signal processing group at the Lincoln Laboratory) [20]. As we will show in the following section, this analogy holds and is applicable for FMCW deramping beat-frequencies by virtue of the radar's transmitter linearity. In 2001 Kauppinen showed a significantly related finding in [21], being that a single frequency sinusoid can be linearly extrapolated by an impulse response of two coefficients. He then generalizes to that the minimum number of coefficients should be twice the number of frequencies in a signal. In 2002 the same author showed that the extrapolation of missing sinusoidal data can be done forwards and backwards from the known samples, hence the term *interpolation* instead of just extrapolation from one side [22]. Interpolation of the FMCW time-domain beat signal at full bandwidth - typically in the MHz, even after deramping - would then require a prohibitively high-order filter with thousands of coefficients [21]. Coefficients estimation for such a high-

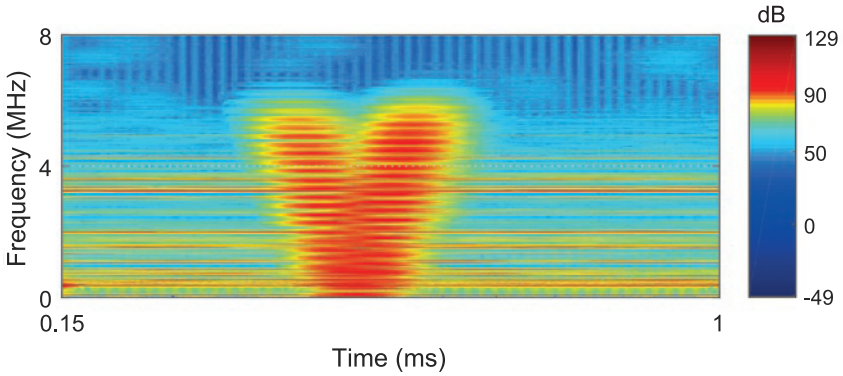
order filter would also typically require the usage of a number of samples at least twice the filter order, which would even further burden the radar.

Decomposing the FMCW time-domain signal in the STFT domain would however relieve the radar from the high-order extrapolation filter requirement, since each frequency (target) will theoretically be represented by a single slice in the STFT time-frequency axes. The idea of working in the STFT domain for speech was indeed also presented by McAulay in the eighties [23] for the purpose of speech analysis and synthesis (reconstruction) back to speech, and in 1997 [24] for radar without further investigation. The work was continued by McAulay's [20] co-author in [25] for the purpose of audio cross-channel interference suppression using the aforementioned sinusoidal model in the STFT domain, followed by an (Inverse Short-Time Fourier Transform) ISTFT for synthesis.

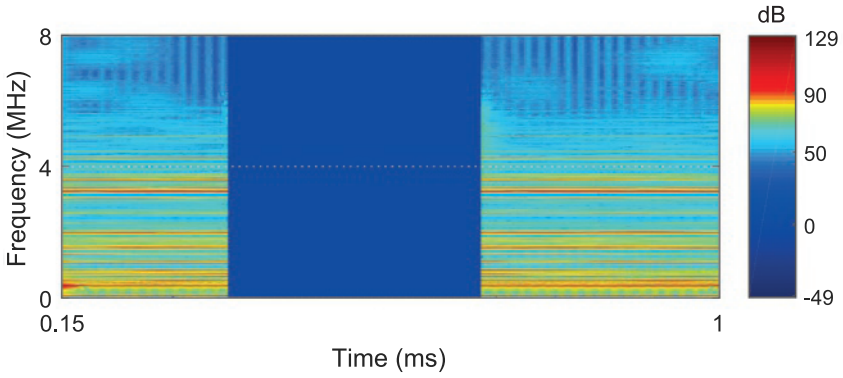
We note that in all the previously cited work, no strict linking of the extrapolated or interpolated data - in the STFT domain - from a phase-continuity point of view has been attempted. The methods suggest none, or just the averaging of the forward and backward extrapolated amplitudes using a cross-fading window. The quality of these reconstruction methods were evaluated subjectively using listening tests. A momentary phase discontinuity might be negligible to the human ear in speech, but remains a limiting factor in radar. There is also no concept of a Coherent Processing Interval (CPI) phase stability (coherence) across multiple sweeps in acoustics. In FMCW however, the end-goal would be to perform FFT operations on the reconstructed sinusoids - after an ISTFT - for range and Doppler information. Phase discontinuities after concatenating the original signal with the interpolated part would cause significantly high sidelobes after performing a range-compression FFT, and as a result, phase stability from pulse-to-pulse will subsequently degrade, resulting in additional high sidelobes after the Doppler (second) FFT.

Considering the suppression/removal of FMCW interferences in the STFT domain and their reconstruction (as in Fig. 2.1 for example), defines the problem as one of the nature of the reconstruction of an amplitude-modulated single-frequency sinusoid per target which was observed in two separate windows. The single-frequency amplitude-modulated sinusoid per target is the simplest beat-frequency signal model, as we will discuss how this varies for real scenarios in Section 2.2.

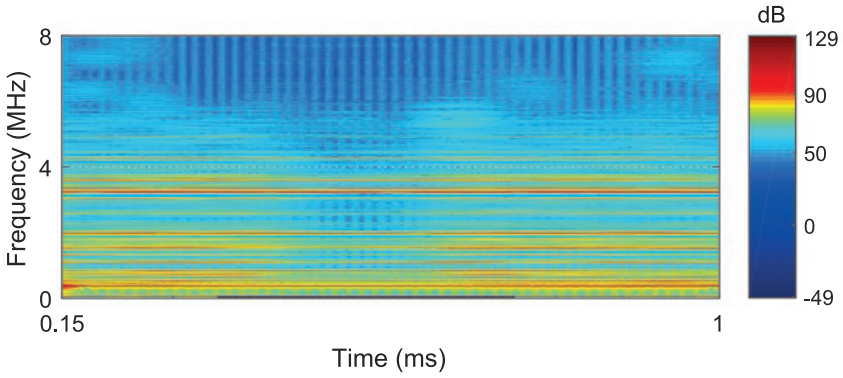
Inspired by acoustics, in this chapter we propose an interference mitigation technique in the STFT domain, tuned for deramping FMCW radar. In our technique, interference-contaminated parts of the beat-frequencies within a sweep are suppressed in the STFT domain. Useful beat-frequencies are to be subsequently reconstructed based on a known signal model (being amplitude-modulated single-frequency sinusoids). The STFT is the analysis tool for the signal model




(a)




(b)




(c)

Figure 2.1: STFT for a single interference contaminated sweep as received using the FMCW radar's Double-Side-Band (DSB) receiver. This sweep is used for the experiment in Section 2.5.2. (a) Interference-contaminated. (b) Interference-contaminated frames suppressed (c) Beat-frequencies interpolated using our proposed technique.

parameters estimation. Linear Prediction (LP) coefficients for the signal parameters are then estimated using Autoregression (AR). These coefficients are estimated for each STFT frequency-slice from the interference-free parts of the sweep, or optionally, in a reconfigurable manner, from a previously known interference -free sweep in the CPI. Suppressed beat-frequencies are then replaced by linear-predicted interpolated ones, followed by a phase matching procedure.

The difference from previous techniques and the novelty in this work is highlighted in:

1. The first ever interference mitigation technique for FMCW radar deramp receivers via model-based beat-frequencies interpolation in the STFT domain;

2. An optional LP interpolation coefficients reconfigurable estimation mode for CPI processing. Coefficients are estimated for the current observation scene using a known single interference-free sweep. These coefficients are then reused for the restoration of subsequent interference-contaminated sweeps in the CPI;

3. The proposed technique is real-time implementable, with a predictable execution delay (latency), based on FFT banks and fixed-length extrapolation filters, as opposed to iterative methods relying on algorithm convergence;

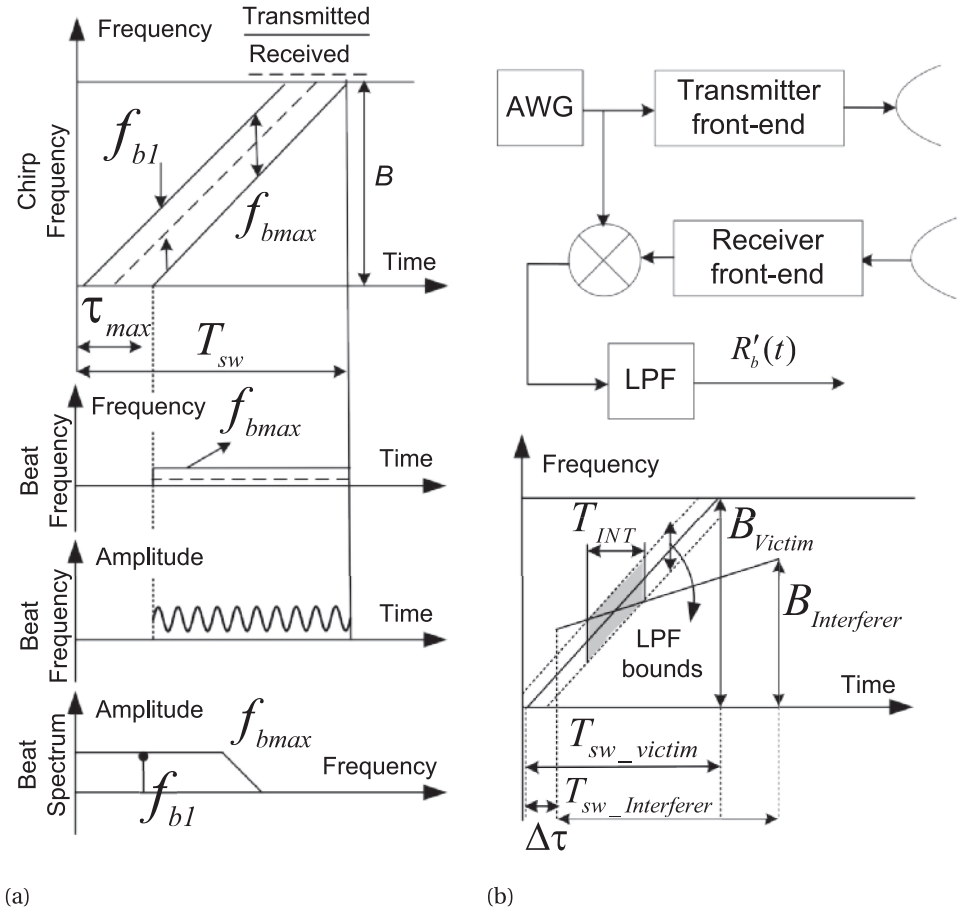
4. An evaluation of the technique's performance in the range-Doppler domain as opposed to range-only (range-profiles) as in previously cited work. The aim is to additionally showcase the maintenance of the radar's coherence over a CPI after interference mitigation;

The rest of the chapter is organised as follows: Section 2.2 presents theoretical aspects related to the proposed technique. Section 2.3 describes the technique used for interference mitigation. Section 2.4 presents technique simulations. Section 2.5 presents experimental results with real radar data and discusses the findings. Conclusions and final remarks are given in Section 2.6.

## 2.2. THEORY

### 2.2.1. DERAMP LINEAR FMCW RECEIVERS

In linear FMCW [26], the transmitted signal can be described as in (1.1), and the received signal as in (1.3). In deramping, the transmitted and received signals are mixed to produce beat-frequencies. This is illustrated in Fig. 2.2 where a receiver's output can be considered as a sum of beat-frequencies. The receiver implementation can be an I/Q (SSB) or DSB. These beat-frequencies are usually




(a) (b)

Figure 2.2: After [7],[5] and [19]. (a) Deramping linear FMCW operational overview. The transmitted and received chirps are mixed to produce beat-frequencies which are usually bound by a LPF. (b) Simplified receiver architecture at the top where $R'_b(t)$ from (2.4) is shown after the LPF. At the bottom, a victim/interferer FMCW interference example where the shaded area represents interferences in a DSB receiver implementation.

bound by a Low Pass Filter (LPF), limiting the maximum frequency in the beat-frequency interval to a desired maximum range. The beat-frequencies are then typically sampled to a point that satisfies the Nyquist criterion for that maximum range. A beat-frequency for a target return after mixing and filtration can also be expressed as [17]:

$$R_{b,i}(t) = A_i \cos[\varphi_i(t)] \tag{2.1}$$

and the receiver output for $M$ multiple responses can be written as:

$$R_b(t) = \sum_{i=0}^{M} R_{b,i}(t) \tag{2.2}$$



confirming that targets' beat-frequencies, like speech, can indeed be considered as a sum of sinusoids with arbitrary amplitudes, frequencies and phases. A full derivation showing all phase terms can be found in [27]. This insight lends itself to working with targets' beat-frequencies in the STFT domain. Each frequency (target) will theoretically be represented by a single slice in the STFT time-frequency axes. Targets with different velocities will later be resolvable in the Doppler domain after processing a CPI. It is worth noting that in the interference mitigation technique presented in this chapter, we do not consider the case where a target might have a considerably high acceleration - causing a frequency change within a *single* sweep - as in ballistic missile applications, for example. The proposed technique can however work in radars experiencing targets range-migration phenomena, as this happens from sweep-to-sweep.

### 2.2.2. FMCW INTERFERENCE

In a victim deramp FMCW radar receiver like the one in Fig. 2.2(b), a received interference from a similar interferer FMCW radar can be described similarly to (1.3) as:

$$R_I(t) = A_I \cos[2\pi(f_c(t-\Delta\tau) + \frac{1}{2}\alpha_I(t-\Delta\tau)^2)] \tag{2.3}$$

where $A_I$ is the interference amplitude, $\Delta\tau$ is the interferer's transmission start time delay with respect to the victim radar transmit start time, and the interferer's chirp rate $\alpha_I = B_I/T_{s_I}$. The interferer's bandwidth is $B_I$ and its sweep time interval is $T_{s_I}$. This interference will be mixed with the transmitted reference, along with useful received echoes. This means that the receiver output in (2.2) can be written as:

$$R'_b(t) = \begin{cases} R_{beat}(t), & -(\frac{T_s}{2}) + \tau_{\max} < t < t_1 \\ R_{beat}(t) + R_I(t), & t_1 \le t \le t_2 \\ R_{beat}(t), & t_2 < t < T_s/2 \end{cases} \tag{2.4}$$

where the interference duration $T_{INT} = t_2 - t_1 + 1$ following the derivations in [5], [17] and [19]. It has been demonstrated that after deramping, the instantaneous frequency of $R_{\mathrm{I}}(t)$ can be expressed as $f_i(t) = (\alpha_{\mathrm{I}} - \alpha)t - \alpha_{\mathrm{I}}\Delta\tau$. The analysis in [19] show that since $f_i(t)$ is bound by the victim's LPF as illustrated in Fig. 2.2(b), the interference duration will be: $T_{INT} \le \left|2LPF/(\alpha_{\mathrm{I}} - \alpha)\right|$. Note that the factor 2 will not be present in a SSB receiver implementation. For a DSB receiver, the

interference appears as a "V" like shape intersecting across the beat-frequencies band, as in Fig. 2.1(a). The assumption in (2.4) is that the interference occurs in the middle of the sweep, causing a discontinuity in useful data. If however the interference occurs in the beginning or end of the sweep, it can simply be discarded without having undesired effects on the range FFT.



### 2.2.3. LINEAR PREDICTION OF FMCW BEAT-FREQUENCIES

In the STFT domain, FMCW target beat-frequencies - as in (2.2), Fig. 2.1 - appear as horizontal (slices) in the time-frequency plane. The full derivation in [27], shows that - except for target range - contributing factors to the phase elements of (1.6) are usually very small in one sweep compared to $\pi$ radians, and can be neglected. It is expected that a noise-free single point-target will have a single constant-amplitude frequency-slice. In reality we however observe amplitude fluctuations on each frequency-slice which depend on factors like: 1) target(s) Radar-Cross-Section (RCS) frequency dependence varying in response to swept instantaneous frequency (Swerling RCS models) in relation to target(s) behavior and nature (point/extended/stable/moving); 2) FFT leakage and resolution degradation due to the fact that the STFT window and hop sizes being typically smaller than the observed signal length; 3) ripple on beat-frequencies as a result of imperfect digital filters' pass-band-ripple. There usually are one or more digital filters in an FMCW radar receiver chain (dc-block, I/Q demodulation, maximum-range, etc.).

Because of the aforementioned reasons, beat-frequencies in the STFT domain can be considered as time sinusoidal signals too, but - as key - with a much lower frequency than the original time domain deramped signal. In the following section we will show that we propose to suppress interference-contaminated beat-frequency frames in the spectrogram, and interpolate them. Since it has long been known in acoustics that time signals' parameters can be modeled using AR, and further extrapolated using these parameters by LP, we propose to do so for FMCW radar beat-frequencies in the STFT domain in this chapter.

In LP, future $y$ values are estimated using a linear combination of previous ones, with the most common representation being:

$$\hat{x}[y] = \sum_{i=1}^{LP_{ord}} a_i x[y-i] \tag{2.5}$$

where $\hat{x}[y]$ is the predicted value, $LP_{ord}$ the prediction filter order and $a_i$ the AR prediction coefficients. AR coefficients estimation algorithms recommend having available samples - to estimate from - at least twice $LP_{ord}$. Noting that when estimating from post-interference-region samples, nothing changes except that samples are flipped-around before being used. This will further be discussed in

Section 2.3. The coefficients are estimated following the Burg method [28] in our implementation. Several methods exist for AR parameters estimation, such as the least-square and Yule-Walker [29]. These methods lead to approximately the same results for large data sets (typically more than 2048 points [30]). It has however been demonstrated that the Burg method is more reliable than the others [30].

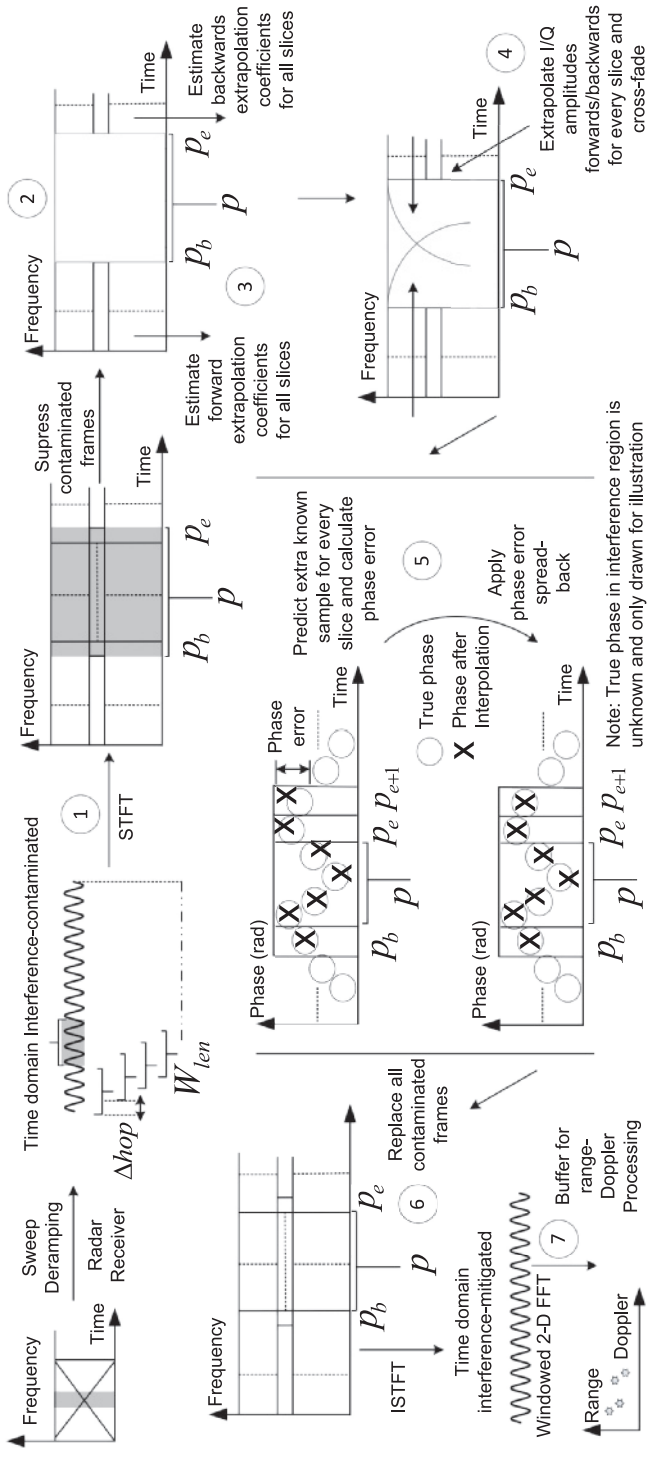



Figure 2.3: Recipe for the proposed interference mitigation technique; and the setup for the first experiment in Section 2.5.2.

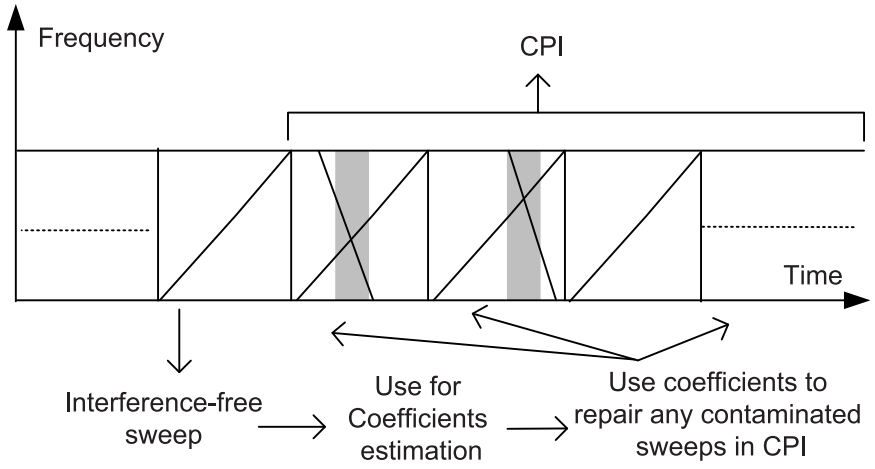



Figure 2.4: Optional reconfigurable LP coefficients scheme for CPI processing. Estimated LP coefficients are retained using a known interference-free sweep, and then used for the interpolation operations in the rest of the CPI.

### 2.2.4. BEAT-FREQUENCIES IN THE STFT DOMAIN

At the output of a typical deramping FMCW receiver, like the one in Fig. 2.2, let a received sweep - as in (2.4) - have $k$ samples, a sampling frequency $f_s$ Hz, a sampling time $t_s$ seconds, yielding an observation time $T_{obs} = k/f_s$ seconds; The beat-frequency resolution of this signal would then be $\Delta f = 1/T_{obs}$ Hz. In the STFT domain, the sweep can be represented as:

$$x_l[n] = \sum_{n=-\frac{W_{len}}{2}}^{\frac{W_{len}}{2}-1} h[n]x[n+l\Delta hop]e^{-i2\pi n/W_{len}} \tag{2.6}$$

where $l$ is the frame number in the STFT, $W_{len}$ is the number of samples for each FFT forming the STFT. $h$ is the analysis window function (Hamming in our case), and $x$ is the input sweep fragment. $\Delta hop$ is the number of samples from successive STFT windows to create an overlap, and $\omega$ the frequency index. The number of frames is defined as $l = 1 + floor((k - W_{len})/\Delta hop)$, where $floor$ is a round-towards-zero operation. The observation time will be determined by $W_{len}$ as $T_{obs_STFT} = W_{len}/f_s$ seconds. The reduced observation time will yield an STFT frequency axis resolution being $\Delta f_{STFT} = 1/T_{obs_STFT}$ Hz. $\Delta f_{STFT}$ will be significantly coarser than $\Delta f$ of the original signal. On the STFT's time axis. The time equivalent of the $\Delta hop$ size is $T_{\Delta hop} = \Delta hop/f_s$, resulting in a different sampling frequency $f_{\Delta hop} = 1/T_{\Delta hop}$. To satisfy the Nyquist criterion, the maximum

STFT beat-frequency-slice fluctuation that can then be unambiguously observed is $f_{\Delta hop}/2$. Note that the STFT is the analysis tool for the signal model (beat-frequencies) parameters estimation.



### 2.2.5. BEAT-FREQUENCY FLUCTUATION MODEL

We model the beat-frequency fluctuations discussed in Section 2.2.3 using a classical amplitude modulation defined with a depth and frequency where:

$$s_m(t) = \frac{A_0}{1+m}\left(1 + m\cos(\omega_m t + \varphi_m)\right)\cos(\omega_b t + \varphi_b) + n(t) \tag{2.7}$$

for $0 < t < T_s$, where $s_m(t)$ is an amplitude modulated STFT beat-frequency-slice, $A_0$ its amplitude, $m$ the modulation depth, $\omega_m$ the modulation frequency, $\varphi_m$ the modulation phase, $\omega_b = 2\pi f_b$ where $f_b$ is the beat-frequency, with an initial phase $\varphi_b$, and $n(t)$ is noise. The modulation frequency $\omega_m = (2\pi/T_s)g$, where $g$ is the number of oscillations per observation period, and $f_m = g/T_s$ the frequency in Hz.

Any of the fluctuation reasons can lead to: 1) $m$ possibly ranging from 0 to 1 in depth; 2) $f_m$ being smaller than $\Delta f_{STFT}$, or being closely spaced to another frequency, and therefore be unresolvable by the STFT on a single frequency-slice; 3) fluctuations periodicity behaviour not being captured by the LP coefficients when the number of oscillations $g$ is too small (depending on the interference duration being suppressed); 4) the SNR affected by the noise amplitude. This model will assist in the trade-offs for the selection of the $W_{len}$, $\Delta hop$ and $LP_{ord}$ parameters in Section 2.3.2, and for simulation in Section 2.4.

## 2.3. METHOD

The following subsections present the steps for beat signal reconstruction, discusses the reconstruction parameters selection trade-offs and CPI processing.

### 2.3.1. BEAT SIGNAL RECONSTRUCTION STEPS

The proposed interference mitigation technique is illustrated in Fig. 2.3. This technique assumes a priori knowledge of the interference location in the sweep, or the usage of the simple method in [10] to identify that location. The steps are:

1. Take a received deramped sweep to the STFT domain;
2. Suppress $p$ interference-contaminated frames where $p$ is the index of the suppressed frames. The suppression is illustrated in Fig. 2.1(b);
3. Estimate IQ amplitude LP coefficients ($a_i$ in (2.5)) for each $n$ frequency-slice from the interference-free parts. The coefficients estimation is done

Table 2.1: Interpolation Parameters Trade-offs

| Parameter | Role/Effect | Size Increase Pros | Size Increase Cons | Limits / Requirement to Satisfy |
|---|---|---|---|---|
| $W_{len}$ | Determines number of STFT frequency-slices (frequency resolution) | Better resolution on the STFT frequency grid ($\Delta f_{STFT}$). More immunity against amplitude fluctuations. Decrease interpolation filter operations computational complexity | Less interference-free samples $l$ to interpolate from. Increase FFT computational complexity | Available samples $l$ to be used for interpolation have to be at least twice the interpolation filter order |
| $\Delta hop$ | Along with $W_{len}$, it determines the time resolution $T_{\Delta hop}$ and value of $l$ | Interpolation filter operations computational complexity decrease | Less interference-free samples $l$ to interpolate from | Nyquist criterion for maximum unambiguously observed amplitude fluctuation for a single beat-frequency slice ($f_{\Delta hop}$). Available samples $l$ to be used for interpolation have to be at least twice the interpolation filter order |
| $LP_{ord}$ | Determines maximum number of frequencies to be interpolated ($f_{\Delta hop}$) (interpolation quality) | Better ability to interpolate more amplitude fluctuations and better noise immunity | Interpolation filter operations computational complexity increase | Order should be less than or equal to $l/2$ |

from the left and right sides of the suppressed frames. As illustrated in Fig. 2.4, in CPI processing, an optional mode allows for the retainment of estimated coefficients from a known interference-free sweep, and the reconfiguring of the LP filters with those coefficients from one CPI to another. This will further be discussed in Section 2.3.2;

4. Extrapolation of IQ amplitudes of (2.6) is done from right and left following (2.5). (noting that this is done on STFT data, which are made up of short FFTs, therefore IQ amplitudes of beat signals on the STFT grid are available. This should not be confused with sweep IQ deramped data from a radar's SSB receiver). A cross-fading window is used to merge the data from both extrapolations, hence the term interpolation. An interpolated frequency slice can be written as:

$$x_n[p] = cw[p]x_{pfw}[p] + \left(1 - cw[p]\right)x_{pbw}[p] \tag{2.8}$$

where $x_{pfw}$ and $x_{pbw}$ are the forward and backward extrapolations respectively. The cross-fading window $cw$ adapted from [31] and [32] is defined as: $cw[p] = c[p]^r$, where $c[p] = 0.5\left(1 + \cos\left(\pi\left(1 + p/(p_b - p_e)\right)\right)\right)$.

The contaminated frames' beginning and end indexes are $p_b$ and $p_e$ respectively.
And $r = \log(0.5)/0.5\left(1 + \cos\left(\pi\left(1 + 0.5/(p_b - p_e)\right)\right)\right)$;

5. Predict an extra sample ($p_{e+1}$) beyond the interference region, with the purpose of checking the predicted phase vs the actual phase at that point. The calculated phase error is then spread backwards in the interpolated data following [32] using the approximation:

$$\varphi_{error} = \hat{\varphi}_{p_{e+1}} - \varphi_{p_{e+1}} \tag{2.9}$$

where $\hat{\varphi}_{p_{e+1}}$ is the phase of the extra predicted sample, $\varphi_{p_{e+1}}$ is the actual phase of the first sample of the interference-free part, and:

$$\hat{\varphi}[p] = \hat{\varphi}[p] + \frac{p - p_b}{p_e - p_b}\varphi_{error} \tag{2.10}$$

where $\hat{\varphi}[p]$ are the phase values of the $p$ previously interpolated samples and $p_b \leq p \leq p_e$. Note that if the forward or backward parts of the sweep are completely contaminated, the technique will work, (2.8) will then only have one part and the phase correction step can be skipped;

6. Convert sweep back to the time-domain, after all $p$ frames have been replaced, using an ISTFT;

7. Normal CPI processing can now take place using a 2-D FFT - with Hamming windows for example - to produce range-Doppler maps.

### 2.3.2. Reconstruction Parameters Selection Trade-offs and CPI Processing

Following the beat-frequency model discussion in Section 2.2.5 and (2.7), interpolation errors can be considered using the trade-offs of the multi dimensional dependence in:

$$error = f(SNR, INT, g, m, k, W_{len}, \Delta hop, LP_{ord}) \tag{2.11}$$

where $INT$ is the interference duration within a sweep. Some of these dependencies will be covered in the simulations in Section 2.4. Trade-offs have to be then made for the selection of $W_{len}$, $\Delta hop$ and $LP_{ord}$ parameters. A guideline for these trade-offs is presented in Table 2.1.

Since the aforementioned fluctuations are not the same for different ranges, target types and different radars, an optimal $LP_{ord}$ selection cannot be generalized and has to be estimated. This can be done by extrapolating *known* interference-free samples (continuously from sweep-to-sweep as a radar background task for example), and choosing an acceptable error percentage threshold against different LP filter orders. An average interpolation error percentage can be calculated as:

$$error = \frac{1}{N}\sum_{n=1}^{N}\left|\frac{x_n - \hat{x}_n}{x_n}\right| \times 100\% \tag{2.12}$$

where $N$ is the number of samples interpolated, $x$ is the interference-free samples and $\hat{x}$ the interpolated samples. If the nature of the beat-frequencies is not foreseen to significantly change from sweep-to-sweep, LP coefficients estimated from a known interference-free sweep can optionally be used for the restoration of an optional number of subsequent interference-contaminated sweeps, or for all subsequent interference-contaminated sweeps in a CPI. This compromise will relief the radar from coefficients estimation from sweep-to-sweep. The CPI coefficients retention mode is illustrated in Fig. 2.4 and has been used in the experiments presented in Section 2.5.

## 2.4. Simulation Results For Presented Technique

To characterize some of the multi-dimensional dependencies in (2.11) for the mitigation technique, a beat-frequency is generated as in Fig. 2.5(a) following (2.7) with: $m = 1$, $T_s = 1$ ms, $g = 25$, $\varphi_m = 0$, $f_c = 100$ kHz, $\varphi_b = 0$ and sampled at an $f_s = 2$ MHz. Additive White Gaussian Noise (AWGN) is used in the simulations. The beat-frequency is then taken to the STFT domain as in Fig. 2.5(b) with: $W_{len} = 64$, $\Delta hop = 4$, where the effects of $g$ and $m$ are clearly visible. The STFT frequency slice at 100 kHz is then plotted in Fig. 2.5(c). For 100 Monte-Carlo simulation runs, Fig. 2.5(d) to Fig. 2.5(i) present box-plots for different

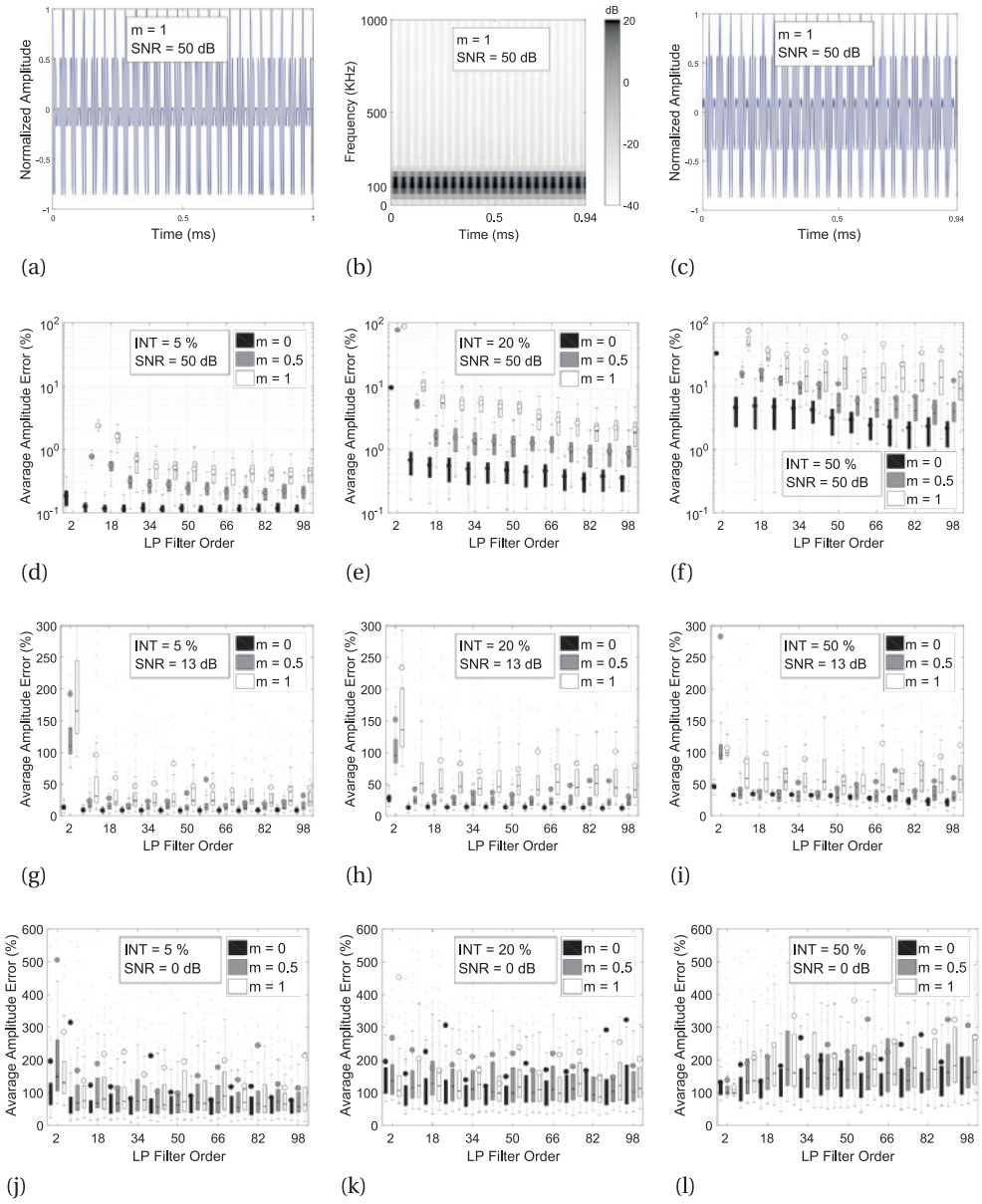



Figure 2.5: Plots for simulation is Section 2.4.(a) Input beat signal in time-domain. (b) STFT of input signal. (c) Amplitude of the 100 kHz frequency slice. Box-plots (d) to (i) are for average amplitude error percentages vs LP filter order for different permutations. In the box-plots, dots represent outliers, horizontal lines the median and circles the mean. In the plots, m: modulation depth from (2.7), INT: interference duration percentage in relation to the time-domain beat signal. SNR values are given for the input time-domain signal. Number of samples used for coefficients estimation: 450.

Table 2.2: Results related to Fig. 2.6 for the strongest target. The difference in signal amplitude (loss) due to the restoration is represented by dP2P, and the difference in peak to sidelobe level is represented by dPSL

| SNR (dB) | 50 | | | 13 | | | 0 | | |
|---|---|---|---|---|---|---|---|---|---|
| INT (%) | 5 | 20 | 50 | 5 | 20 | 50 | 5 | 20 | 50 |
| dP2P (dB) | 0.3 | 0.3 | 0.3 | 0.3 | 0.3 | 0.3 | 0.4 | 0.4 | 1.0 |
| dPSL (dB) | 1.8 | 2.0 | 2.3 | 6.0 | 6.0 | 7.0 | 6.0 | 6.0 | 3.0 |

beat-frequencies with different dependencies of (2.11). SNR and INT percentages are related to the time-domain beat-frequency signal before the STFT (an INT of 50% for example would mean that 0.5 ms of the beat-frequency signal is interference-contaminated). The duration of which the signal in Fig. 2.5(c) is to be suppressed in relation to different interference percentages is calculated using the equation for $l$ STFT frames in Section 2.2.4. The floor operation when calculating $l$ is the reason the STFT beat-frequency has a 0.94 ms duration as opposed to the 1 ms duration of its time-domain representation. Average amplitude errors are calculated using (2.12) and are related to the amplitudes of the specific frequency-slice under test in the STFT domain. From the simulations, we found that the interference duration and modulation depth have a great impact on the errors. As the input SNR is reduced, the fluctuations do not play a major role and the interference duration is more important. Despite that results are shown for a $g$ value of 25, we found that high values of $g$ are better, as the periodicity behavior is more easily then being captured by the LP coefficients. The average amplitude errors seem dramatic because they are calculated sample per sample without any thresholding, and therefore random noise is also compared. To relate those errors to a detection scenario, Fig. 2.6 presents the signal spectrum related to Fig. 2.5(h) after restoration. The combination of $g$ and $m$ appear as three targets. The difference in signal amplitude (loss) due to the restoration is represented by dP2P, and the difference in peak to sidelobe level is represented by dPSL. Table 2.2 presents the results for all simulated cases in dB regardless of probability of detection and false alarm. In simulation, the reference noise-free samples - before adding white noise - are known, therefore another way to evaluate the reconstruction results is to do so for the beat-frequency time-domain signal by calculating a Restoration SNR (RSNR) [21] as:

$$RSNR = 10\log \frac{\sum_{n=1}^{N} {z_n}^2}{\sum_{n=1}^{N} |(z_n - z'_n)|^2} \tag{2.13}$$

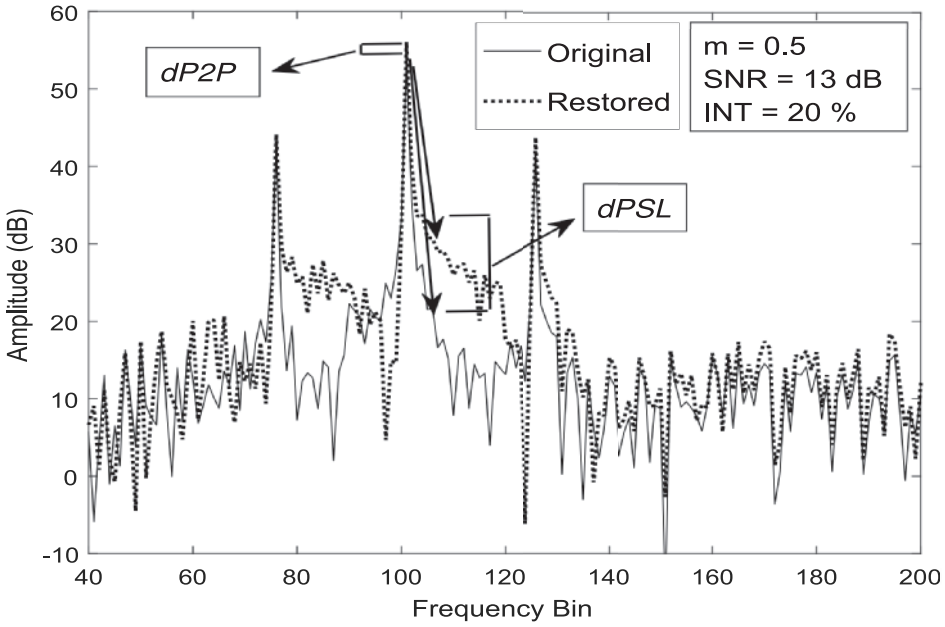



Figure 2.6: Signal spectrum related to Fig. 2.5(h) after restoration. The difference in signal amplitude (loss) due to the restoration is represented by dP2P, and the difference in peak to sidelobe level is represented by dPSL. Refer to Table 2.2 for these results for all simulated cases.

where $N$ is the number of interference-contaminated samples (in the beat-frequency time-domain signal). $z$ are the reference noise-free samples, $z'$ the reconstructed samples. The denominator represents the noise that is the error due to the reconstruction imperfection. The RSNR can also be interpreted as how much of the beat-frequency SNR is restored due to the reconstruction, and to show the reconstruction's dependence on the input beat-frequency SNR. The RSNR is calculated only over the interference-contaminated region in the beat-frequency time signal and is presented in Fig. 2.7. For the permutations in these simulations, LP orders of from 18 to 34 were sufficient to achieve stable error results. Similar simulations can be done for different FMCW radars to determine acceptable error thresholds as discussed in Section 2.3.2.

## 2.5. EXPERIMENTAL VERIFICATION

### 2.5.1. EXPERIMENTAL SETUP

The performance of the proposed interference mitigation technique is demonstrated experimentally using the full-polarimetric TU Delft PARSAX [33] radar depicted in Fig. 2.8(a). PARSAX is mounted on the roof of the electrical engineering, mathematics and computer science building at the TU Delft. The radar

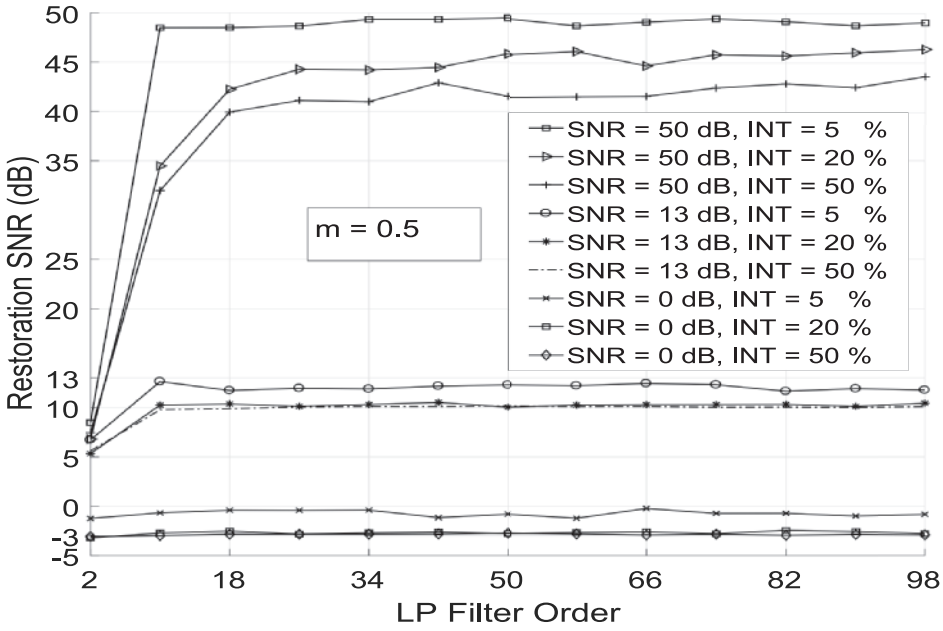



Figure 2.7: RSNR for simulations in Section 2.4. RSNR values indicate how much of the signal power (in the interference region) is restored due to the proposed mitigation technique. This is an advantage over merely suppressing interferences in time-domain. As the input SNR increases, the better the RSNR. Increasing interference durations give worst results.

operates in S-band (3.1315 GHz) and uses an Intermediate Frequency (IF) of 125 MHz. The radar is equipped with a horizontal and a vertical polarization transmit channels. PARSAX has four receiver channels providing for cross and co-polarization configurations. A simplified PARSAX block diagram is depicted in Fig. 2.9. On every receiver channel, transmitted and received signals are sampled at IF using a pair of Analog-to-Digital Converters (ADCs) on an Innovative Integrations X5-400M Xilinx Virtex5SX95T FPGA card. The ADCs are 14-bit devices with sampling rates up to 400 Mega Samples per Second (MSPS). Deramping signal processing is performed digitally on the FPGAs. Beat-frequencies are transferred to a computer via the PCI-express bus for interference mitigation and range-Doppler processing.

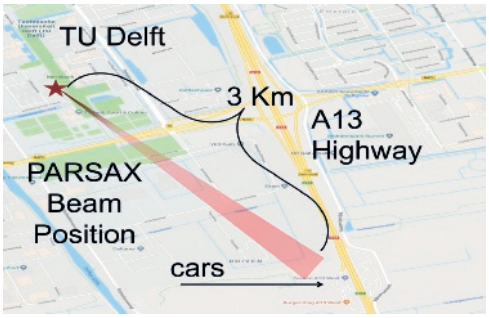
PARSAX can be used to create FMCW interferences in the form of cross-channel interferences. This is done by simultaneously generating an up-chirp and a down-chirp on the horizontal and vertical polarization channels respectively. This waveform will cause a leakage around the time when the up and down chirps intersect. The interference is in agreement with the theory in Section 2.2.2, except that the interferer and victim radars are different polarization channels within the same radar. This is illustrated at the bottom right of Fig. 2.9 for the SSB receiver



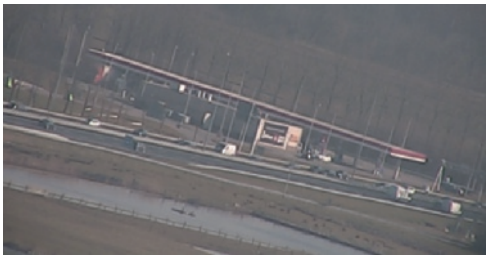

(a)



(b)




(c)



(d)

Figure 2.8: Experimental setup. (a) The PARSAX radar (b) Industrial chimney as a stable-target in experiment 1 (c) location of highway in relation to PARSAX for experiment 2 (d) Photo of the illuminated highway area for experiment 2.

case used in the second experiment. The interference duration in PARSAX for DSB and SSB receivers is approximately 20% and 10% respectively [7]. PARSAX can also be used in an interference-free mode where only a single chirp is generated on a single polarization channel.

Experiments were conducted using the configuration options shown in Table 2.4.

The filter order was selected after analyzing radar data STFT frequency-slices following the discussion in Section 2.3.2. The lowest filter order which gives stable minimum errors for the worst-case frequency-slice (target) was selected. The worst-case frequency-slices for both experiments are illustrated in Fig. 2.10. For simplicity, that filter order was used for all frequency-slices in both experiments.

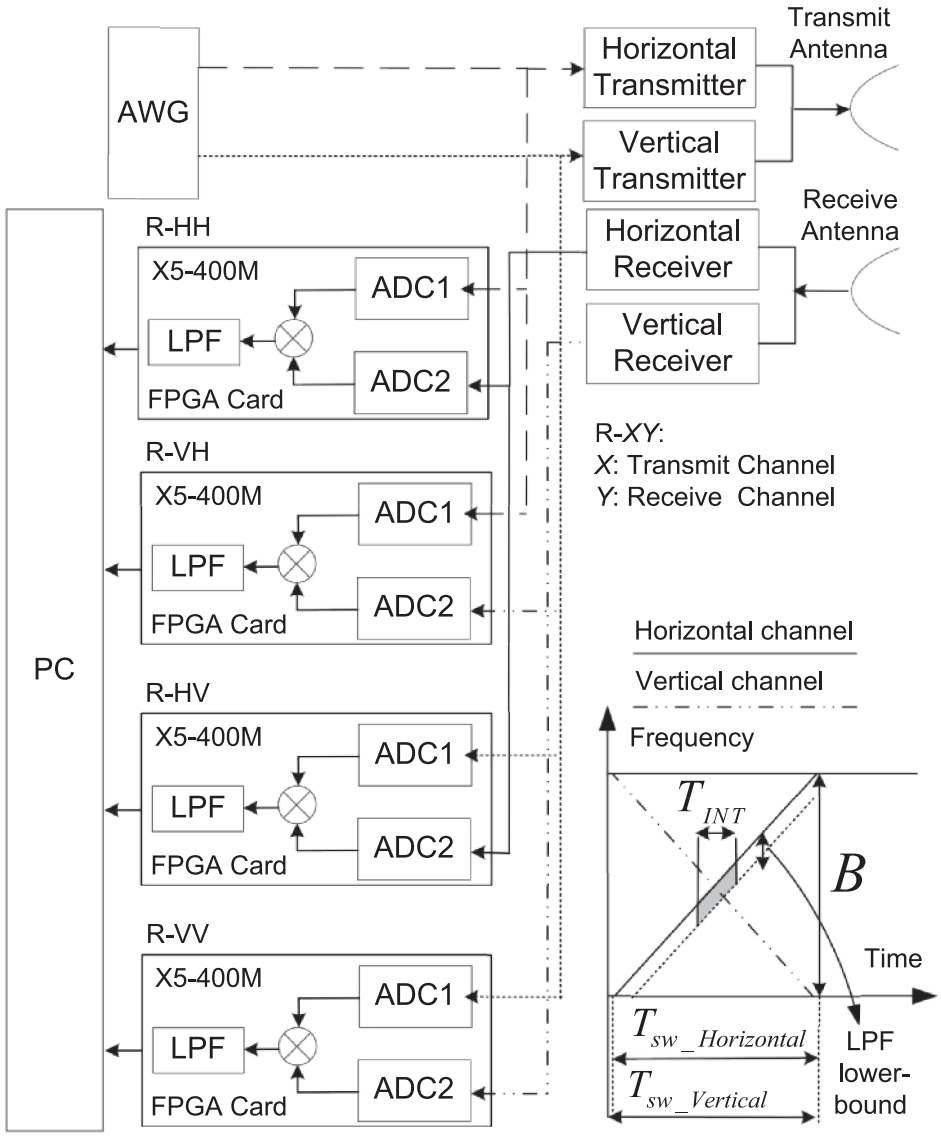



Figure 2.9: Simplified simultaneous polarimetric PARSAX radar block diagram. The radar has two co- and two cross-polarization channels. FPGAs allow for implementing a DSB or a SSB receiver. Data transfer to the PC via PCI-express. The interference scenario in the bottom-right represents the simultaneous polarimetric mode and a SSB receiver.

### 2.5.2. EXPERIMENT 1: INTERFERENCE MITIGATION FOR A SINGLE SWEEP (RANGE-PROFILE)

The setup for the first experiment is illustrated in Fig. 2.3. In this experiment we observe an industrial factory chimney in a stable targets scene, using simultane-

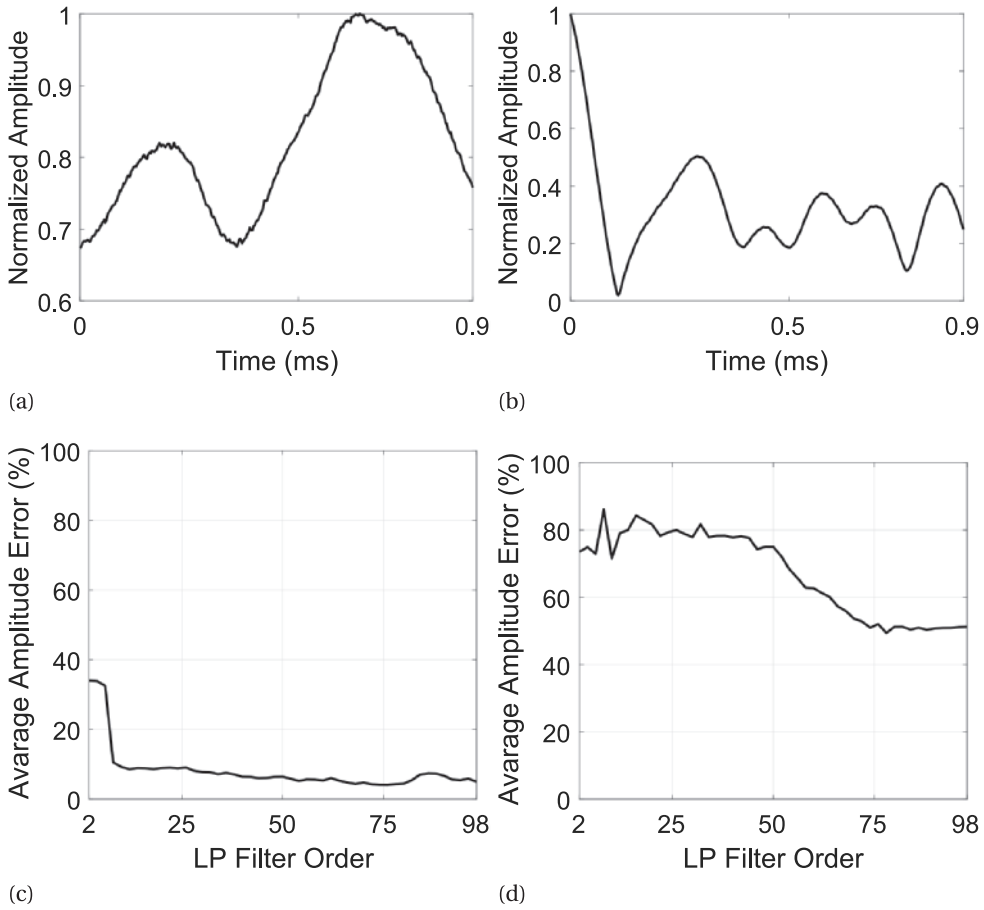



Figure 2.10: Filter order selection based of average interpolation errors of interference-free beat-frequency-slice amplitude fluctuations. For radar-measured data, (a) and (b): Beat-frequency-slice amplitude fluctuation for the worst-case-targets in experiments 1 and 2 respectively. (c) and (d): A filter order of 75 was selected for both experiments. A filter order of 75 was selected because it is the lowest order which gives stable error results.

ous transmission on the horizontal and vertical polarization channels, and using the radar's co-polarimetric receiver (R-HH) with a DSB implementation for an interference duration of 20%. The chimney is depicted in Fig. 2.8(b). This will result in an interference-contaminated sweep due to the vertical channel's leakage into the horizontal one. The aim is to use our interference mitigation technique for this sweep, and illustrate the results for a range-profile. We observe the interference in the STFT domain shown in Fig. 2.1(a). The data is then processed using the proposed technique, inverse cosine windowing and zeroing for comparison.

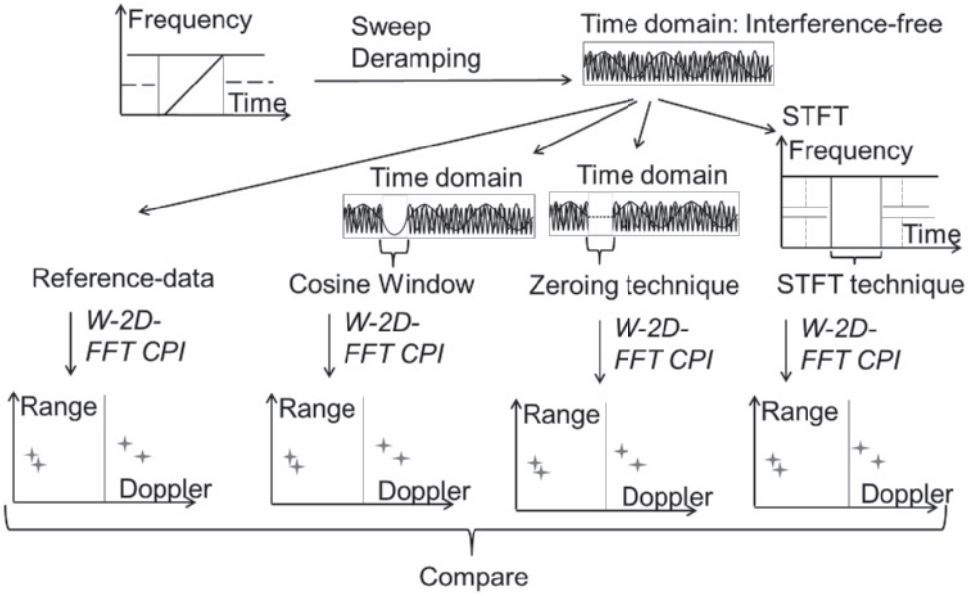



Figure 2.11: Setup for the second experiment in Section 2.5.3. The zeroing, inverse cosine windowing and the proposed techniques are compared in range-Doppler against reference interference-free data. W-2D-FFT indicates performing a windowed (Hamming, in our implementation) range-Doppler two-dimensional FFT.

The inverse cosine window is applied to the interference region in time-domain and is defined as:

$$W_c(t) = \frac{1-\cos\left(\pi\left(\frac{1+2t}{T_s}\right)\right)}{2} \tag{2.14}$$

where $t_1 \leq t \leq t_2$ as in (2.4) and $T_{INT} = t_2 - t_1 + 1$.

### 2.5.3. EXPERIMENT 2: INTERFERENCE MITIGATION IN A RANGE-DOPPLER CPI

The experiment Setup is illustrated in Fig. 2.11. In this experiment, we observe automobiles on a highway, transmitting on only the radar's horizontal channel, and using the radar's co-polarimetric receiver (R-HH) with a SSB implementation. This will result in interference-free sweeps. The highway and its location are depicted in Fig. 2.8(c) and Fig. 2.8(d). These interference-free sweeps are used as reference-data. The data is then processed - as if it had interferences - using the proposed technique, inverse cosine windowing and zeroing for comparison. The aim is to evaluate our proposed technique on range-Doppler maps for a CPI in the case of a moving targets scene. Three copies of the data are made available. On the first, a section of each interference-free sweep is removed by the zeroing

technique. On the second, the inverse cosine window is applied to that same section. And on the third copy, the same section is removed and interpolated by the proposed technique. Three durations of 15%, 25%, and 50% are selected to examine the effects of different possible interference durations. All three techniques are then compared against the reference-data in range-Doppler. A segment - representing a cluster of targets - of the range-Doppler maps from the compared cases is presented in Fig. 2.12, before and after applying a threshold of -30 dB lower than the strongest target peak in each map (different thresholds will also be considered as will be seen in the next subsection). This range-Doppler segment/cluster will be used for further comparisons.



### 2.5.4. RESULTS AND DISCUSSION

For the first experiment, results are shown in Fig. 2.1(c) for our technique in the STFT domain where the "V" shaped interference is removed. In Fig. 2.13 the range-profile for the compared techniques is shown. The range-profile shows that weaker targets clearly emerge after the reduction of the interference-induced noise floor. The inverse cosine window does not perform as well as zeroing - throughout the range-profile - because of it being a compromise between completely eliminating interferences and smoothing the area between the signal and the interference to reduce SLL in the frequency domain. The "V" shaped interference will not completely be removed by the inverse cosine window. The zeroing technique however suffers from higher residual-sidelobes due to the discontinuity in the FFT frequency estimation. For the second experiment, results are calculated on the previously mentioned thresholded range-Doppler maps in Fig. 2.12[(b),(d), (f) and (h)] for multiple threshold levels. The range-Doppler maps show high sidelobes and signal energy spread in the case of zeroing and inverse cosine windowing, whereas a fine restoration is achieved after interpolation. This is also evident in the range and Doppler cuts illustrated in Fig. 2.14 and Fig. 2.15. The figures correspond to the interference duration of 15% in Table 2.3.

The results in Table 2.3 measure performance criteria from different points of view. We found that if we were to evaluate only at target peaks - even after data normalization - it would not be a fully representative restoration accuracy measure, since the zeroing technique can cause peak-deformation into more than one. While this might not be very evident in simulation data, we found it to be so for experiments with the radar. We therefore calculate the performance criteria on the thresholded range-Doppler maps - instead of just at normalized peaks - for more representative results.

A 2-D correlation coefficient [34] calculated as:

$$r = \frac{\sum_{s=1}^{S}\sum_{j=1}^{J}(x_{sj}-\bar{x})(x'_{sj}-\bar{x}')}{\sqrt{\sum_{s=1}^{S}\sum_{j=1}^{J}(x_{sj}-\bar{x})^2 \sum_{s=1}^{S}\sum_{j=1}^{J}(x'_{sj}-\bar{x}')^2}} \tag{2.15}$$

where $x$ is the reference interference-free data, $\bar{x}$ its mean, $x'$ the data processed by the mitigation technique being evaluated and $\bar{x}'$ its mean. The 2-D matrix indices are $s$ and $j$.

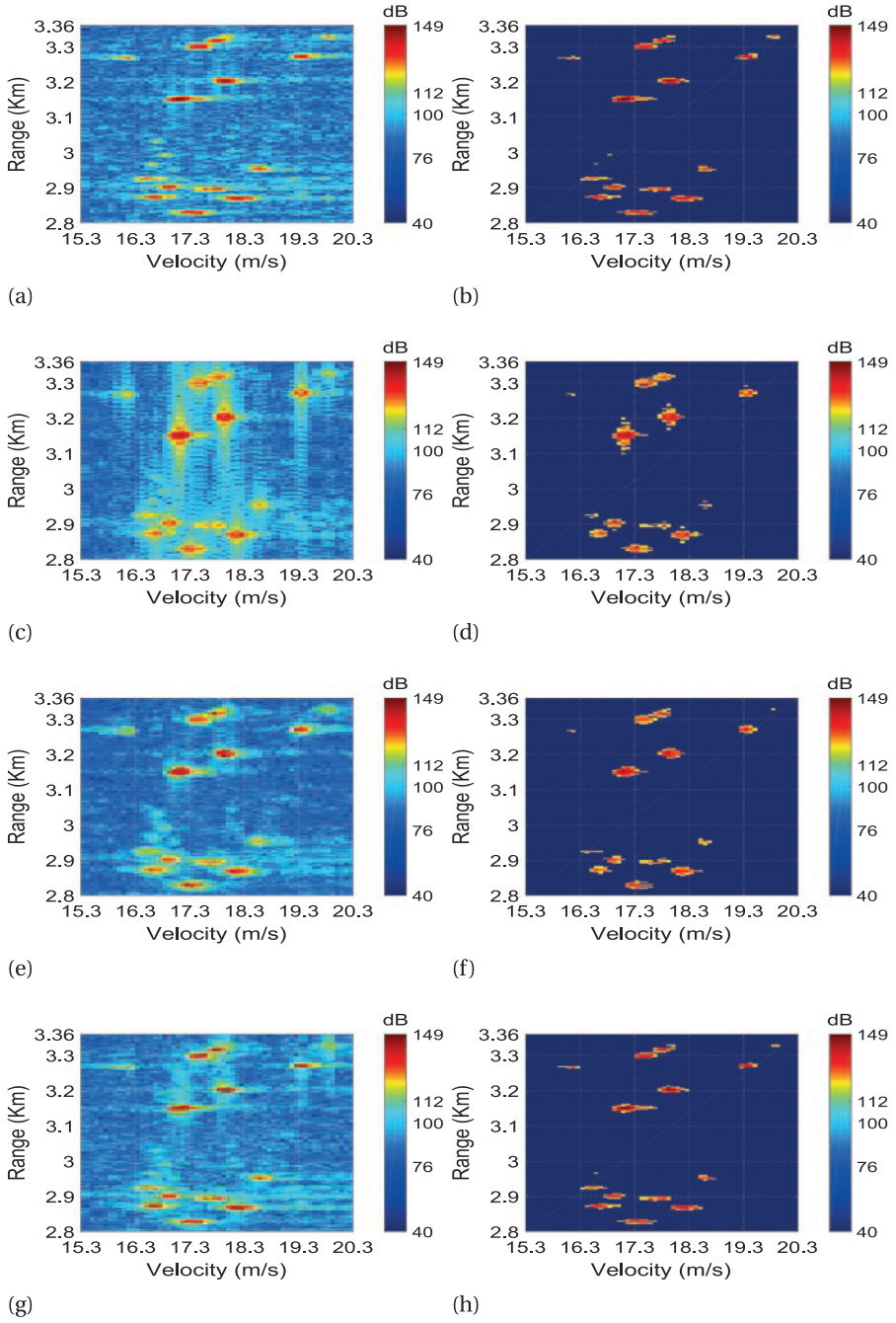



Figure 2.12: Range-Doppler maps used in the second experiment (Section 2.5.3), and illustrated in Fig. 2.11. (a) Reference-data (b) Reference-data thresholded at -30 dB from its strongest peak. (c) Zeroing technique processing of the reference-data (d) Zeroing technique processing of the reference-data thresholded at -30 dB from its strongest peak.(e) Inverse cosine window technique processing of the reference-data (f) Inverse cosine window technique processing of the reference-data thresholded at -30 dB from its strongest peak (g) STFT interpolation technique processing of the reference-data (h) STFT interpolation technique processing of the reference-data thresholded at -30 dB from its strongest peak.

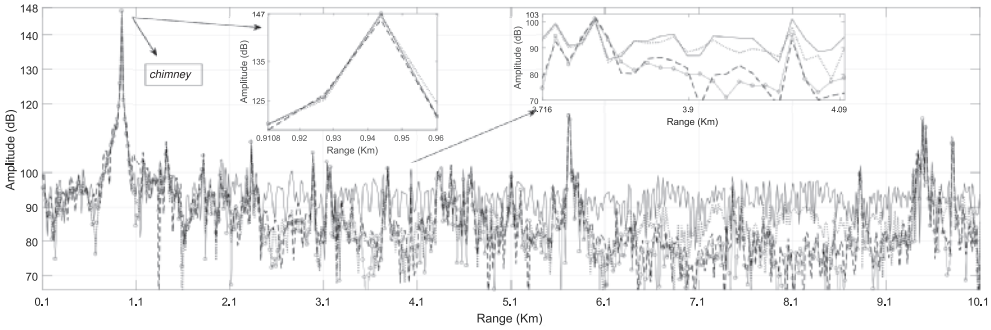



Figure 2.13: Range profile for the sweep in Fig. 2.1 (fist experiment, Section 2.5.2) after processing with zeroing, inverse cosine windowing and the proposed interpolation technique. A drop in the interference-induced noise-floor is visible and weak targets emerge after processing.

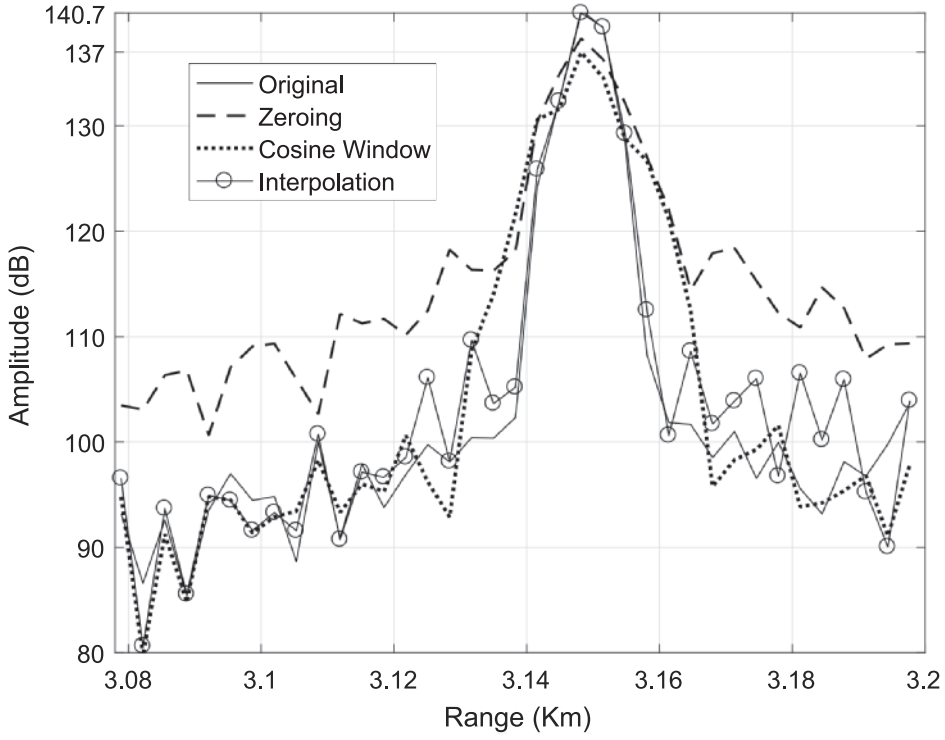



Figure 2.14: A cut through the range-Doppler maps in Fig. 2.12 before any thresholding, at 17.34 m/s velocity. The interpolation technique outperforms the zeroing and inverse cosine window techniques in terms of signal energy spread and SLL.

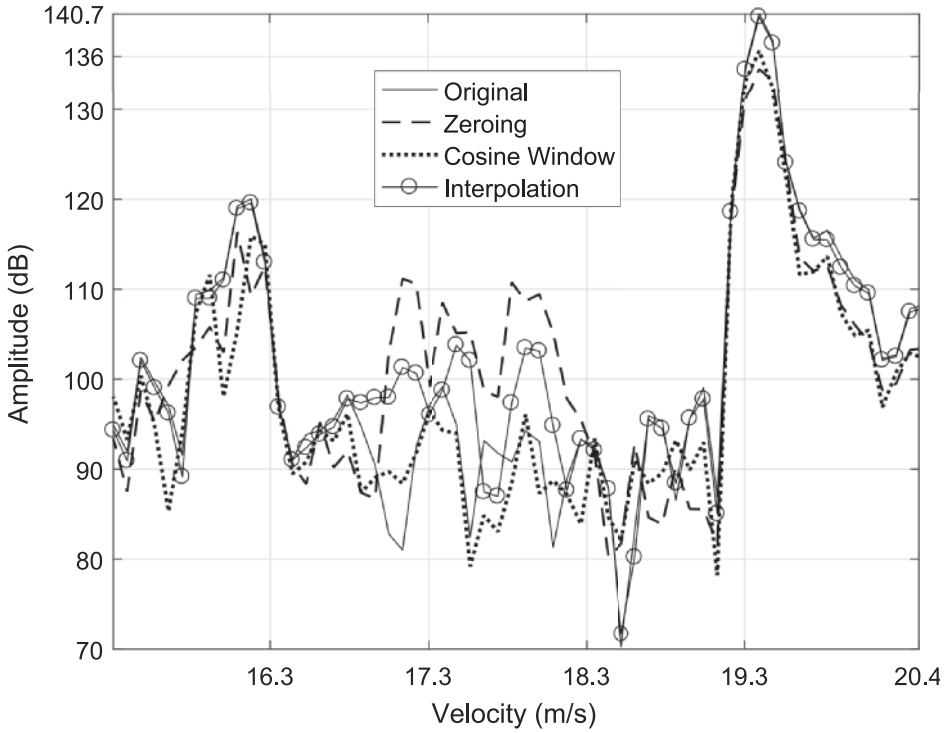



Figure 2.15: A cut through the range-Doppler maps in Fig. 2.12 before any thresholding, at 3.27 km range. The interpolation technique outperforms the zeroing and inverse cosine window techniques in terms of signal energy spread and SLL.

Table 2.3: Results of the second experiment (Section 2.5.3) for different interference durations, threshold values and mitigation techniques. T1: zeroing, T2: Inverse Cosine Window, T3: proposed STFT interpolation technique

| Interference Duration (%) | 15 | | | | | | | | | | | | | | | | | |
|---|---|---|---|---|---|---|---|---|---|---|---|---|---|---|---|---|---|---|
| Threshold from Strongest Peak (dB) | -10 | | | -20 | | | -30 | | | -40 | | | -50 | | | | | |
| Mitigation Technique | T1 | T2 | T3 | T1 | T2 | T3 | T1 | T2 | T3 | T1 | T2 | T3 | T1 | T2 | T3 | | | |
| 2-D Correlation Coefficient | 0.62 | 0.78 | 0.97 | 0.66 | 0.74 | 0.95 | 0.54 | 0.72 | 0.90 | 0.44 | 0.69 | 0.79 | 0.37 | 0.62 | 0.71 | | | |
| Amplitude Average Error (%) | 40.98 | 24.50 | 4.81 | 47.37 | 26.53 | 5.53 | 62.67 | 38.46 | 7.99 | 109.97 | 79.74 | 18.26 | 194.53 | 110.53 | 36.79 | | | |
| Phase Average Error (%) | 111.66 | 32.47 | 4.87 | 157.96 | 85.54 | 19.83 | 170.94 | 100.47 | 21.80 | 272.56 | 118.55 | 61.94 | 247.97 | 107.29 | 67.14 | | | |
| Phase RMSE (radian) | 0.74 | 0.24 | 0.05 | 0.91 | 0.59 | 0.08 | 1.00 | 0.69 | 0.17 | 1.12 | 0.73 | 0.37 | 1.29 | 0.73 | 0.52 | | | |
| Interference Duration (%) | 25 | | | | | | | | | | | | | | | | | |
| Threshold from Strongest Peak (dB) | -10 | | | -20 | | | -30 | | | -40 | | | -50 | | | | | |
| Mitigation Technique | T1 | T2 | T3 | T1 | T2 | T3 | T1 | T2 | T3 | T1 | T2 | T3 | T1 | T2 | T3 | | | |
| 2-D Correlation Coefficient | 0.42 | 0.66 | 0.89 | 0.54 | 0.75 | 0.79 | 0.49 | 0.77 | 0.70 | 0.40 | 0.72 | 0.64 | 0.32 | 0.60 | 0.53 | | | |
| Amplitude Average Error (%) | 44.84 | 34.45 | 12.93 | 49.61 | 38.63 | 14.97 | 59.27 | 46.68 | 22.26 | 93.31 | 67.67 | 59.25 | 162.15 | 63.86 | 108.76 | | | |
| Phase Average Error (%) | 116.89 | 77.98 | 18.53 | 242.93 | 96.49 | 32.92 | 256.18 | 221.83 | 80.18 | 293.25 | 162.07 | 125.27 | 268.86 | 107.66 | 127.19 | | | |
| Phase RMSE (radian) | 0.93 | 0.56 | 0.16 | 1.24 | 0.81 | 0.27 | 1.36 | 0.91 | 0.48 | 1.47 | 1.00 | 0.68 | 1.50 | 0.85 | 0.83 | | | |
| Interference Duration (%) | 50 | | | | | | | | | | | | | | | | | |
| Threshold from Strongest Peak (dB) | -10 | | | -20 | | | -30 | | | -40 | | | -50 | | | | | |
| Mitigation Technique | T1 | T2 | T3 | T1 | T2 | T3 | T1 | T2 | T3 | T1 | T2 | T3 | T1 | T2 | T3 | | | |
| 2-D Correlation Coefficient | 0.40 | 0.68 | 0.72 | 0.51 | 0.76 | 0.70 | 0.51 | 0.77 | 0.64 | 0.40 | 0.72 | 0.55 | 0.30 | 0.57 | 0.42 | | | |
| Amplitude Average Error (%) | 45.78 | 38.35 | 25.57 | 49.27 | 41.97 | 33.13 | 55.05 | 52.19 | 47.18 | 89.54 | 71.92 | 112.47 | 165.10 | 72.36 | 156.15 | | | |
| Phase Average Error (%) | 234.58 | 107.62 | 52.70 | 282.78 | 162.61 | 103.44 | 366.70 | 156.21 | 155.07 | 337.11 | 174.41 | 194.67 | 287.42 | 125.77 | 180.74 | | | |
| Phase RMSE (radian) | 1.09 | 0.67 | 0.43 | 1.45 | 0.88 | 0.71 | 1.51 | 0.91 | 0.80 | 1.57 | 0.91 | 1.00 | 1.62 | 0.79 | 1.08 | | | |

For the −10 dB threshold case, a correlation of 0.97 is calculated compared to 0.78 and 0.62 for the interpolation, inverse cosine windowing and zeroing techniques respectively. A close correlation (the closer to 1 the better) between the original and restored range-Doppler maps for the proposed technique is observed. 2-D correlation coefficients are indicators of how well Sidelobe-Levels (SLL) are reduced. It is worthwhile noting that the results are slightly biased towards inverse cosine windowing in the second experiment. Inverse cosine windowing performs considerably better than zeroing - and in a few instances even better than interpolation - because it is applied to reference interference-free data. There is - in this case - no "V" shaped interference to battle against, and no compromise has to be made between completely eliminating interferences and smoothing the area between the signal and the interference.

An average error percentage is used to quantify accuracy for amplitudes and phases using (2.12) where $N$ is the number of elements in a range-Doppler map, $x_{ref}$ is the reference interference-free data and $x'$ is the data processed by the mitigation technique being evaluated. The results show that - for the -10 dB threshold case - the interpolation technique reduces amplitude and phase errors from 40.98% and 24.5% - for zeroing and inverse cosine windowing respectively - to 4.81% and from 111.66% and 32.47% - for zeroing and inverse cosine windowing respectively - to 4.87%. The differences in the results confirms peaks power-spread and high sidelobes in the case of the zeroing and inverse cosine windowing techniques, which is also in agreement with the 2-D correlation coefficients' results. A phase Root-Mean-Square Error (RMSE) is added as an additional method for phases evaluation in radian. The RMSE is calculated using:

$$RMSE = \sqrt{\frac{1}{N}\sum_{n=1}^{N} |x_n - \hat{x}_n|^2} \tag{2.16}$$

where $N$ is the number of samples, $x$ is the reference interference-free data phases in radian and $x'$ is the phases in radian for data processed by the mitigation technique being evaluated. The interpolation technique offers better phase maintenance. Phase stability is of great importance in polarimetric radars, where target polarimetric information is directly dependent on phase variations between the co- and cross-polarimetric receiver channels (as in the configuration in Fig. 2.9). At high threshold levels, results are more related to target peaks, but as the threshold drops, sidelobes and noise become more evident, and therefore have greater effects in worsening the results. At the lowest threshold of −50 dB we are already marginally comparing noise and the results are not very representative.

Conforming to simulations observations, as interference durations increases, the interpolation quality decreases because of errors accumulating over time. In

Table 2.4: Setup parameters for experiments in Section 2.5

| Experiments 1 and 2 | | |
|---|---|---|
| Parameter | Value | Unit |
| Bandwidth | 40 | MHz |
| PRF | 1 | kHz |
| Maximum beat-frequency | 5 | MHz |
| Total number of samples per sweep | 16384 | Samples |
| STFT window length | 3072 | Samples |
| STFT hop size | 32 | Samples |
| Linear prediction filter order | 75 | n/a |
| Experiment 1 | | |
| Receiver type | DSB | n/a |
| Waveform | Simultanious up/down chirps on horizontal and vertical polarization channels | n/a |
| Experiment 2 | | |
| Receiver type | SSB | n/a |
| Waveform | Up-chirp on horizontal channel | n/a |
| Retain linear prediction coefficients for entire CPI | Yes | n/a |
| CPI length | 512 | Sweeps |
| CPI time | 512 | ms |

such cases we observed worst target sidelobes in range and in Doppler. We observed neither the introduction of *new/false* strong target peaks nor a rise in the noise-floor. We believe this to be due to the LP's linear nature in the sense that its extrapolated values depend on a linear combination of previous ones. This is also evident in that no new targets falsely appear in the noise regions between targets. On the other hand, zeroing or inverse cosine windowing should be selected - at low SNR scenarios - if the error in (2.12) exceeds a selected threshold by the radar designer, as motivated in the discussion in Section 2.3.2.

## 2.6. CONCLUSION

A novel interference mitigation technique for FMCW radar using beat-frequencies interpolation and phase matching in the STFT domain has been presented. After the suppression of interference-contaminated frames of beat-frequencies in a sweep in the STFT domain, useful beat-frequencies are subsequently reconstructed based on a known beat signal model. The beat signal model parameters estimation analysis is done using the STFT. LP coefficients for the signal parameters are then estimated using AR for the current observation scene - for each STFT frequency-slice - from the interference-free parts of each slice, or optionally - in a reconfigurable manner - from a previously known interference-free sweep in the CPI. Suppressed beat-frequency frames are then replaced by the linear-predicted interpolated ones, followed by a phase matching procedure. The proposed technique satisfies our requirement to keep using the FFT as the radar's beat-frequency estimation tool. It furthermore does not require target detection/thresholding - at the strongest target peak - to begin with, nor algorithm convergence. The technique is real-time implementable with a predictable execution delay (latency), based on FFT banks and fixed-length extrapolation filters. We have demonstrated the technique's performance improvement with respect to the known zeroing and inverse cosine windowing solutions, against interference for a stable targets scenario. We have then evaluated the technique's performance in range-Doppler for a moving targets scenario, where an interference-free reference-data CPI is processed using the zeroing technique and vs inverse cosine windowing in comparison to ours. Our technique has shown significant improvements in 2-D correlation coefficients, amplitude and phase average error percentages and phase RMSE.

The proposed technique is also applicable for radars experiencing targets range-migration phenomena, but not applicable to applications where targets might have a considerably high acceleration - causing a frequency change within a single sweep - as in ballistic missile applications, for example.

## REFERENCES

[1] S. Neemat, O. Krasnov, and A. Yarovoy, "An interference mitigation technique for fmcw radar using beat-frequencies interpolation in the stft domain," *IEEE Transactions on Microwave Theory and Techniques*, vol. 67, no. 3, pp. 1207–1220, March 2019.

[2] D. Giuli, M. Fossi, and L. Facheris, "Radar target scattering matrix measurement through orthogonal signals," *IEE Proc. for Radar and Signal Process.*, 1993.

[3] G. M. Brooker, "Mutual interference of millimeter-wave radar systems," *IEEE Trans. Electromagn. Compat.*, 2007.

[4] M. Goppelt, H. L. Blöcher, and W. Menzel, "Automotive radar - investigation of mutual interference mechanisms," *Adv. Radio Sci.*, 2010.

[5] T. Schipper, M. Harter, T. Mahler, O. Kern, and T. Zwick, "Discussion of the operating range of frequency modulated radars in the presence of interference," *Int. J. Microwave Wireless Technolog.*, 2014.

[6] M. Goppelt, H. L. Blöcher, and W. Menzel, "Analytical investigation of mutual interference between automotive FMCW radar sensors," *German Microwave conf.*, 2011.

[7] G. Babur, "Processing of dual orthogonal CW polarimetric radar signals," Ph.D. dissertation, TU Delft, 2009.

[8] S. Sasanka, "Radar to radar interference for 77 GHz automotive radar," *TU Delft Elect. Engineering, Mathematics and Comput. Science*, 2017.

[9] M. Barjenbruch, D. Kellner, K. Dietmayer, J. Klappstein, and J. Dickmann, "A method for interference cancellation in automotive radar," *IEEE MTT-S Int. conf. on Microwaves for Intelligent Mobility*, 2015.

[10] S. Murali, K. Subburaj, B. Ginsburg, and K. Ramasubramanian, "Interference detection in fmcw radar using a complex baseband oversampled receiver," *2018 IEEE Radar conf. (RadarConf18)*, 2018.

[11] O. A. Krasnov, G. P. Babur, Z. Wang, L. P. Ligthart, and F. van der Zwan, "Basics and first experiments demonstrating isolation improvements in the agile polarimetric FM-CW radar - PARSAX," *Int. J. Microwave Wireless Technolog.*, 2010.

[12] G. Babur, Z. Wang, O. A. Krasnov, and L. P. Ligthart, "Design and implementation of cross-channel interference suppression for polarimetric LFM-CW radar," *SPIE - The Int. Soc. for Optical Engineering*, 2010.

[13] Y. Kim, "Identification of FMCW radar in mutual interference environments using frequency ramp modulation," *European conf. on Antennas and Propagation (EuCAP)*, 2016.

[14] T. N. Luo, C. H. E. Wu, and Y. J. E. Chen, "A 77-GHz CMOS automotive radar transceiver with anti-interference function," *IEEE Trans. Circuits Syst. I*, 2013.

[15] J. Bechter, C. Sippel, and C. Waldschmidt, "Bats-inspired frequency hopping for mitigation of interference between automotive radars," *IEEE MTT-S Int. conf. on Microwaves for Intelligent Mobility (ICMIM)*, 2016.

[16] J. Bechter, M. Rameez, and C. Waldschmidt, "Analytical and experimental investigations on mitigation of interference in a DBF MIMO radar," *IEEE Trans. Microw. Theory Techn.*, 2017.

[17] J. Bechter and C. Waldschmidt, "Automotive radar interference mitigation by reconstruction and cancellation of interference component," *IEEE MTT-S Int. conf. on Microwaves for Intelligent Mobility (ICMIM)*, 2015.

[18] J. Bechter, F. Roos, M. Rahman, and C. Waldschmidt, "Automotive radar interference mitigation using a sparse sampling approach," *European Radar conf. (EURAD)*, 2017.

[19] F. Uysal and S. Sanka, "Mitigation of automotive radar interference," *2018 IEEE Radar conf. (RadarConf18)*, 2018.

[20] R. McAulay and T. Quatieri, "Speech analysis/synthesis based on a sinusoidal representation," *IEEE Trans. Acoust., Speech, Signal Process.*, 1986.

[21] I. Kauppinen, J. Kauppinen, and P. Saarinen, "A method for long extrapolation of audio signals," *J. Audio Eng. Soc.*, 2001.

[22] I. Kauppinen and J. Kauppinen, "Reconstruction method for missing or damaged long portions in audio signal," *J. Audio Eng. Soc.*, 2002.

[23] R. McAulay and T. Quatieri, "Speech processing based on a sinusoidal model," *The Lincoln Laboratory J.*, 1988.

[24] B. E. Tullsson, "Topics in FMCW radar disturbance suppression," *Radar conf. (RadarConf)*, 1997.

[25] T. F. Quatieri and R. G. Danisewicz, "An approach to co-channel talker interference suppression using a sinusoidal model for speech," *IEEE Trans. Acoust., Speech, Signal Process.*, 1990.

[26] A. G. Stove, "Linear FMCW radar techniques," *IEE Proc. or Radar and Signal Process.*, 1992. [Online]. Available: http://dx.doi.org/10.1002/andp.19063240204

[27] K. Peek, "An analysis of the effects of digital phase errors on the performance of a FMCW-Doppler radar," M.Sc. Thesis, University of Twente, 2011.

[28] S. Kay, *Modern Spectral Estimation: Theory and Application*. Prentice Hall, 1999.

[29] S. Haykin, *Nonlinear Methods of Spectral Analysis*. Springer-Verlag Berlin Heidelberg, 1983.

[30] M. J. L. de Hoon, T. H. J. J. van der Hagen, H. Schoonewelle, and H. van Dam, "Why yule-walker should not be used for autoregressive modelling," *Ann. Nucl. Energy*, 1996.

[31] P. Saarinen, "New tools in spectral analysis," Ph.D. dissertation, University of Turku, 1996.

[32] M. Lagrange, S. Marchand, and J.-b. Rault, "Long interpolation of audio signals using linear prediction in sinusoidal modeling," *J. Audio Eng. Soc.*, 2005.

[33] O. A. Krasnov, L. P. Ligthart, Z. Li, G. Babur, Z. Wang, and F. van der Zwan, "PARSAX: High-resolution doppler-polarimetric FMCW radar with dual-orthogonal signals," *18th Int. conf. on Microwave Radar and Wireless Communications (MIKON)*, 2010.

[34] D. Salomon, *A Guide to Data Compression Methods*. Springer New York, 2013.

# 3

# DECOUPLING THE DOPPLER AMBIGUITY INTERVAL FROM THE MAXIMUM OPERATIONAL RANGE AND RANGE RESOLUTION IN FMCW RADARS

*Classical sawtooth Frequency Modulated Continuous Wave (FMCW) radars experience a coupling between the maximum unambiguous Doppler-velocity interval, maximum operational range, range resolution and processing gain. Operationally, a trade-off is often necessarily made between these parameters. In this chapter, we propose a waveform and a processing method that decouples the aforementioned parameter dependencies at the price of using multiple receiver channels within the radar. The proposed method exploits the fact that beat-frequency signals have the same baseband frequency, even if the transmitted and received chirps occupy different radio frequency bands, and have different center-frequencies. We concatenate those baseband signals in the time-frequency domain to restore the range resolution and processing gain. An overview of the FMCW parameters trade-off for different waveforms and a feasibility analysis of implementing the*

This chapter is based on:
**S. Neemat**, O. Krasnov, Fred van der Zwan, and A. Yarovoy, "Decoupling the Doppler Ambiguity Interval from the Maximum Operational Range and Range Resolution in FMCW Radars," *IEEE Sensors Journal.* to be published, DOI: 10.1109/JSEN.2020.2972152. © 2020 IEEE with permission.

*proposed processing method are presented. The proposed method is verified by simulations and experiments with an FMCW radar for stable, moving and extended-moving targets. We found that the proposed method indeed allows for the unambiguous Doppler-velocity interval extension, without compromising the operational maximum range, range resolution and processing gain. We furthermore discussed the method's limitations and imperfections.*



## 3.1. INTRODUCTION

Frequency Modulated Continuous Wave (FMCW) radars [1], [2], operating with chirp-sequence sawtooth waveforms in deramping (stretch-processing) mode – are widely used for numerous applications from weather observation, automotive sensing and navigation [3], and biomedical applications [4]. The deramping processing concept is based on the mixing of the transmitted signal with the received echoes, resulting in baseband signals known as beat-signal, which are proportional to targets' ranges. Appropriate Radio Frequency (RF) conversion and filtering operations are used for a reliable deramping design, depending on available resources and desired operational band [5]. The radar's range-resolution is a criterion by which the radar's ability to separate targets that are close in range is measured. Deramping FMCW radars' range-resolution is defined by the transmitted bandwidth. The radar's chirp-rate defines the ratio between the transmitted bandwidth and the sweep time (PRI). Deramping FMCW radar's maximum operational range is defined by its maximum beat-frequency, which is typically set by a Low Pass Filter (LPF) placed subsequent to the mixing of the transmitted and received signals. Targets' velocities are typically calculated from Doppler frequency estimation across multiple targets' returns from multiple sweeps in a Coherent Processing Interval (CPI). The radar's sweep repetition frequency (PRF) is therefore the Doppler sampling frequency, and in consequence defines the radar's maximum unambiguous velocity. The FT is widely used for the estimation of target ranges and velocities, for its compatibility with most processing architectures, linearity and predictable latency.

The problem this chapter offers a solution for is the coupling of the radar's Doppler-velocity ambiguity interval – as defined by the PRF – with its range resolution and its maximum operational range. This is in the sense that if there is an operational requirement for the observation of fast(er) moving targets, conventional FMCW radar requires the utilization of a higher PRF, which in turn degrades the range-resolution due to the reduced transmitted bandwidth because of the reduced observation time. But, if the transmitted bandwidth is to be maintained as it was before increasing the PRF – by increasing the chirp-rate, which is not always possible for legacy systems – the maximum operational range will be reduced due to the fixed LPF cutoff frequency. The developed solution for

the aforementioned problem shall not require any detection or a-priori information about the observed scene, shall be applicable to very-extended targets like rain/clouds, and shall only use the FT – as opposed to iterative frequency estimation techniques.

Previous work used under-sampling or antenna-spacing schemes are ways to restore range-resolution, but still suffer from Doppler ambiguities [8], [9]. The work in [11] utilizes a Bandwidth Extrapolation (BE) method which uses an Auto Regressive (AR) model to interpolate beat-signals to connect multiple RF sub-band returns in fast-time. The technique is not suitable for systems with an LPF cutoff of a few MHz – in addition to a usually unknown number of observed targets – yielding a fast-time signal which would require an AR filter order in thousands to interpolate, which is very difficult to realize and implement in a practical system. The improvement from BE methods is also typically limited to small durations of a sweep, and it would not be realistic if there is a desire to increase the PRF by a factor of 2, which would mean that half of the original signal would have to be interpolated. The method in [12] is also a BE technique for matched-filter processing and is not applicable to deramping systems. An iterative frequency estimation method for target's beat-signals is presented in [13]. The method gives more freedom in terms of restrictions to the maximum center-frequency separation between utilized sub-bands, but does not rely on the FT, making its latency unpredictable since it relies on algorithm convergence. An interesting approach which unbinds the Doppler ambiguity interval from the PRF is presented in [15], but requires the usage of time-shifted opposite-slope chirps, and is iterative along target-peaks, making it unsuitable for extended meteorological targets like rain.

The solution proposed in this chapter is the multiplexing of multiple chirps within one sweep, and a processing method that decouples the aforementioned parameter dependencies at the price of using multiple receiver channels within the radar. The processing method will exploit the fact that beat-frequency signals have the same baseband frequency – even if the transmitted and received chirps occupy different RF bands, and have different center-frequencies (with restrictions discussed at the end of the chapter). The fusion of those – same frequency – baseband signals will be done in the time-frequency domain using phase shift operations. The solution will enable the radar to continuously operate at a high PRF, liberating it from post range-Doppler resolution improvement techniques which might suffer from Doppler frequency spectrum folding due to the ambiguities related to a low PRF.

A concept sketch of the idea is presented in Fig.3.1.

The novelty of this work and difference from previous techniques is highlighted in:

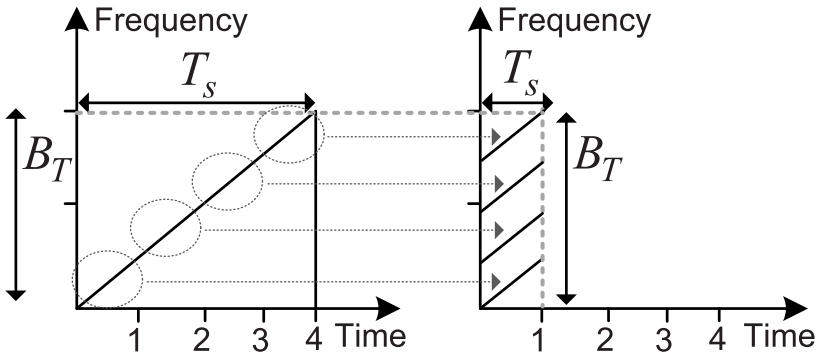



Figure 3.1: Concept sketch of the solution waveform presented in this chapter, where the multiplexing of multiple chirps within one sweep and a processing method is proposed. The solution decouples FMCW operational parameter dependencies at the price of using multiple receiver channels in the radar. The total transmitted bandwidth $B_T$ and processing gain is maintained, but the PRF is increased, all while maintaining the same chirp-rate. In Section 3.2.2, the pros and contras between the suggested waveform and a chirp-rate increase will be discussed.

1. The first ever processing method for the coherent integration of frequency multiplexed chirps within one sweep/PRI – for deramping FMCW radar in the time-frequency domain, which allows the decoupling of the Doppler ambiguity interval from the maximum range, processing gain and range resolution.

2. The method constructs a single fast-time slow-time matrix – with an extended Doppler ambiguity interval, restored range resolution and restored CPI processing gain – in one go.

3. The method does not use iterative algorithms with unpredictable latencies, nor requires any detection or a-priori information about the observed scene, and is applicable to very-extended targets like rain/clouds.

The rest of this chapter is organized as follows: Section 3.2 presents related theoretical aspects. Section 3.3 presents the method for multiple sub-bands sweeps concatenation in the time-frequency domain. Section 3.4 discusses the implementation feasibility of the proposed method. Section 3.5 presents simulations, experimental verification with real radar data and discusses the findings. Conclusions and final remarks are covered in Section 3.6.

## 3.2. THEORY

### 3.2.1. RELATED FMCW RADAR BACKGROUND

Refer to Section 1.3 for related FMCW radar background and equations. Note that waveforms presented in Table. 3.1 and Table. 3.2 will be further used in this chapter for discussions, simulations and experiments, and that the frequency values are in intermediate frequency (IF) before up-conversion to RF.



### 3.2.2. OPERATIONAL PARAMETERS TRADE-OFFS, AND PARAMETERS DECOUPLING

The waveform in the first column (W.a) of Table. 3.1 is to be taken as the reference case for the following trade-off analysis. If there is a desire to increase $v_u$ by a factor of 2 for the unambiguous observation of fast(er) moving targets, the PRF needs to be increased by a factor of 2. The options for this – in standard processing – are presented in cases (W.b) and (W.c), where the number of sweeps in a CPI $N_{CPI}$ is increased by a factor of 2 in an attempt to recover any possible processing gain loss. For waveform (W.b), changing the chirp-rate to cover the entire available bandwidth might not be possible for legacy systems, and will result in a maximum range $R_m$ loss by a factor of 2 for the same LPF cutoff frequency. The benefits on the other hand would be that the range-resolution $\Delta R$ and the processing gain $G_{\text{CPI}}$ will not degrade by a factor of 2. For waveform (W.c), $R_m$ is maintained in reference to (W.a), but $\Delta R$ and $G_{\text{CPI}}$ are worst by almost a factor of 2 – due to not using the entire available bandwidth – even for the same $N_{CPI}$.

The method described in Section 3.3 exploits the fact that beat-signals have the same baseband frequency, even if the transmitted and received chirps occupy different RF bands. The method will show how these beat-signals can be chained together for further usage. This will mean that the more chirps the radar can transmit and receive, the more beat-frequency samples are available for usage. The feasibility and limitations of this will be covered in Section 3.4. These extra beat-frequency samples will mean that we can increase the PRF, and therefore increase the unambiguous Doppler-velocity interval (while maintaining the same chirp-rate and maximum range $R_m$). All that without compromising on the range resolution and CPI processing gain. If $M$ is the number of frequency chirps multiplexed in a sweep, and is therefore also the number of receivers in the system. This is shown in the drawings and calculations of waveforms (W.d). The improvement in the processing gain in (1.15) after concatenating M sweeps can now be expressed as:

$$G_r = B_e T_o M. \tag{3.1}$$

Table 3.1: Worked-out trade-offs for waveforms discussed in the theory Section 3.2.2, the simulations and experimental verification in Section 3.5. Waveforms W.a, W.b and W.c represent classical operation, whereas W.d the proposed waveform and processing method. References to corresponding equation numbers in the text are presented in the first column.

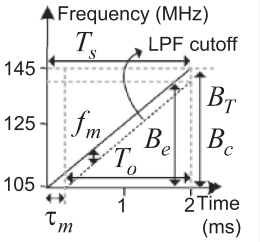
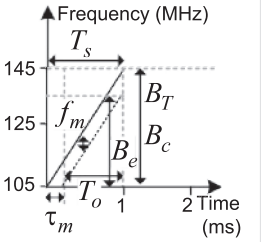
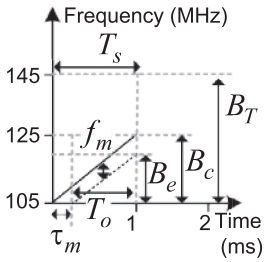
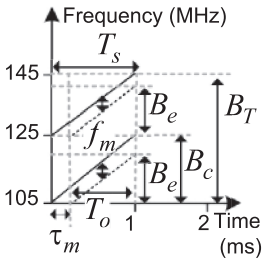
| |  |  |
|---|---|---|
| Waveform | W.a | W.b |
| Description | Standard reference chirp | Double the PRF and increase sweep-rate to cover entire available bandwidth |
| Chirps per sweep/PRI $M$ | 1 | 1 |
| Sweeps in CPI $N$ | 32 | 64 |
| Max. round-trip time $\tau_{\max}$ (1.5) ($\mu s$) | 100 | 100 |
| Max. beat-freq. $f_m$ (LPF) (1.7) (MHz) / Max. range $R_{\mathrm{m}}$ (1.7) (Km) | 2 / 15 | 2 / 7.5 |
| Sweep time $T_s$ (1.1) (ms) / PRF (1.1) (KHz) | 2 / 0.5 | 1 / 1 |
| Max. Unambiguous Doppler Velocity (1.11) (m/s) | 11.3 | 22.6 |
| Observation time (1.4) (ms) | 1.9 | 0.9 |
| Total available bandwidth $B_T$ (1.1) (MHz) | 40 | 40 |
| Transmitted chirp bandwidth $B_c$ (1.2) (MHz) | 40 | 40 |
| Effective bandwidth $B_e$ (1.9) (MHz) | 38 | 36 |
| Chirp-rate $\alpha$ (1.2) (GHz/s) | 20 | 80 |
| Range resolution $\Delta R$ (1.10) (m) | 3.9 | 4.1 |
| CPI processing gain $G_{\mathrm{CPI}}$ (1.16) | 2310400 | 2073600 |

Table 3.2: (Continued) Worked-out trade-offs for waveforms discussed in the theory Section 3.2.2, the simulations and experimental verification in Section 3.5. Waveforms W.a, W.b and W.c represent classical operation, whereas W.d the proposed waveform and processing method. References to corresponding equation numbers in the text are presented in the first column.

| | | |  | |  | |
|---|---|---|---|---|---|---|
| Waveform | | | W.c | | W.d | |
| Description | | | Double the PRF but keep sweep-rate as in W.a | | Double the PRF and keep sweep rate as in W.a, but use two chirps | |
| Chirps per sweep/PRI $M$ | | | 1 | | 2 | |
| Sweeps in CPI $N$ | | | 64 | | 64 | |
| Max. round-trip time $\tau_{\max}$ (1.5) ($\mu s$) | | | 100 | | 100 | |
| Max. beat-freq. $f_m$ (LPF) (1.7) (MHz) | Max. range $R_{\mathrm{m}}$ (1.7) (Km) | 2 | 15 | 2 | 15 | |
| Sweep time $T_s$ (1.1) (ms) | PRF (1.1) (KHz) | 1 | 1 | 1 | 1 | |
| Max. Unambiguous Doppler Velocity (1.11) (m/s) | | | 22.6 | | 22.6 | |
| Observation time (1.4) (ms) | | | 0.9 | | 0.9 | |
| Total available bandwidth $B_T$ (1.1) (MHz) | | | 40 | | 40 | |
| Transmitted chirp bandwidth $B_c$ (1.2) (MHz) | | | 20 | | 20 per chirp | |
| Effective bandwidth $B_e$ (1.9) (MHz) | | | 18 | | 18 per chirp | |
| Chirp-rate $\alpha$ (1.2) (GHz/s) | | | 20 | | 20 | |
| Range resolution $\Delta R$ (1.10) (m) | | | 8.3 | | 4.1 | |
| CPI processing gain $G_{\mathrm{CPI}}$ (1.16) | | | 1036800 | | 2073600 | |

## 3.3. METHOD: SUB-BANDS SWEEPS CONCATENATION

Chirps form different sub-bands in a sweep are coherently concatenated in the time-frequency domain using phase-shift operations, as depicted in Fig. 3.2. The steps are:

1. Store the deramped time-domain beat-frequency signal output from each receiver in the system. These signals can be expressed as $x_{m,n}[k]$. The receiver number is $m$, and $1 \leq m \leq M$, where $M$ is the number of receivers in the system. The sweep number in the CPI is $n$, and $1 \leq n \leq N$, where $N$ is the total number of sweeps in that CPI.

2. Take sweeps from all receivers to the time-frequency domain by applying an STFT, where a sweep can be expressed in matrix form as

$$\mathbf{A}_{m,n}[l,y] = \left[ \sum_{q=-\frac{W}{2}}^{\frac{W}{2}-1} w[q]\, x_{m,n}[q - l\Delta h]\, e^{-i2\pi qy/W} \right]_{Y \times L} \tag{3.2}$$

with $Y$ rows and $L$ columns, where $l$ is the STFT frame index, $l = 1,...,L$, and $L = 1 + \lfloor (k - W)/\Delta h \rfloor$. The analysis window length is $W$. The STFT hop size is $\Delta h$, and $\lfloor \cdot \rfloor$ denotes the floor operation. The frequency-slice index in the STFT frequency grid is $y$, where $y = 0,...,Y$, and $Y$ is the maximum beat-frequency index. The analysis window (for instance, Hamming) is $w$.

3. Form concatenated slices in the STFT domain from all receivers as:

$$\mathbf{P}_n = [\ \mathrm{A}_{1,n} \quad \mathrm{A}_{2,n} \circ \mathbf{C}_{2,n} \quad \dots \quad \mathrm{A}_{m,n} \circ \mathbf{C}_{m,n}\ ]_{Y \times (ML)} \tag{3.3}$$

where '$\circ$' denotes the Hadamard product. The phase matching term $\mathbf{C}$ has $L$ identical columns, and is defined as

$$\mathbf{C}_{m,n} = \begin{bmatrix} e^{i\Delta\varphi_m(f_0)} & \dots & e^{i\Delta\varphi_m(f_0)} \\ \vdots & \vdots & \vdots \\ e^{i\Delta\varphi_m(f_Y)} & \dots & e^{i\Delta\varphi_m(f_Y)} \end{bmatrix}_{Y \times L} \tag{3.4}$$

where

$$\Delta\varphi_m(f_y) = (\varphi_{m-1,L}(f_y) - \varphi_{m,1}(f_y)) + (2\pi f_y t_h). \tag{3.5}$$

The frequency value at a frequency-slice index is $f_y$, and the hop time $t_h = \Delta h / f_s$. Since this is done in the time-frequency domain, the term $2\pi f_y t_h$ in (3.5) can alternatively be calculated by taking the mean of the differences between the – unwrapped – phase values for every frequency slice. Note that the phase matching operations insure phase continuity for each frequency slice when performing an Inverse STFT (ISTFT) in the next step.

4. Form the new time-domain concatenated beat-frequency sweep by applying an ISTFT as

$$\bar{x}_n = \text{ISTFT}(\mathbf{P}_n). \tag{3.6}$$

## 3.4. IMPLEMENTATION FEASIBILITY



The following subsections analyze the feasibility of operating a multi receiver channel radar with waveform (W.d) in Table. 3.2.

### 3.4.1. RECEIVER CHANNELS CALIBRATION

As will be demonstrated in the experiments Section 3.5.2, multiple receivers used for the collection of beat-signals need to be calibrated in amplitude and phase. Mismatches in a fast-time slow-time matrix before – Doppler processing – can be thought of as the superimposition of a second sin wave on top of an original one that is sampled for Doppler processing. That then causes grating lobe in the opposite Doppler-velocity spectrum, which can interpreted as ghost targets.

### 3.4.2. MAXIMUM CHIRPS' CENTER-FREQUENCY DIFFERENCE

For the same observed target with two different center-frequency $f_c$ chirps within the same sweep/PRI, the beat-frequency follow the form as in (1.6). The only difference in the calculated frequency terms in the beat frequency $f_b$ is then: $\Delta f_b = \frac{2v(f_{c_2} - f_{c_1})}{c}$. Since the method described in Section 3.3 concatenates beat-frequency slices in the STFT domain, the target will appear in the same STFT slice grid, as long as the difference is smaller than the STFT frequency grid resolution as: $\Delta f_b < \Delta f_{STFT}$, where $\Delta f_{STFT} = f_s/W$, and $W$ is the STFT window length as in (3.2).

### 3.4.3. LIMITATIONS

The limitations for the proposed method are, SNR system non-linearities – in the transmitter and receiver – and accumulating concatenation errors. Because of non-linearities, even a point-target will have a certain 3 dB spectral width dictated by the radar's non-linearities [5] as: $\Delta f_{\text{target}} = \Delta f_{\text{target}} + (\chi/100)\Delta f_{\text{target}}$, where $\chi$ is the non-linearity in percentage. Any concatenation errors will also result in grating-lobes and spectral width widening. The method described is not suitable for targets which have a substantially high acceleration, to the point that a target's beat-frequency changes *within* one sweep, with a value greater than that of the STFT frequency grid resolution. An example is missile tracking applications.

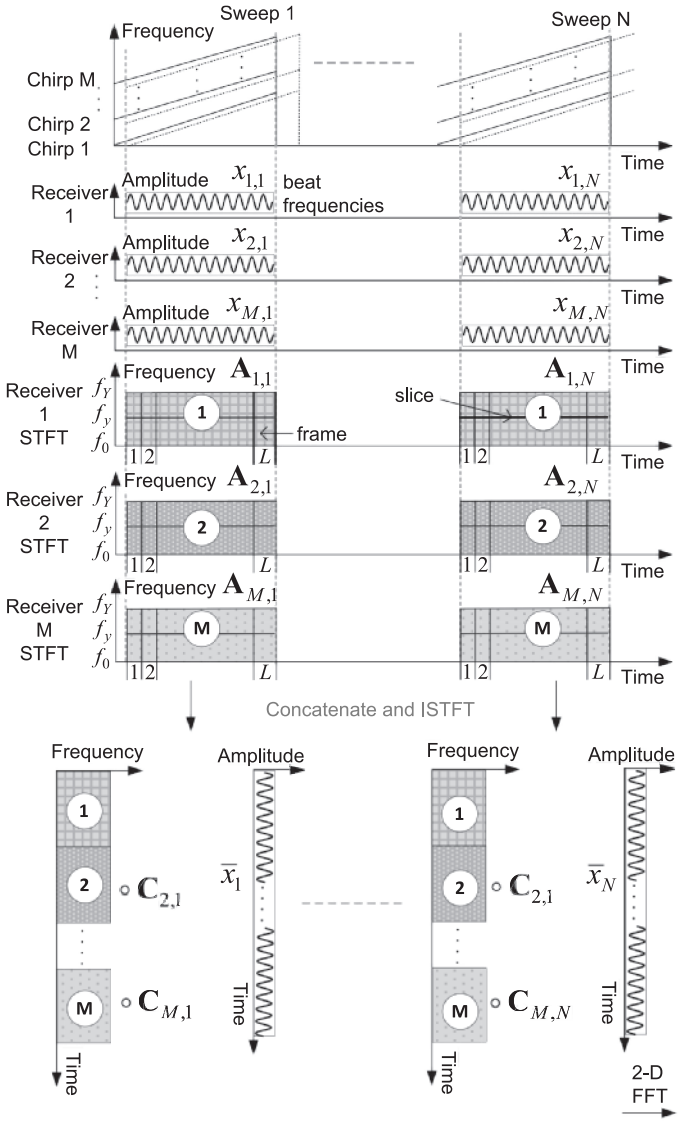



Figure 3.2: Graphical illustration of the proposed processing technique described in Section 3.3. STFT data from multiple chirps in the same sweep – handled by multiple receivers – are concatenated in the STFT domain to produce longer coherent signals for further range-Doppler processing. Note that 'slice' indicates a frequency-slice ($f_y$ for example), and 'frame' indicates a time-frame ($L$ for example). The slant frequency-time and amplitude-time representations at the bottom of the figure are a depiction of the resultant concatenated time frequency matrices and the resultant extended beat frequency signal respectively.

Table 3.3: Simulation and processing parameters.

| Simulation Parameters | | | |
|---|---|---|---|
| Target number | Range (m) | Velocity (m/s) | Wavelength $\lambda$ (m) |
| G1 | 375 | 0 | 0.0905 |
| G2 | 449 | 17.5 | |
| STFT Processing Parameters | | | |
| Window length $W$ | 7168 | | |
| Hop size $\Delta h$ | 8 | | |



## 3.5. SIMULATIONS AND EXPERIMENTAL VERIFICATION

### 3.5.1. SIMULATIONS

A simulation of the different waveform cases in Table. 3.1 and Table. 3.2 is presented in this section with the parameters in Table. 3.3 for two point-targets. White Gaussian noise is added and targets are simulated for different SNR values (20 , 13 , 0 and −40 dB). Note that the chirp frequency values in Table. 3.1 and Table. 3.2 are in Intermediate Frequency (IF) before up-conversion to S-band RF, where the 125 MHz is up-converted to an $f_c$ equal to 3.315 GHz. This $f_c$ is selected to match that of the experimental radar in Section 3.5.2. For the 20 dB SNR case, the range-Doppler results for (W.a), (W.b), (W.c), and (W.d) are presented in Fig. 3.3(a) to Fig. 3.3(d) respectively. The stable target G1 remains at zero-Doppler for all waveforms as expected. Target G2 has a velocity of 17.5 m/s, but $v_u$ for (W.a) is 11.3 m/s, causing the target to be ambiguously folded to around -5 m/s. For the remaining cases, the velocity is unambiguously estimated after increasing the PRF to 1 kHz. The range resolution degradation for both targets is apparent for case (W.c), and its maintenance in relation to (W.a) can be seen in cases (W.b), and to a large extent in (W.d). A range-cut through the range-Doppler maps for target G2 is presented in Fig. 3.4(a), (b), (c) and (d) for SNR values of 20 , 13 , 0 and −40 dB respectively, where the effects on the target response function width for all cases is presented. In Fig. 3.4(d) the SNR is dropped to −40 dB, and the proposed method suffers from concatenation errors as discussed in the limitations subsection.

The following subsections describe an experimental setup with a radar, fallowed by three experiments on different target types (stable, moving and extended-moving), and a results discussion.

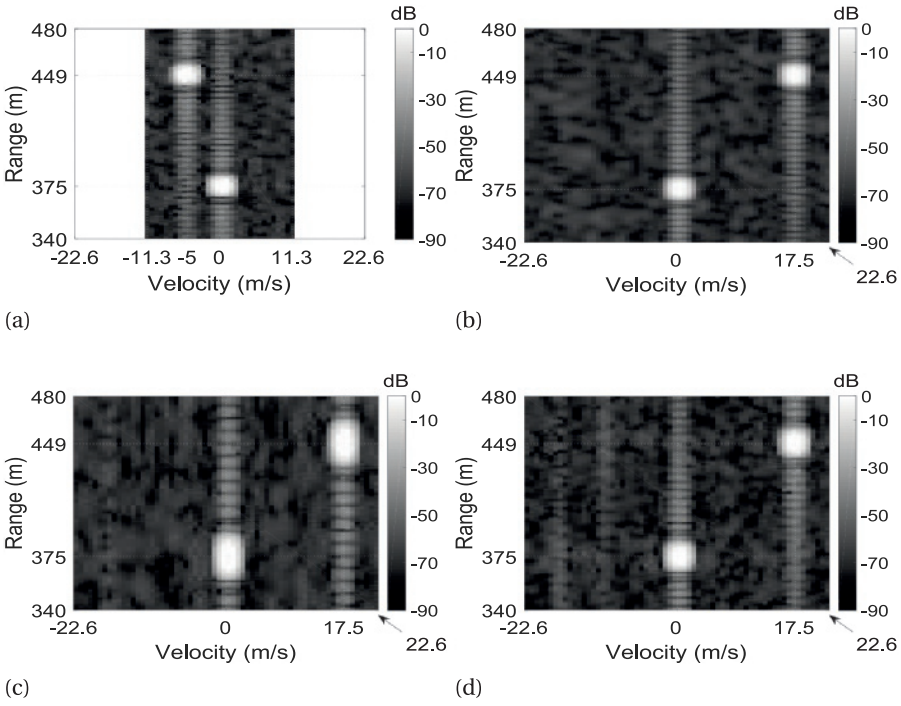



Figure 3.3: Simulation results for the different waveforms in Table 3.1 and Table 3.2. Two target are simulated, G1 and G2, with the parameters in Table. 3.3, and an SNR of 20 dB. The extension of the unambiguous Doppler-velocity interval allows for target G2's velocity of 17.5 m/s to be unambiguously estimated for waveforms (W.b), (W.c) and (W.d), as shown in (b), (c) and (d) respectively.

### 3.5.2. EXPERIMENTAL SETUP

The decoupling of the range resolution from the Doppler ambiguity interval is experimentally demonstrated using the Delft University of Technology (TU Delft) PARSAX FMCW radar [19] mounted on a building roof on campus, as shown in Fig. 3.5.

The experiment was setup to always have a reference waveform to compare against, and that being (W.a) from Table. 4.1, without causing any cross-channel interferences in the experiments. PARSAX operates in S-band with an $f_c$ of 3.315 GHz, has an IF of 125 MHz and a $B_T$ of 40 MHz. A block diagram of the experimental setup is presented in Fig.3.6. The FPGA receiver cards (R-1) and (R-2) sample the transmitted and received signals in IF after down-conversion. The cards are from Innovative Integration model X5-400M, with Virtix-5 FPGAs and equipped with two 14-bit 400 MSPs ADCc. An SSB I/Q deramping receiver architecture is implemented on the FPGAs with a 2 MHz LPF cutoff, and beat-frequency signals are transferred to a PC via PCIe interfaces connected to a PCIe-expansion back-

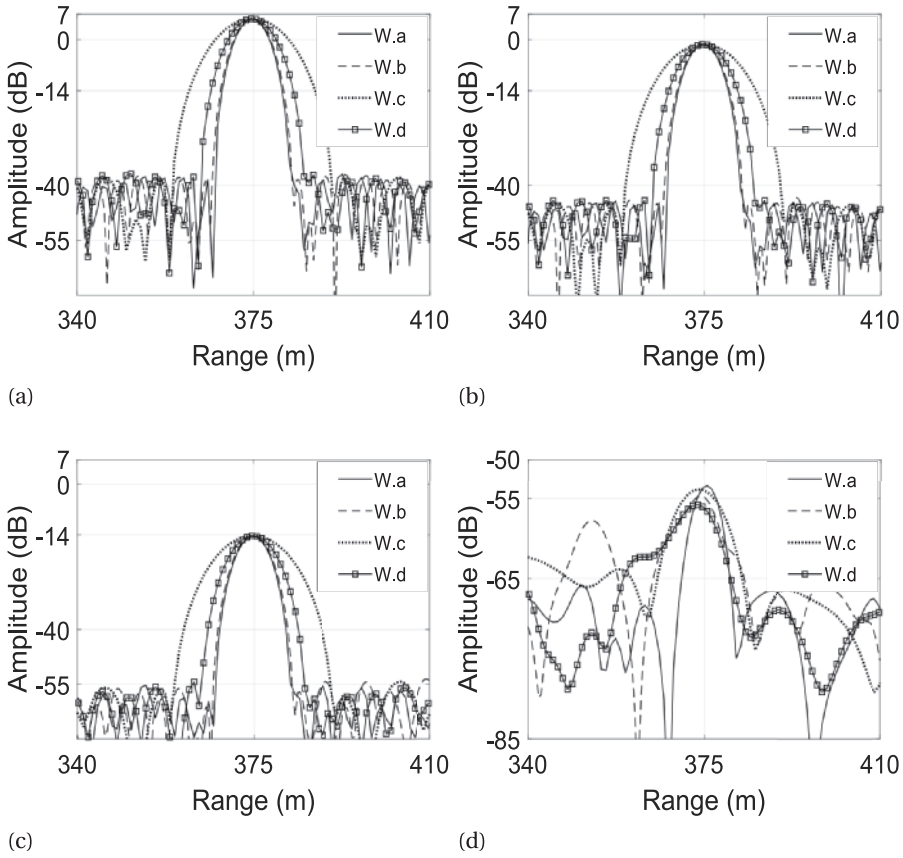



Figure 3.4: Simulation results for the different waveforms in Table 3.1 and Table 3.2. A range cut through zero-Doppler shows the response function width achieved by all waveforms for target G2. Sub-figures (a), (b), (c) and (d) are for simulations with SNR values 20 , 13 , 0 and −40 dB respectively. In (d), the SNR is −40 dB, and the proposed method suffers from concatenation errors as discussed in the limitations subsection.

plane. Waveform (W.a) is created on the AWG Ch1. A waveform resembling (W.c) is created on Ch2, but with an alternating high and low parts, as seen in Fig. 3.6. Waveforms from Ch1 and Ch2 are combined in analog and sent to the transmitter circuit. A similar splitting operation is performed by an analog splitting circuit upon reception. A depiction of the resultant combined waveforms is also presented in Fig. 3.6, where waveform (W.c) is realized using only the lower parts of the combined waveform (see horizontal shading in the figure), by extracting beat-frequency signals from both receiver boards on the PC in an alternating manner. Note that the starting phase is set to be the same for the waveform in Ch1 and the lower part of the waveform in Ch2. This allows Doppler process-

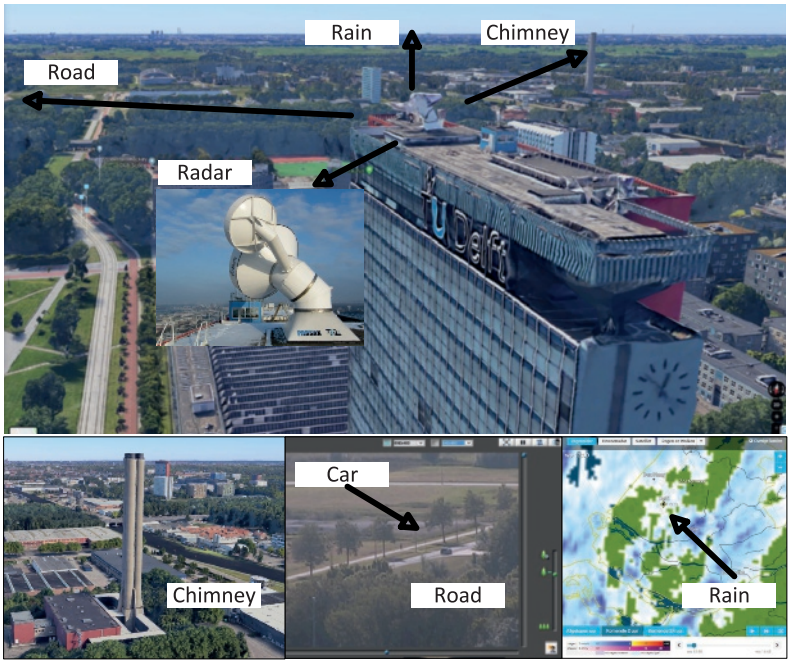



Figure 3.5: The experimental PARSAX radar mounted on the roof, and targets used for experiments in Section 3.5.2.

ing on the lower part of the combined waveforms, and thus realizing waveform (W.c). Waveform (W.d) is realized as shown by the vertical shaded area, where data is extracted from alternating receivers as well. Note the triggering at 500 Hz and 1 kHz for R-1 and R2 respectively, as shown in the figure. A photograph of the experiment setup is shown in Fig. 3.7(a). The Arbitrary Waveform Generator (AWG) and the FPGA cards are shown in Fig. 3.7(b). The IF combining and splitting circuits are shown in Fig. 3.7(c) and Fig. 3.7(d) respectively. The SNR for all the experiments was around 70 dB.

### 3.5.3. Experiments Description

- **Experiment-1: A Stable Target**: The industrial chimney shown in the bottom left corner of Fig. 3.5 is selected as a stable target in this experiment. Its height allows the radar beam to be pointed to its top part, while avoiding most of the ground clutter. A measurement was taken before and after channels calibration to observe the effect discussed in Section 3.4.1.

- **Experiment-2: A Moving Target**: A car on a traffic-quiet road on campus was selected as a moving target. A camera mounted on the radar captured its images quasi-synchronously with the radar transmission – as shown at

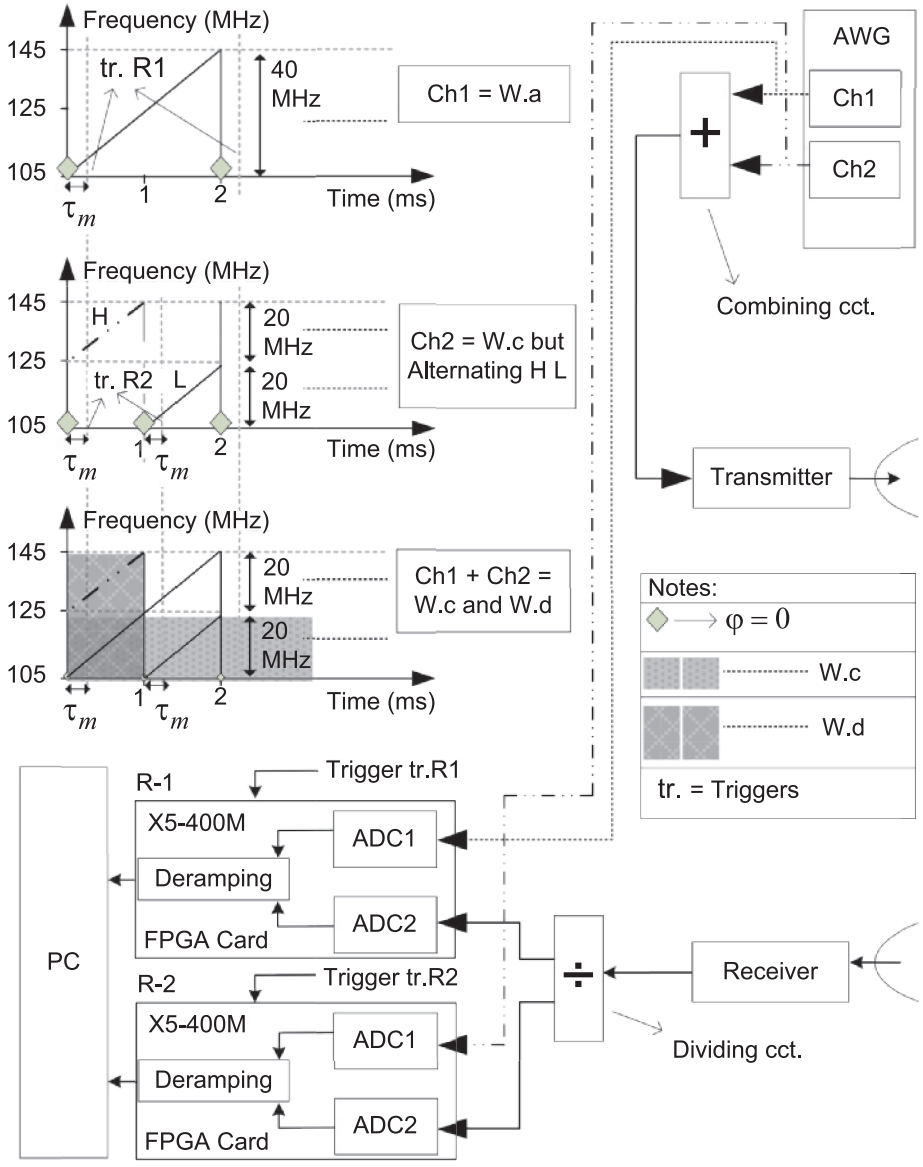



Figure 3.6: Simplified radar block diagram.

the bottom center of Fig. 3.5. The car was driving at a velocity of around 12.5 m/s (45 km/h) away from the radar. The car will be ambiguous for a 500 Hz PRF, but will be unambiguous at a PRF of 1 kHz.

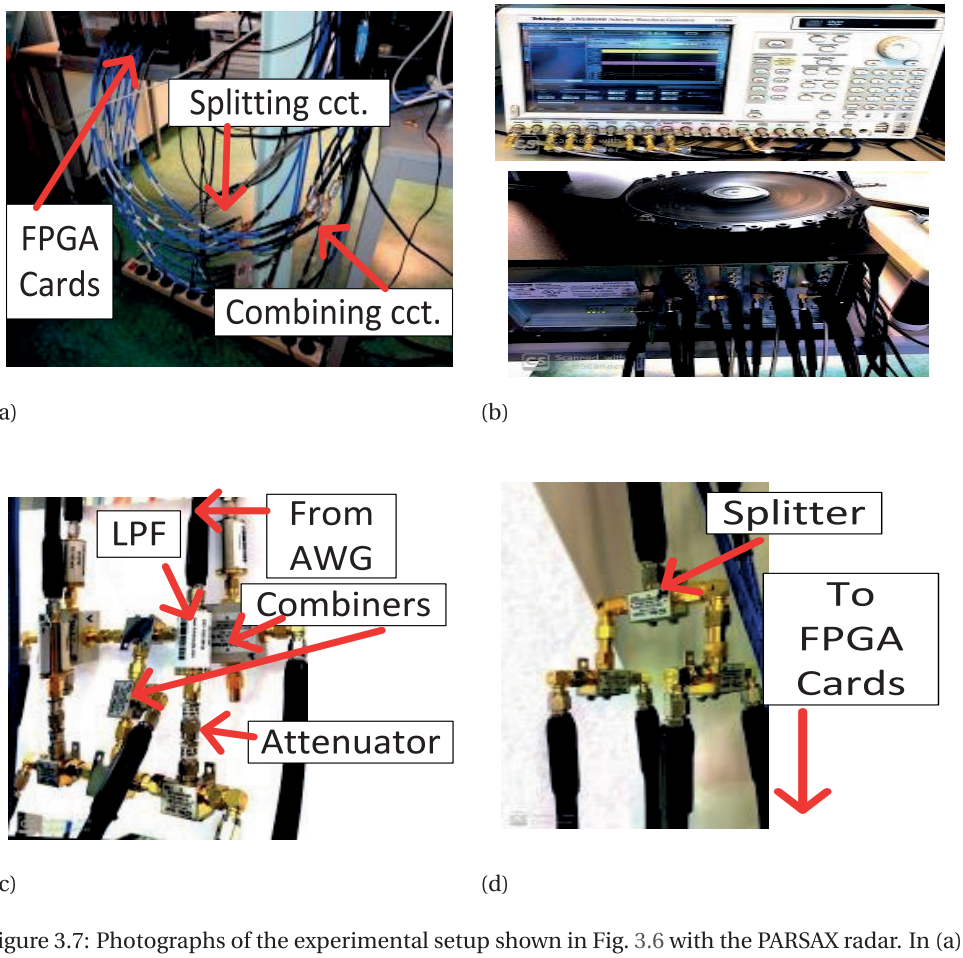



Figure 3.7: Photographs of the experimental setup shown in Fig. 3.6 with the PARSAX radar. In (a), the connections to and from the FPGA cards are shown. In (b), the AWG – where the waveforms and triggers are setup to match what is shown at the top of Fig. 3.6 – and the FPGA cards on the PCIe backplane are shown. The combining and splitting circuits are shown in (c) and (d) respectively.

- **Experiment-3: An Extended-Moving Target**: A rain and clouds formation is selected as an extended-moving target. The weather formation at the moment of experiment is shown in the bottom right corner of Fig. 3.5, where a reported rainfall rate of between 0.1 mm/h to .3 mm/h (from the color-code) is reported over Delft.

### 3.5.4. EXPERIMENTS RESULTS AND DISCUSSION

The results of the first experiment are presented in Fig.3.8.

Waveform (W.a) – as a reference – is shown in Fig.3.8(a), and (W.c) – before

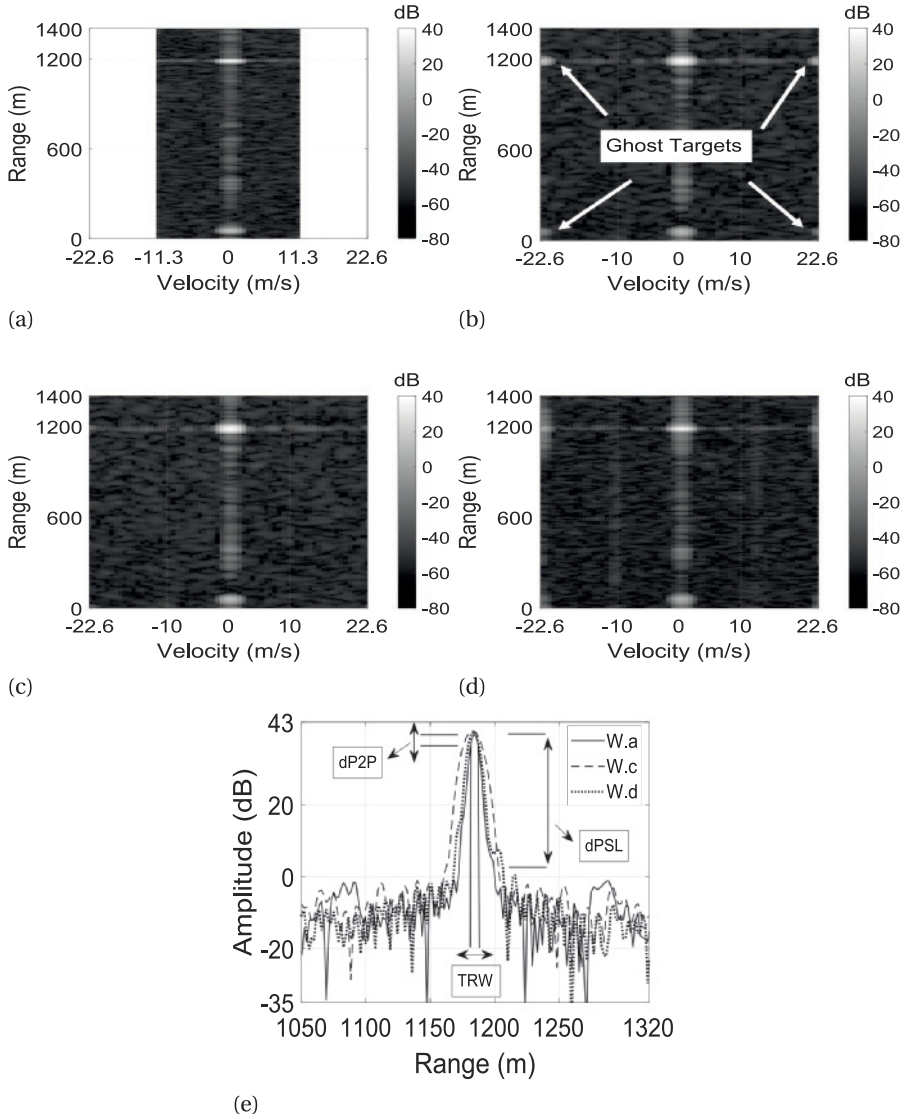



Figure 3.8: Range-Velocity maps presenting results for the chimney stable-target described in Section 4.6.2. The result for waveform (W.a) - as described in Table. 4.1 – is shown in (a), for waveform (W.c) before and after channels-calibration in (b) and (c) respectively, and for waveform (W.d) in (d). Processing artefacts due to the method's imperfections are also visible in (d). A range cut through zero-Doppler around the chimney is shown in (e), where the resolution closely matches that of (W.a), but with the Doppler ambiguity interval extension. The dP2P, dPSL and TRW parameters related to Table 3.4 are symbolically depicted in (e) to visualize their meaning.

Table 3.4: Results related to the target range cuts for the first and second experiments (Fig.3.8(e) and Fig. 3.9(d)). The difference in signal amplitude (loss) for the target peak compared to the reference waveform is represented by dP2P. For all waveforms, the peak to sidelobe is represented by dPSL and the target response function width is represented by TRW.

| | dP2P (dB) | | dPSL (dB) | | TRW (m) | |
|---|---|---|---|---|---|---|
| Experiment Number | 1 | 2 | 1 | 2 | 1 | 2 |
| (W.a) | n/a | n/a | 42 | 32 | 5 | 9 |
| (W.c) | .7 | .2 | 42 | 32 | 11 | 20 |
| (W.d) | 1 | 2.5 | 39 | 31 | 7 | 11 |



channels-calibration – in Fig.3.8(b) where ghost targets appear due to the phenomenon discussed in Section 3.4.1. Post channels-calibration, results for (W.c) are shown in Fig.3.8(c), where the ghost targets are still visible, but strongly suppressed, and the unambiguous Doppler-velocity interval extension from 11.3 m/s to 22.6 m/s is observed. An apparent resolution loss is noted for the chimney (at a range around 1200 m) for (W.c) can be seen in Fig.3.8(c), compared to (W.a) in Fig.3.8(a), and its close restoration via waveform (W.d) in Fig.3.8(d) in comparison to (W.a). A range cut across zero-Doppler for the ranges around the chimney is presented in Fig.3.8(e) where (W.d) closely restores the range-resolution compared to (W.a), but with a higher peak to sidelobe level due to method errors and imperfections as discussed in Section 3.4.3.

To relate the results to a detection scenario – regardless of probability of detection and false alarm – three parameters are measured. The difference in signal amplitude (loss compared to (W.a)) for the target peak is represented by difference peak-to-peak (dP2P), the difference in peak-to-sidelobe level is represented by (dPSL), and the target response function width at the −3 dB line is represented by (TRW). These parameters are presented in Table 3.4, and a depiction of their definition is shown in Fig.3.8(e). (W.d) compared to (W.a) suffers a 1 dB loss for dP2P, and is 3 dB worst for dPSL due to concatenation errors as discussed in Section 3.4.3. As expected, (W.d) however improved the TRW from 11 m for (W.c) to 7 m.

Similar findings can be inferred about the results for experiment-2 as presented in Fig. 3.9. The car is ambiguous at a velocity of around 10.5 m/s via (W.a) in Fig. 3.9(a), but its velocity is unambiguously estimated via (W.c) and (W.d) in Fig. 3.9(b) and Fig. 3.9(c) respectively – due to the PRF increase. The car's resolution for (w.d) is improved compared to (W.c), and a range cut through the car's Doppler-velocity bin is presented in Fig. 3.9(d). The demonstrated improvement for (w.d) is less than the theoretical expectation of it to match the performance of (w.a) is due to the processing method errors and imperfections as discussed in Section 3.4.3. The parameters in Table 3.4 show that (W.d) compared to (W.a)

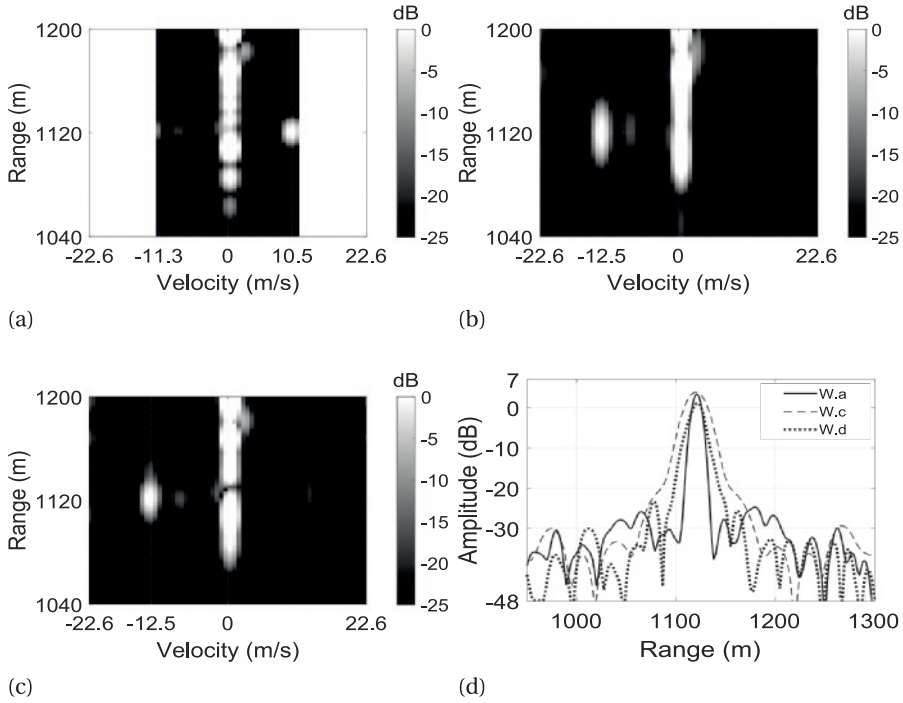



Figure 3.9: Range-Velocity maps presenting results for the car moving-target described in (Experiment-2: A Moving Target). The result for waveform (W.a) - as described in Table. 4.1 – is shown in (a), where the car is ambiguous at 10.5 m/s, but after the PRF increase for waveform (W.c) (W.d) shown in (b) and (c) respectively, the car's velocity is unambiguously estimated at -12.5 m/s receding from the radar. A resolution improvement can be observed in (c) compared to (a), as can also be seen in range cut through car's Doppler bin. The demonstrated improvement for (w.d) is less than the theoretical expectation of it to match the performance of (w.a) is due to the processing method errors and imperfections as discussed in Section 3.4.3.

suffers a 2.5 dB loss for dP2P, and is 1 dB worst in dPSL. As expected, (W.d) however improved the TRW from 20 m for (W.c) to 11 m.

The results for the weather formation of experiment-3 are presented in Fig. 3.10. The range-velocity matrix's zero-Doppler is clipped for all ranges, and it is then thresholded at -40 dB from its strongest peak. A weighted mean Doppler velocity is then calculated for each range in the range-velocity matrix as:

$$\bar{\mathbf{v}} = \frac{\sum_{i=-V_{\min}}^{V_{\max}} i\, v_i}{\sum_{i=-V_{\min}}^{V_{\max}} v_i} \tag{3.7}$$

where $V_{\min}$ and $V_{\max}$ are the minimum and maximum velocities in the unam-

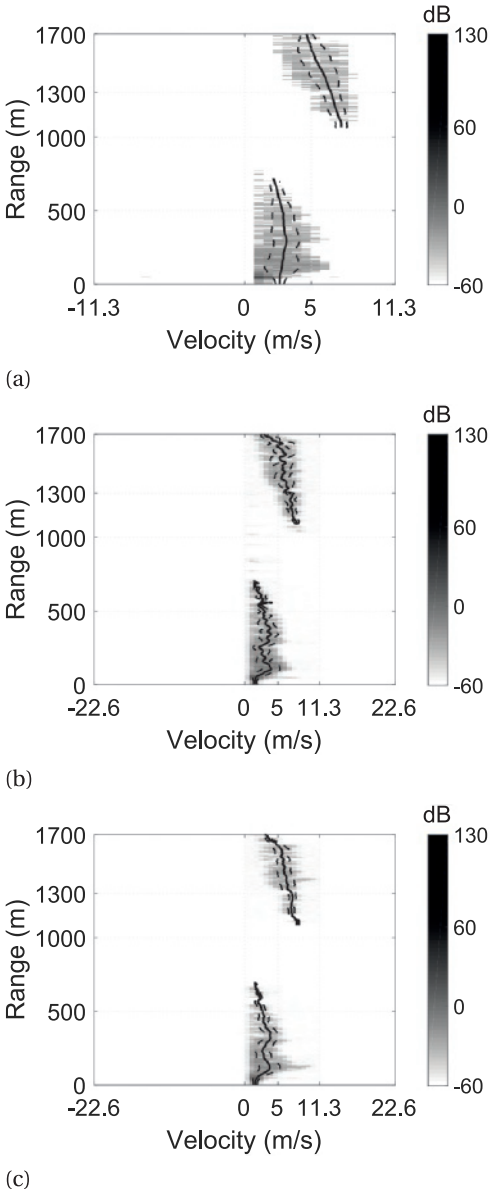



Figure 3.10: Range-Velocity maps presenting results for the extended moving target described in (Experiment-3: An Extended-Moving Target). The mean velocity is presented by the solid line, and the Doppler width (positive and negative) with the dashed lines. The result for waveform (W.a) - as described in Table. 4.1 – is shown in (a), where the weather formation is unambiguous and has a positive velocity as expected for rainfall. The formation's shape is maintained for waveforms (W.c) and (W.d) as seen in (b) and (c) respectively.

biguous velocity interval respectively, and $v$ is the Doppler power spectrum. A Doppler width is similarly calculated for each range as:

$$\sigma = \sqrt{\frac{\sum_{i=-V_{\min}}^{V_{\max}} (i-\bar{v})^2 v_i}{\sum_{i=-V_{\min}}^{V_{\max}} v_i}} \tag{3.8}$$

where $\bar{v}$ is the average velocity for that range following (3.7). The mean velocity and Doppler width are also presented in Fig. 3.10.

An average error percentage is used to quantitatively compare the mean velocity and Doppler width for the different waveforms. This error is defined as:

$$\text{error} = \frac{1}{R}\sum_{r=1}^{R}\left|\frac{x_r - \hat{x}_r}{x_r}\right| \times 100\% \tag{3.9}$$

where $R$ is the number of ranges tested for, $x_r$ is the mean velocity or the Doppler width for (W.a) as a reference, and $\hat{x}_r$ is the mean velocity or Doppler width for the waveforms compared against. The mean velocity errors for (W.c) and (W.d) are 11.9% and 12.3% respectively. The Doppler width errors for (W.c) and (W.d) are 28.8% and 18.2% respectively. Errors related to (W.c) are due to resolution loss, and errors for (W.d) are due to the method's imperfections and concatenation errors creating sidelobes around the 5 m/s velocity point, as seen in Fig. 3.10(c).

The rain and clouds' shape and velocity-spread are maintained when extending the PRF for waveforms (W.c) and (W.d) as seen in Fig. 3.10(b) and Fig. 3.10(c), compared to (W.a) in Fig. 3.10(a).

## 3.6. CONCLUSION

In this chapter we proposed a novel waveform and a processing method to decouple the Doppler ambiguity interval from the maximum operational range, range-resolution and processing gain in frequency multiplexed FMCW Radar. The method allowed the keeping of the radar's operational parameters while increasing the PRF – to unambiguously observe fast(er) moving targets, without having to trade-off these operational parameters. The solution proposed was to exploit the fact that beat-frequency signals have the same baseband frequencies, even if the transmitted and received chirps occupied different RF bands. That is in the sense that these baseband signals can be concatenated in the time-frequency domain to restore any operational parameters' losses due to the PRF increase. The price to be paid is to use more receiver channels in the radar. We

have presented the method's limitations and an implementation feasibility analysis, and have also discussed the maximum chirps' center-frequency difference. The method is verified by simulations and experiments with an FMCW radar for stable, moving and extended-moving targets. We found that the proposed method indeed alleviates the trade-off between FMCW operational parameters, and have highlighted its non-idealities in the experiments.

## REFERENCES

[1] D. E. Barrick, "FMCW radar signals and digital processing," *NOAA Technical Report ERL 283-WPL 26*, 1973.

[2] A. G. Stove, "Linear FMCW radar techniques," *IEE Proc. or Radar and Signal Process.*, 1992. [Online]. Available: http://dx.doi.org/10.1002/andp.19063240204

[3] A. Asensio López, A. Duque de Quevedo, F. Salmerón Yuste, J. Muñoz Dekamp, V. Aparicio Mequiades, V. Medel Cortés, D. García Cobeña, D. Madueño Pulido, F. Ibañez Urzaiz, and J. Gismero Menoyo, "Coherent signal processing for traffic flow measuring radar sensor," *IEEE Sensors Journal*, vol. 18, no. 12, June 2018.

[4] S. Kim and K. Lee, "Low-complexity joint extrapolation-music-based 2-d parameter estimator for vital fmcw radar," *IEEE Sensors Journal*, vol. 19, no. 6, pp. 2205–2216, March 2019.

[5] M. Jankiraman, *Design of Multi-Frequency CW Radars*. SciTech, 2007.

[6] N. B. Jones and J. D. Watson, *Digital signal processing: principles, devices, and applications*. P. Peregrinus Ltd. on behalf of the Institution of Electrical Engineers, 1990.

[7] Y. Li and S. O'Young, "Method of doubling range resolution without increasing bandwidth in FMCW radar," *Electron. Lett.*, vol. 51, no. 12, pp. 933–935, 2015.

[8] V. Trees and H. L., *Optimum Array Processing: Part IV of Detection, Estimation, and Modulation Theory*. Wiley Interscience, 2002.

[9] N. Levanon, E. Mozeson, and C. Levanon, *Radar Signals*. John Wiley, 2004.

[10] D. E. Maron, "Frequency-jumped burst waveforms with stretch processing," in *IEEE Int. Conf. on Radar*, May 1990, pp. 274–279.

[11] J. Yu and J. Krolik, "Multiband chirp synthesis for frequency-hopped FMCW radar," in *Forty-Third Asilomar Conf. on Signals, Systems and Comp.*, Nov 2009, pp. 1315–1319.

[12] V. K. Nguyen and M. D. Turley, "Bandwidth extrapolation of LFM signals for narrowband radar systems," in *Int. Conf. on Radar*, Sep. 2013, pp. 140–145.

[13] M. Pan, B. Chen, and M. Yang, "A general range-velocity processing scheme for discontinuous spectrum FMCW signal in HFSWR applications," *Int. J. of Antennas and Propagation*, 2016.

[14] S. Neemat, F. Uysal, O. Krasnov, and A. Yarovoy, "Reconfigurable range-doppler processing and range resolution improvement for fmcw radar," *IEEE Sensors Journal*, vol. 19, no. 20, pp. 9294–9303, Oct 2019.

[15] B. G. M. A. Lulu, "Phase matching of coincident pulses for range-doppler estimation of multiple targets," *IEEE Signal Processing Lett.*, vol. 26, no. 1, pp. 199–203, Jan 2019.

[16] W. L. Melvin and J. A. Scheer, *Principles of Modern Radar: Volume 3 : Radar Applications*. SciTech Publishing Inc, 2014.

[17] M. A. Richards, *Fundamentals of Radar Signal Processing, Second Edition*. McGraw-Hill, 2014.

[18] G. M. Brooker, "Understanding millimetre wave FMCW radars," in *1 st Int. Conf. on Sensing Technol., IEEE, New Zealand*, 2005, pp. 152–157.

[19] O. A. Krasnov, L. P. Ligthart, Z. Li, G. Babur, Z. Wang, and F. van der Zwan, "PARSAX: High-resolution doppler-polarimetric FMCW radar with dual-orthogonal signals," *18th Int. conf. on Microwave Radar and Wireless Communications (MIKON)*, 2010.

[20] B. Sun, M. Yeary, F. Uysal, N. Goodman, C. Fulton, and R. Rincon, "Digital radar implementation with amplitude predistortion," in *IEEE Radar Conf.*, May 2017, pp. 1691–1696.

# 4

# Reconfigurable Range-Doppler Processing and Target Response Function Width Improvement for FMCW Radar

*A reconfigurable range-Doppler processing method for FMCW radar is presented. By concatenating beat-frequency signals from more than one sweep, continuous targets' observation time is extended beyond that of a single chirp duration, leading to target response function width improvement. Multiple two-dimensional slow-time fast-time matrices can be created – in the digital domain – with the same number of elements as in the original matrix. This offers a realization of a software defined pulse/sweep repetition rate (PRF) for Range-Doppler processing. The signal concatenation is done in the Short-time Fourier Transform (STFT) domain, where beat-frequency slices are extrapolated to compensate for the observation time lost in the transient region between sweeps, then a phase correction is applied to each frequency-slice as appropriate, followed by an Inverse STFT (ISTFT). The proposed method is verified with simulation and experiments with*

This chapter is based on:
**S. Neemat**, F. Uysal, O. Krasnov, and A. Yarovoy, "Reconfigurable range-Doppler processing and range resolution improvement for FMCW radar," *IEEE Sensors Journal*, vol. 19, no. 20, pp. 9294–9303, 2019. © 2019 IEEE with permission.

*two FMCW radars for stable and moving target scenarios. We found that the method allows for target response function width improvement. It additionally allows the decoupling of the transmitted PRF from the Doppler processing PRF, permitting the facility to observe different unambiguous Doppler velocity intervals from one CPI, without compromising on the total CPI processing gain. Method limitations and shortcomings are additionally highlighted.*

## 4.1. INTRODUCTION



Deramping Frequency Modulated Continuous Wave (FMCW) radars operate by mixing a transmitted chirp signal with received returns, and filtering the resulting beat signal [1]. After deramping – for a single point-target, the time delay between the probing signal transmission and the scattered signal reception will result in a single-tone signal, known as a beat-frequency, whose frequency is proportional to that target's range. Range is therefore defined by frequency.

To elaborate, this single-tone beat-signal for that point-target is observed during a certain time interval within the radar's sweep time. Classical signal compression is then done by converting this single-tone signal to the spectral domain. As a result, the point-target is represented as a sinc function shaped spectral line which has a bandwidth that is inversely proportional to the duration of the signal observation time interval. The conversion of this compressed signal from the spectral domain to the range domain (to produce a range-profile) is done by rescaling the spectrum grid to a range grid using a scaling equation. As a result, the sinc function shaped spectral line – related to that point-target – is converted into what can be called a point target response function (analogous to the impulse response function in pulse-compression radar). In classical FMCW processing, the width of this response function after scaling is inversely proportional to the transmitted bandwidth during the observation time interval. This width represents the actual radar range resolution, which is directly proportional to the target's range localization accuracy. The range-resolution granularity defines the width of what is known as radar's range bins. A radar's range-resolution is a criterion by which the radar's ability to separate targets that are close in range is evaluated. The Fourier Transform (FT) is typically used to convert beat signals to the spectral domain. The FT frequency spectral width is defined by the signal observation time, or by the combination of the number of observed samples and the sampling frequency [2].

Legacy computer architectures used in FMCW radars are highly compatible with the FT for its reduced computational requirements and predictable latency. Target velocities are calculated from Doppler processing - also typically using the FT - across radar's range bins from multiple sweeps [3]. The radar Pulse/sweep Repetition Frequency (PRF) is therefore the Doppler sampling frequency. The

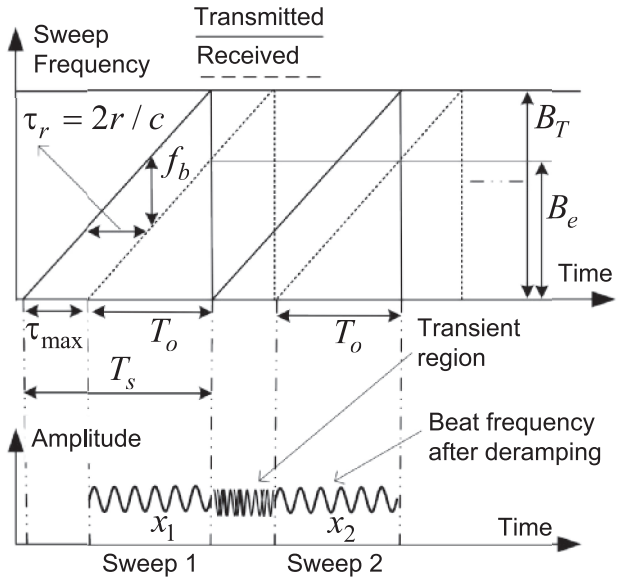



Figure 4.1: Deramping operational overview, highlighting beat-frequency signals and the transient region. Here, $\tau_{\max}$ is the maximum transient time, and is dependant on the desired radar maximum range.

time spent to gather multiple sweeps for range and Doppler processing is typically known as a Coherent Processing Interval (CPI). Sweeps in a CPI are typically arranged in a fast-time slow-time matrix, where fast-time is the time within a sweep, and slow-time is the time across multiple sweeps. The total processing gain in a CPI is contributed to the matrix's 2-D FT processing gain. It is typical for radars to transmit at different PRF values, across multiple CPIs to unambiguously determine targets' ranges and velocities [4] or to provide different input to radar classification algorithms. In FMCW, the observation time is limited by what is known in the literature as the "transient" or "fly-back" region (dead-time) between frequency sweeps [5]. The received signal is typically only sampled after the transient region, which causes discontinuities in received beat-frequencies (demarking the end of a received sweep), and puts a limit on the possibility of having a continuous observation time. The transient region is shown in Fig.4.1.

The problems this chapter addresses are:

1. The existence of the transient regions in received beat-frequency sweeps in a CPI, in the sense that its existence does not allow for longer targets observations. If a method were to be developed to extend the observation time by coherently concatenating/processing beat-frequencies from more

than one sweep at a time, that would result in a target response function width improvement.

2. With such a concatenation method, there would be a tool to decouple the Doppler processing PRF from the transmitted signal PRF. This is in the sense that it becomes possible to – in parallel and from one CPI – create different lengths fast-time slow-time matrices, without compromising on the total processing gain in any of the created matrices. That would therefore allow the implementation of PRF velocity disambiguation techniques, or provide different inputs to target classification algorithms for example, from a single CPI.



3. If a target response function width improvement is possible, would that translate to range resolution improvement?

4. Is the same analogy for improving the target response function width by concatenating multiple sweeps in time be used for when concatenating frequency multiplexed chirps within one sweep? (in the previous chapter two chirps in one sweep were concatenated. What if more chirps were to be stacked in the sweep and concatenated?).

The solution proposed in this chapter is to concatenate beat-frequency slices in the Short-time Fourier Transform (STFT) domain, by applying a phase correction to each frequency slice as appropriate, followed by an Inverse STFT (ISTFT). A second optional realization of this solution is to first extrapolate beat-frequency slices, to compensate for the observation time lost in the transient region, then concatenate the slices as aforementioned.

Previous work on the topic is scarce, in the sense that a method does not exist where such a method:

- is applicable to deramping processing (as opposed to matched filtering),
- only relies on the FT (as opposed to more computationally intensive or iterative frequency estimation algorithms),
- does not improve the range resolution by stitches sweeps from multiple discontinuous bands, and therefore technically requiring more overall system bandwidth,
- does not require target detection as a prerequisite,
- is applicable to extended-targets.

Techniques that work by coherently processing data post range-Doppler may not be suitable for wide-band systems where range migration causes targets' energy to be spread across multiple range-Doppler bins. An interesting method for doubling the range resolution refinement without increasing the bandwidth can be found in [6]. Their method is restricted to the radar's intermediate frequency being an integer multiple of the transmitted bandwidth, and to being operable only with a real Double-Side-Band (DSB) deramping receiver. Bandwidth extrapolation techniques like in [7], [8] and [9] use prediction techniques to synthetically extrapolate the data to improve the range resolution. There usually is a practical limit to how much will extrapolated data really represent target returns as associated with their Radar-Cross-Section (RCS). The work in [10] uses waveform diversity to decouple the Doppler cycle from the PRF, but does not address target response function width nor range resolution improvement.



The difference from previous techniques and the novelty in this work is highlighted in:

1. The first ever method for deramping FMCW radar multiple sweeps coherent concatenation in the STFT domain.

2. The method allows for target response function width improvement without transmitting additional bandwidth.

3. The method offers the ability to - in parallel - generate different size fast-time slow-time matrices, and decouples the transmitted PRF from the Doppler processing PRF, without compromising on the total CPI processing gain. This offers the ability to observer different unambiguous Doppler velocity intervals in one CPI.

4. The method does not require target(s) detection as a prerequisite.

## 4.2. THEORY

### 4.2.1. FMCW RADAR BACKGROUND

Refer to Section 1.3 for related FMCW radar background and equations. The deramping transient region is shown in Fig.4.1.

### 4.2.2. BEAT FREQUENCY SPECTRAL WIDTH AND PROCESSING GAIN IMPROVEMENT

It is well known from FT signal processing that for a signal like:

$$S_r(t) = A_0 \text{rec}\,(t/T_o)\cos(2\pi f_b t + \varphi_0) \tag{4.1}$$

the FT will result in an impulse function - assuming that $f_b$ is on a frequency grid point - and a sinc function, and that the frequency spectrum resolution is defined by the 3 dB width of that sinc function centered at $f_b$ [4]. The 3 dB width of a sinc function in the frequency domain is inversely proportional to that signal's integration time $T_e$ [2] as:

$$\Delta f = \frac{1}{T_e}. \tag{4.2}$$

This concept is depicted in Fig. 4.2. The method proposed in Section 4.3 increases the integration time in (4.2), as depicted in Fig.4.2, by coherently concatenating $d$ sweeps, and therefore improving the sinc function spectral width, which can be expressed as:



$$\Delta f_d = \frac{1}{T_o d} \tag{4.3}$$

where $d$ is the concatenation factor as well as the spectral width improvement factor, and noting that in classical processing $d = 1$.

The range processing gain in FMCW radar is known as the compression gain or the time-bandwidth product (BT product) [11]. From (1.15), the improvement in the processing gain after sweeps concatenation can be expressed as:

$$G_r = B_e T_o d. \tag{4.4}$$

### 4.2.3. RECONFIGURABLE RANGE-DOPPLER PROCESSING

In classical FMCW radar processing, a CPI of a certain duration is selected as a system parameter. Received sweeps in the CPI are typically stored in a 2-D matrix (commonly named the fast-time slow-time matrix), after which, a 2-D FT is performed on that matrix to produce range-Doppler maps. The total processing gain in the CPI is the range compression gain (BT product) multiplied by the number of sweeps in the CPI (1.16). Operationally, to maintain this processing gain, the total number of samples stored in a CPI is typically kept the same when changing the PRF, and a tradeoff is made between the range resolution and the unambiguous Doppler velocity interval. This is in the sense that more sweeps of shorter durations are received in High PRF (HPRF) mode, and less sweeps of longer duration in low PRF mode. If the radar operates in a HPRF mode, different unambiguous Doppler velocity intervals can be created by simply discarding every other sweep(s) in the fast-time slow-time matrix, but that would result in a total processing gain loss. The unambiguous velocity interval is related to the PRF as defined in (1.11).

We propose the creation of different lengths fast-time slow-time matrices by operating the radar in a HPRF mode, and concatenating sweeps for different concatenation factor values ($d$) in parallel.

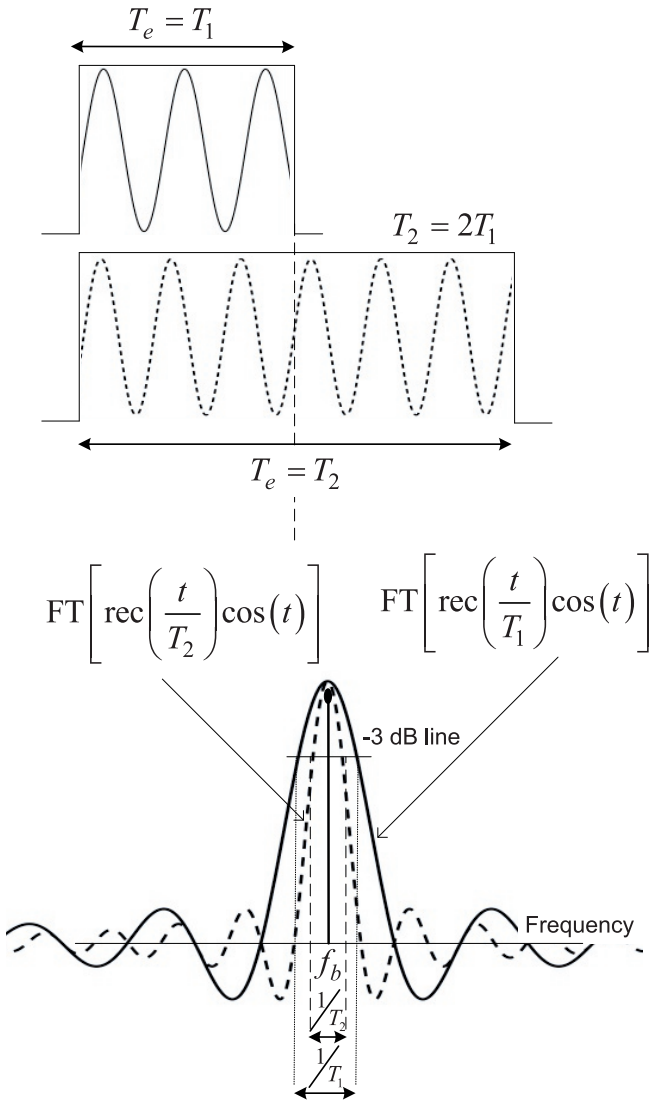



Figure 4.2: Simplified sinc function spectral bandwidth illustration for signals with different durations. When coherently concatenating two sweeps, the sinc function 3 dB width will reduce.

This will allow the creation of different 'processing' PRF values from the operational HPRF, while maintaining the total processing gain. The created different processing PRF values will allow for the evaluation of multiple unambiguous Doppler velocity intervals from the same CPI. This reconfigurable processing concept is illustrated in Fig. 4.3, where as the number of concatenated sweeps increase, the unambiguous Doppler velocity intervals is reduced, but all samples

Table 4.1: Flexible CPI processing gain vs Maximum Unambiguous Doppler Velocity tradeoff example. Assumptions are: Transmitted PRF = 2kHz, $T_s$ = 500 $\mu$s, $T_o$ = 400 $\mu$s, $N$ = 8 sweeps in the CPI, CPI length = 4000 $\mu$s, $B_e$ = 32 MHz, wavelength $\lambda$ = 0.0905 m. Note that when $d$ = 1, this is the case for classical processing.

| Concatenation Factor $d$ | Range Processing Gain | N CPI Doppler Processing Gain | Total CPI Processing Gain = Range Processing Gain x N CPI Doppler Processing Gain | PRF (kHz) | Maximum Unambiguous Doppler Velocity (m/s) |
|---|---|---|---|---|---|
| 1 | 12800 | 8 | 102400 | 2 | 45.25 |
| 2 | 25600 | 4 | 102400 | 1 | 22.62 |
| 4 | 51200 | 2 | 102400 | 0.5 | 11.31 |
| 8 | 102400 | 1 | 102400 | N/A | N/A. Only a range profile is available. |



are still used and therefore the processing gain is maintained. The processing PRF can be expressed as:

$$\text{PRF}_d = \frac{\text{PRF}}{d}. \tag{4.5}$$

A calculated example is furthermore given in Table 4.1. It can be seen in the example that when $d = 2$ for instance, the processing PRF becomes 1 kHz, which is half the transmitted PRF of 2 kHz, while still maintaining the same total processing gain of 102400 in both cases because of not discarding any samples.

The value of $d$ should become a radar system parameter. We will show in Section 4.3 that different size slow-time fast-time matrices can be created in parallel from a single CPI, by processing for different values of $d$. Noting that, practically, the maximum concatenation factor $d$ will be bound by errors and limitations as discussed in Section 4.5.4. The maximum concatenation factor $d$ which we have tested for is 8 in the experiment in Section 4.6.4.

## 4.3. METHOD: SWEEPS CONCATENATION WITH TRANSIENT REGION EXTRAPOLATION

In the time-frequency domain, beat-frequency slices are first extrapolated to cover the transient region between sweeps, and then coherently concatenated using a phase-shift operation, as depicted in Fig. 4.4. The steps are:

1. Store digitally sampled beat-frequencies for sweeps from the output of the deramping receiver. A sweep can be expressed as $x_n[k]$, where $n$ is the sweep number, and $1 \leq n \leq N$. The number of sweeps in a conventional Coherent Processing Interval (CPI) is $N$, and $N \in \mathbb{Z}$, and $\mathbb{Z}$ denotes the set

of all integers. The time domain sample index in a sweep is $k$ , where $k = 1,...,K$, and $K = f_s T_o$. The sampling frequency is $f_s$.

2. Take sweeps to the time-frequency domain by applying an STFT, where a sweep can be expressed in matrix form as

$$\mathbf{S}_n[l,y] = \left[ \sum_{q=-\frac{W}{2}}^{\frac{W}{2}-1} w[q]x[q-l\Delta h]e^{-i2\pi qy/W} \right]_{Y\times L} \tag{4.6}$$

with $Y$ rows and $L$ columns, where $l$ is the STFT frame index, $l = 1,...,L$, and $L = 1+\lfloor (k-W)/\Delta h)\rfloor$. The analysis window length is $W$. The STFT hop size is $\Delta h$, and $\lfloor\cdot\rfloor$ denotes the floor operation. The frequency-slice index in the STFT frequency grid is $y$, where $y = 0,...,Y$, and $Y$ is the maximum beat-frequency index. The analysis window (for instance, Hamming) is $w$.

3. Using the Burg algorithm [15], estimate in-phase and quadrature (IQ) Linear Prediction (LP) coefficients $[\mathbf{a}]_{Y\times o}$ in matrix form for amplitudes of each frequency-slice $y$ in each of the $N$ sweeps. The prediction filter order is $o$, and $o$ should be between 2 and $\lfloor L/3\rfloor$.

4. Extrapolate $R$ frames for each $y$ frequency-slice, for each of the $N$ sweeps. Note that $R = 1 + \left\lfloor ((\tau_r f_s) - W) \,/\, \Delta h) \right\rfloor$, and the extrapolated frames can be written as

$$\mathbf{A}_y[r] = \left[ \sum_{i=1}^{o} \mathbf{a}[y,i]\, \mathbf{S}[y,i]_{y,i} \right]_{1\times R} \tag{4.7}$$

where $r = 1,...,R$. After extrapolating for all $y$ frequency-slices, an extrapolated sweep can then be written as

$$\mathbf{E}_n = \left[ \begin{array}{cc} \mathbf{A}_n & \mathbf{S}_n \end{array} \right]_{Y\times \bar{L}} \tag{4.8}$$

where $\bar{L} = L + R$. Note that the purpose of the extrapolation is to restore any SNR loss due to the transient region. The phase continuity after extrapolation will be handled in the following steps. Note that If the radar is to operate with long delays between sweeps, steps 3 and 4 can be skipped because of the extrapolation quality degradation.

5. Select a concatenation factor $d$ which indicates the desired number of sweeps to be concatenated, where $d \in \mathbb{Z}$, and $\mathbb{Z}$ denotes the set of all integers. Noting that $d = N/\overline{N}$. The number of concatenated sweeps in the CPI is $\overline{N}$, and $d = 2,...,N$ with the constraint that $(N/d) \in \mathbb{Z}$.

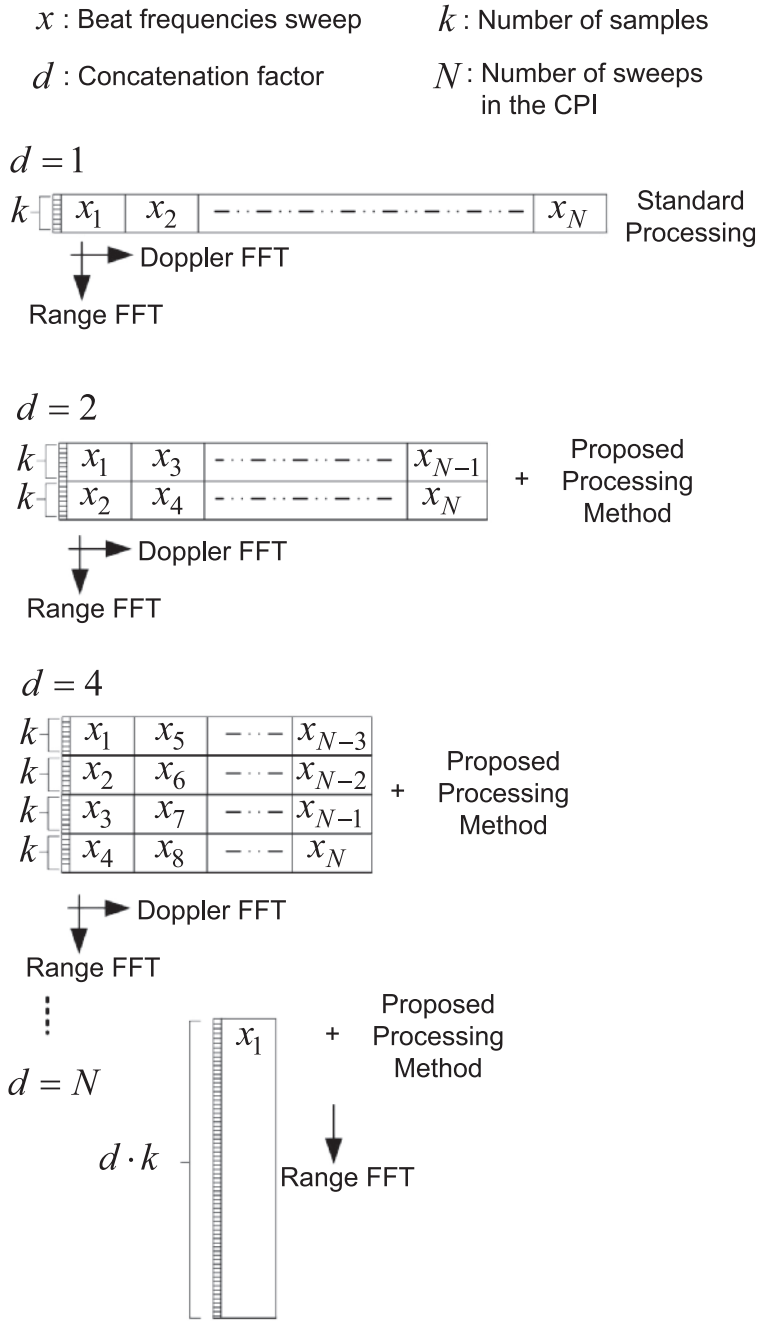



Figure 4.3: Reconfigurable range-Doppler processing permutations of fast-time slow-time received sweeps. The total CPI processing gain is maintained. Depending on the number of sweeps concatenated, there is a tradeoff between the target response function width and the maximum unambiguous Doppler velocity interval. Note that for realistic small values of N, and when $d = N$, only a range profile is provided because the matrix is then one dimensional.

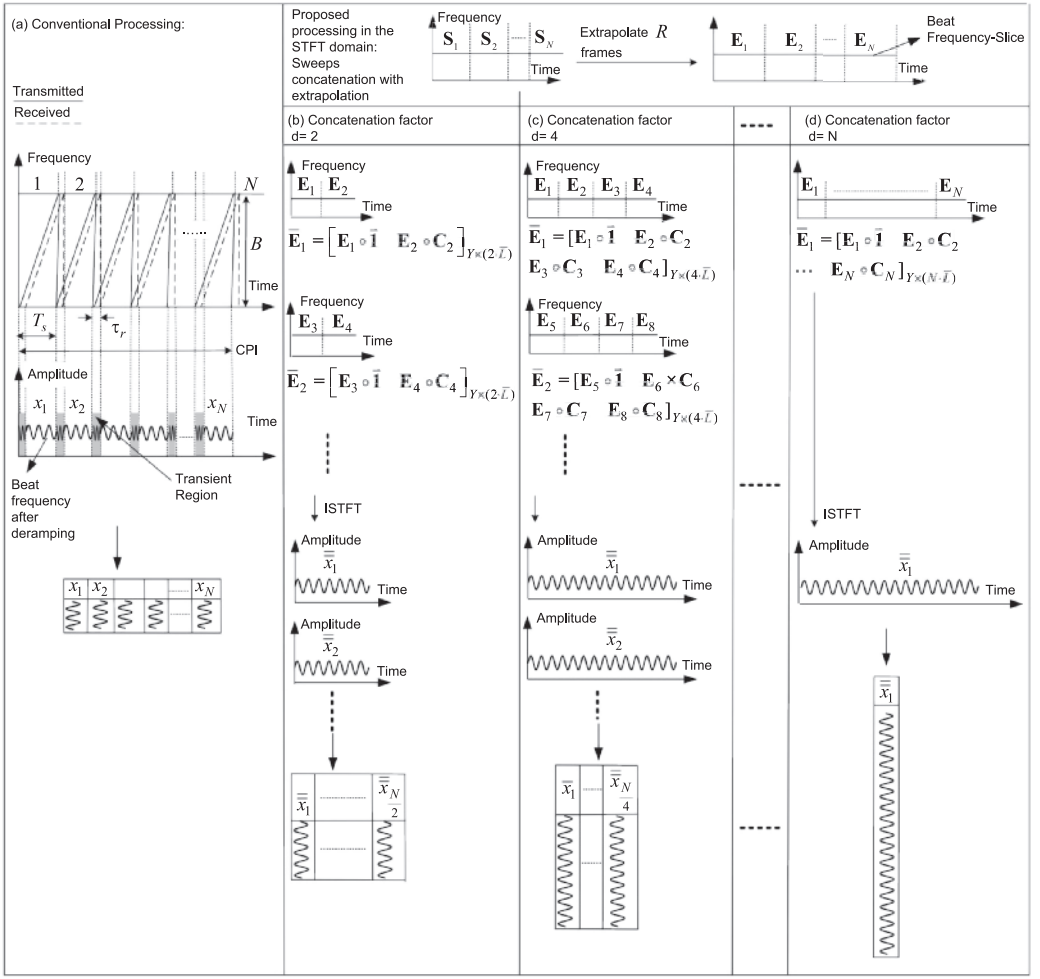



Figure 4.4: Examples for reconfigurable CPI processing with transient region frames extrapolation. Different values of the concatenation factor $d$ are shown for sweep concatenation.

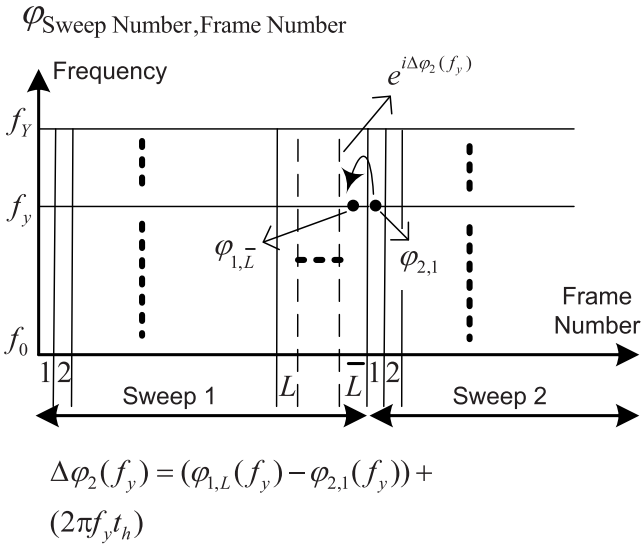



Figure 4.5: Depiction of phase matching in the STFT domain after transient region frames extrapolation, as discussed is Section 4.3.

6. Form concatenated sweeps in matrix-form in the STFT domain as

$$\bar{\mathbf{E}}_m = [\ \mathbf{E}_{dm-(d-1)} \quad \mathbf{E}_{dm-(d-2)} \circ \mathbf{C}_{dm-(d-2)} \quad \cdots \quad \mathbf{E}_{dm} \circ \mathbf{C}_{dm}]_{Y \times (d \cdot L)} \tag{4.9}$$

where $m$ is the sweep number after concatenation, $m = 1,...,\overline{N}$, and the $\mathbf{E}$ matrices are of the form as in (4.8), '$\circ$' denotes the Hadamard product. At this point, there is still a phase discontinuity. To solve this, the phase matching term $\mathbf{C}$ has $L$ identical columns, and is defined as

$$\mathbf{C}_i = \begin{bmatrix} e^{i\Delta\varphi_i(f_0)} & \cdots & e^{i\Delta\varphi_i(f_0)} \\ \vdots & \vdots & \vdots \\ e^{i\Delta\varphi_i(f_Y)} & \cdots & e^{i\Delta\varphi_i(f_Y)} \end{bmatrix}_{Y \times L} \tag{4.10}$$

where

$$\Delta\varphi_i(f_y) = (\varphi_{i-1,\bar{L}}(f_y) - \varphi_{i,1}(f_y)) + (2\pi f_y t_h). \tag{4.11}$$

Here $f_y$ is the frequency value at frequency-slice index $y$, and the hop time $t_h = \Delta h / f_s$. The phase matching is illustrated in Fig. 4.5.

7. Perform an Inverse STFT (ISTFT) to form the new concatenated sweeps as

$$\bar{\bar{x}}_m = \text{ISTFT}(\bar{\mathbf{E}}_m). \tag{4.12}$$

8. Perform these steps in parallel for different values of $d$ to create multiple fast-time slow-time matrices from the same CPI. If no transient region extrapolation is desired, sweeps can be directly concatenated, where the process then begins at step 5.

## 4.4. SIMULATIONS FOR SWEEPS CONCATENATION FOR DIFFERENT VALUES OF $d$

To evaluate the reconfigurable range-Doppler and target response function width improvement method, a simulation and processing scenario for five point-targets is setup using the parameters in Table 4.2 and illustrated in Fig. 4.6.



On the one hand, the simulation compares 2-D FT results for the standard case with a PRF of 1 kHz (Fig. 4.6(a)), the creation of a second Doppler velocity ambiguity interval by manually discarding every other sweep from the CPI resulting in a Doppler sampling PRF of 500 Hz (Fig. 4.6(b)), and the creation of a third interval by manually using one sweep from every four sweeps from the CPI resulting in a Doppler sampling PRF of 250 Hz (Fig. 4.6(c)). On the other hand this is compared with the proposed processing with $d = 2$ (Fig. 4.6(d)) and $d = 4$ (Fig. 4.6(e)) to create the same velocity ambiguity intervals, but with improving the target response function width. Hamming windowing is used for both the range and Doppler processing. The simulation results are presented in Fig. 4.7. Target G1 wraps around the unambiguous velocity intervals as expected, as it can be seen at a velocity of around -9 m/s in Fig. 4.7(b) and (d), and at around 3 m/s in Fig. 4.7(c) and (e). Targets G2 and G3 have a velocity which is always within the ambiguity intervals, and therefore do not fold. Targets G2 and G3 are only distinguishable when processing with $d = 4$, because of the improved target response function width,

as seen in Fig. 4.7(e). This is also the case for targets G4 and G5, which are at zero velocity.

## 4.5. POSSIBLE RANGE-RESOLUTION IMPROVEMENT INVESTIGATION

### 4.5.1. POSSIBLE RANGE-RESOLUTION IMPROVEMENT FOR DIFFERENT VALUES OF $d$

Referring back to the discussion in the introduction, this section investigates if the improvements in the target response function width (due to the sinc function width improvement in the spectral domain when increasing the beat frequency integration time from more than one sweep) could result in range resolution improvement. The work in [6] proposes a method to double the range

Table 4.2: Simulation setup parameters.

| Simulated Targets' Specifications | | |
|---|---|---|
| Target Number | Range (m) | Velocity (m/s) |
| G1 | 348.28 | 13.85 |
| G2 | 362.98 | 1.38 |
| G3 | 364.45 | 1.38 |
| G4 | 379.14 | 0 |
| G5 | 380.61 | 0 |
| CPI Parameters | | |
| Parameter | Value | Unit |
| Waveform | Linear sawtooth | n/a |
| PRF | 1 | KHz |
| $T_s$ | 1000 | $\mu$s |
| $T_o$ | 950 | $\mu$s |
| N CPI | 64 | sweeps |
| CPI length | 0.064 | s |
| $B_e$ | 49.5 | MHz |
| wavelength $\lambda$ | 0.0905 | m |
| Extrapolation Parameters | | |
| Parameter | Value | Unit |
| Window length $W$ | 8192 | samples |
| Hop size $\Delta h$ | 8 | samples |
| Extrapolation filter order $o$ | 120 | coefficients |
| Flexible Range-Doppler Processing | | |
| Concatenation Factor | Maximum unambiguous Doppler Velocity $v_u$ (m/s) | |
| $d = 1$ (standard) | $\pm$ 22.1 | |
| $d = 2$ | $\pm$ 11 | |
| $d = 4$ | $\pm$ 5.5 | |

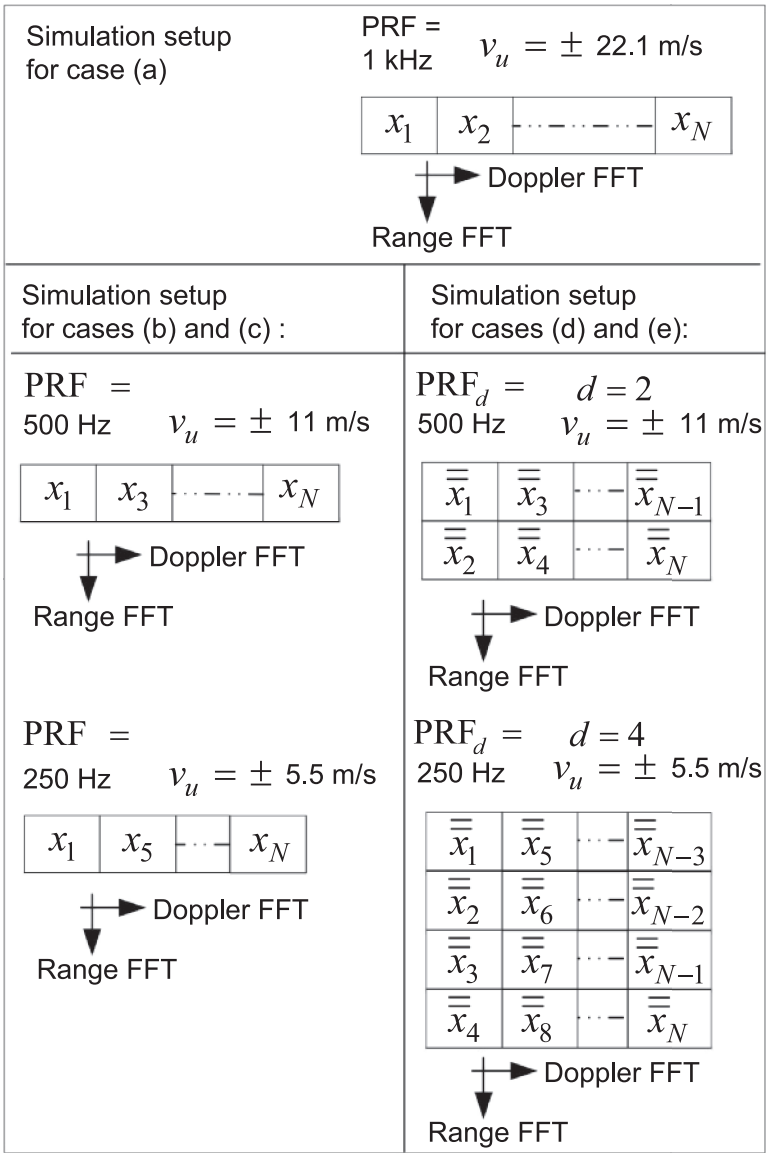



Figure 4.6: Simulation setup for the results presented in Fig. 4.7, where cases (a) to (e) correspond to Fig. 4.7 sub-figure labels.

resolution refinement without increasing the transmitted bandwidth, but is restricted to the chirp center-frequency being an integer multiple of the total transmitted bandwidth, and without improvement to the Doppler ambiguity interval. In [13], we overestimated the method's ability to improve range-resolution with-

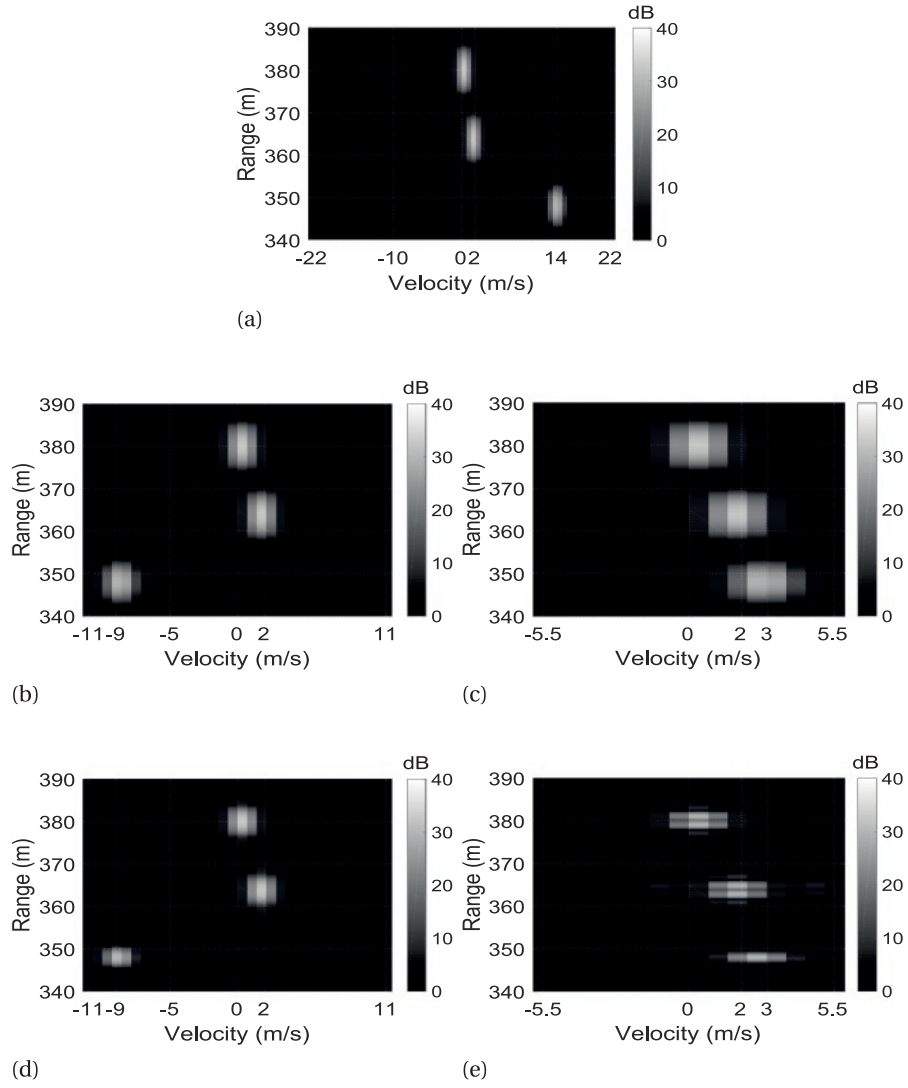



Figure 4.7: Simulation Results for the scenario setup using the parameters in Table 4.2 and illustrated in Fig. 4.6 with five targets. (a) Standard processing, PRF = 1 kHz. (b) Dropped sweeps to create PRF = 500 Hz. (c) Dropped sweeps to create PRF = 250 Hz. (d) Proposed processing with $d = 2$. (e) Proposed processing with $d = 4$ where the target's range response function width is significantly improved and targets G2, G3 and G4, G5 are resolvable as expected. Processing artefacts due to the method's imperfections are also visible in (e).

out solid proof. In this subsection, we present the hypothesis of possible range-resolution improvement, and leave the door open for future research. An experiment around this issue will be presented in Section 4.6.4 where the resolution is improved in terms of targets' resolvability in relation with the transmitted band-

width, but with range estimation errors.

From (1.7), (1.8) and (4.2), for two targets $r_1$ and $r_2$ to be separable in the frequency domain, they need to meet the requirement:

$$\frac{2B_e r_1}{T_o c} - \frac{2B_e r_2}{T_o c} \geq \frac{1}{T_e} \tag{4.13}$$

which can be simplified to:

$$r_1 - r_2 = \Delta R = \frac{c}{\left(\frac{2B_e}{T_o}\right) T_e}. \tag{4.14}$$

It should be noted that in typical FMCW processing, $T_o = T_e$, yielding

$$\Delta R = \frac{c}{2B_e} \tag{4.15}$$

which is the classical form of FMCW range resolution. But as seen in (4.14), if there were a way to increase the integration time, the hypothesis is that the range-resolution can be improved when concatenation $d$ multiple sweeps as follows:

$$\Delta R_d = \frac{c}{\left(\frac{2B_e}{T_o}\right) d T_e} = \frac{c}{2B_e d} \tag{4.16}$$

Noting that, practically, the maximum concatenation factor $d$ will be bound by errors and limitations as discussed in Section 4.5.4. The maximum concatenation factor $d$ which we have tested for is 8 in the experiment in Section 4.6.4.

### 4.5.2. POSSIBLE RANGE-RESOLUTION IMPROVEMENT FOR DIFFERENT VALUES OF $M$

In Chapter 3, we demonstrated the concatenating of two chirps from the same sweep/PRI using two receivers. But, more chirps and more receiver channels could be be used to produce even more samples. This concept in presented in Table 4.3, which follows the same structure of Table 3.1 and Table 3.2. If the chirp sampling frequency is $f_s$, the spectral width improvement can be expressed in number of samples instead of time, as in (4.3), since the extra samples come from the same sweep/PRI. Assuming the time domain sample index in a chirp is $k$, where $k = 1,...,K$, and $K = f_s T_o$. The spectral width improvement can thus be expressed as:

$$\Delta f_M = \frac{f_s}{kM} \tag{4.17}$$

where $M$ is the number of frequency chirps multiplexed in a single sweep and is therefore the number of receivers in the system, as shown in Table 4.3.

Following the hypothesis in (4.16) where the improvement is expressed in number of concatenated sweeps $d$, a similar hypothesis is presented for possible range-resolution improvement, to leave the door open for future research. The hypothesis is that the range-resolution can be improved when concatenation $M$ chirps from one sweep as follows:

$$\Delta R_M = \frac{c}{\left(\frac{2B_e f_s}{k}\right)\frac{Mk}{f_s}} = \frac{c}{2B_e M}. \tag{4.18}$$

Note that the maximum number of chirps which can be stacked in a single sweep/PRI – assuming the radar receiver channels implement a deramping Single-Sideband (SSB) I/Q architecture with the ability to reject negative frequencies – is:

$$M_{\max} = \left\lfloor \frac{B_T - B_c}{f_m} \right\rfloor + 1 \tag{4.19}$$

where the SSB's LPF cutoff-frequency defines $f_m$ as in (1.7). It is worth noting that this assumes a sharp filter cutoff with no guard-band, where in reality, such a filter is difficult to realize. Note that the SSB receiver is what allows each radar receiver to reject interfering echos from other receivers. This is in the sense that a positive frequency echo for one chirp will appear as a negative echo for another chirp, and with the SSB I/Q implementation, these interfering echos can easily be rejected.

### 4.5.3. SIMULATIONS FOR SWEEPS CONCATENATION FOR $M_{\max}$

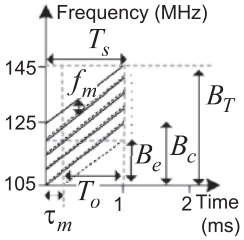
Simulations comparing waveform (W.e) (corresponding to the waveform shown in Table 4.3) to Chapter 3 waveforms in Table 3.1 and Table 3.2 are presented in Fig. 4.8. Two target are simulated, G1 and G2, with the parameters in Table. 3.3. The extension of the unambiguous Doppler-velocity interval allows for target G2's velocity of 17.5 m/s to be unambiguously estimated for waveforms (W.b), (W.c), (W.d), and (w.e) as shown in sub figures (b), (c), (d) and (e) respectively. Simulation results for the different waveforms in Table. 4.1. Targets' response functions width are significantly improved when using (w.e). A range cut through zero-Doppler shows the target response function width achieved by all waveforms for target G2.

This simulation only aimed at showing the target response function width improvement when using (W.e). No closely spaced targets were simulated and no experiment was performed to test the hypothesis in Section. 4.5.2.

### 4.5.4. RECONFIGURABLE RANGE-DOPPLER PROCESSING LIMITATIONS

The limitations for the proposed method are, SNR system non-linearities – in the transmitter and receiver – and accumulating concatenation errors. Because of

Table 4.3: Worked-out example for the discussion in Section 4.5.2 for possible range resolution improvement from the concatenation of $M$ chirps in a single sweep. The table structure follows that of Table 3.1 and Table 3.2.

| | | | |
|---|---|---|---|
| |  | | |
| Waveform | | W.e | |
| Description | | Double the PRF and keep sweep rate as in W.a, but use five chirps | |
| Chirps per sweep/PRI $M$ | | 5 | |
| Sweeps in CPI $N$ | | 64 | |
| Max. round-trip time $\tau_{\max}$ (1.5) ($\mu s$) | | 100 | |
| Max. beat-freq. $f_m$ (LPF) (1.7) (MHz) | Max. range $R_{\mathrm{m}}$ (1.7) (Km) | 2 | 15 |
| Sweep time $T_s$ (1.1) (ms) | PRF (1.1) (KHz) | 1 | 1 |
| Max. Unambiguous Doppler Velocity (1.11) (m/s) | | 22.6 | |
| Observation time (1.4) (ms) | | 0.9 | |
| Total available bandwidth $B_T$ (1.1) (MHz) | | 40 | |
| Transmitted chirp bandwidth $B_c$ (1.2) (MHz) | | 20 per chirp | |
| Effective bandwidth $B_e$ (1.9) (MHz) | | 18 per chirp | |
| Chirp-rate $\alpha$ (1.2) (GHz/s) | | 20 | |
| Range resolution $\Delta R$ (4.18) (m) | | 1.6 | |
| CPI processing gain $G_{\mathrm{CPI}}$ (1.16) | | 5184000 | |

non-linearities, even a point-target will have a certain 3 dB spectral width dictated by the radar's non-linearities [14] as: $\Delta f_{\text{target}} = \Delta f_{\text{target}} + (\chi/100)\Delta f_{\text{target}}$, where $\chi$ is the non-linearity in percentage. Any concatenation errors will also result in grating-lobes and spectral width widening. The method described is not suitable for targets which have a substantially high acceleration, to the point that a target's beat-frequency changes *within* one sweep, with a value greater than that of the STFT frequency grid resolution. An example is missile tracking applications. The expected gain from using the concatenation method of different sweeps in time is also limited to when range migration can be neglected, or first corrected for.



## 4.6. EXPERIMENTAL VERIFICATION

### 4.6.1. PARSAX EXPERIMENTAL SETUP

The reconfigurable processing improvement method is demonstrated experimentally using the Delft University of Technology (TU Delft) PARSAX FMCW radar [16] shown in Fig. 4.9(a). The radar is mounted on the roof of the electrical engineering, mathematics and computer science (EEMCS) building at the TU Delft. It operates in S-band (3.1315 GHz) and uses an Intermediate Frequency (IF) of 125 MHz. A simplified PARSAX block diagram is depicted in Fig. 4.10 along with the experimental setup. On every receiver channel, transmitted and received signals are sampled at IF using a pair of Analog-to-Digital Converters (ADCs) on an Innovative Integrations X5-400M Xilinx Virtex5SX95T FPGA card. The ADCs are 14-bit devices with sampling rates up to 400 Mega Samples per Second (MSPS). Deramping Single-Sideband (SSB) signal processing is performed digitally on the FPGAs. Beat-frequencies are transferred to a computer via the PCI-express bus for further processing. Experiments were conducted using the experiments-applicable configuration options shown in Table 4.4.

The transmitted waveform from the AWG channel-1 was created by combining two frequency slopes of bandwidths 40 MHz and 20 MHz respectively. Receivers R-1 and R-2 separate the received beat-frequencies from the 40 MHz and 20 MHz respectively. Both receivers are SSB IQ ones, with the ability to reject either positive or negative frequencies.

The aim here is to demonstrate that the target response function width from processing the 20 MHz waveform can be improved to match that of the 40 MHz one, using the proposed method with a concatenation factor $d = 2$.

### 4.6.2. PARSAX EXPERIMENT 1: A STABLE TARGET

The PARSAX radar is used in this experiment where we observe an industrial factory chimney as depicted in Fig. 4.9(a) and (b). The chimney is chosen as a stable

Table 4.4: PARSAX experiment setup parameters.

| CPI Parameters | | |
|---|---|---|
| Parameter | Value | Unit |
| Waveform | Linear sawtooth | n/a |
| PRF | 2 | KHz |
| $T_s$ | 500 | $\mu$s |
| $T_o$ | 450 | $\mu$s |
| N CPI | 64 | sweeps |
| CPI length | 0.033 | s |
| $B_e$ | R-1: 38<br>R-2: 19 | MHz |
| wavelength<br>$\lambda$ | 0.0905 | m |
| Extrapolation Parameters | | |
| Parameter | Value | Unit |
| Window<br>length<br>$W$ | 6144 | samples |
| Hop<br>size<br>$\Delta h$ | 3 | samples |
| Extrapolation<br>filter order<br>$o$ | 120 | coefficients |
| Flexible Range-Doppler Processing | | |
| Concatenation Factor | Maximum unambiguous Doppler Velocity $v_u$ (m/s) | |
| $d = 1$ (standard) | $\pm$ 44.4 | |
| $d = 2$ | $\pm$ 22.16 | |

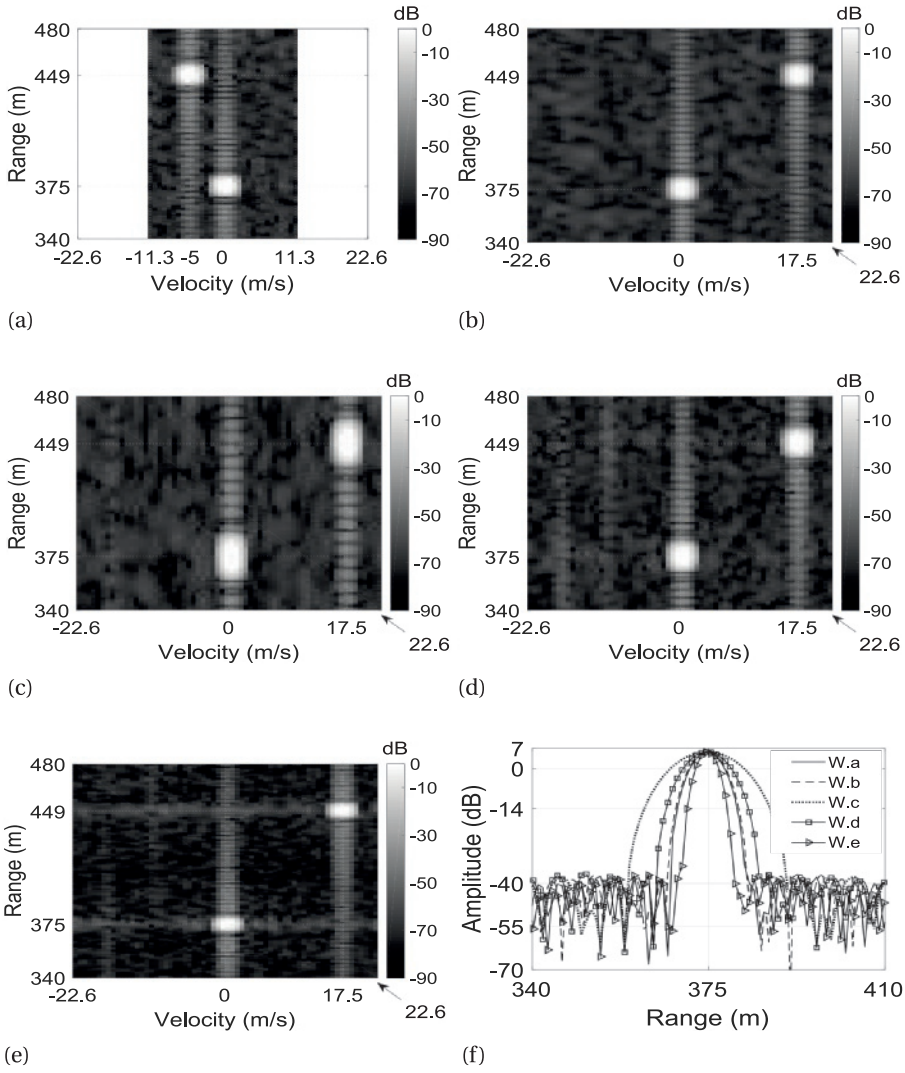



Figure 4.8: A repetition of the simulation results presented in Fig. 3.3, but with the addition of results for waveform (W.e) (corresponding to the waveform shown in Table 4.3) with its results shown in sub figures (e) and (f), where a target response function width improvement can be observed compared to all the other cases in Fig. 3.3.

target. The chimney is made up of multiple sub-chimneys.

### 4.6.3. PARSAX EXPERIMENT 2: A MOVING TARGET

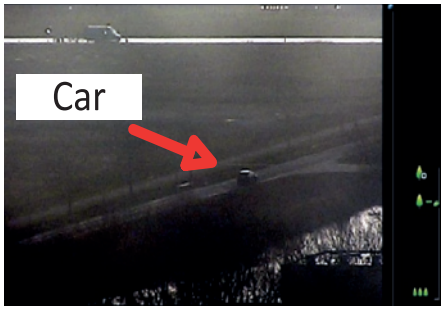
The PARSAX radar is used in this experiment where we observe an automobile on a quiet road as depicted in Fig. 4.9(a) and (c). The automobile driving at a




(a)



(b)




(c)

Figure 4.9: (a) The PARSAX FMCW radar situated at the top of the TU Delft building was used for the experiments. (b) Industrial chimney used as a stable target in the first experiment. (C) An automobile used as a moving target in the second experiment.

velocity of around 19 m/s (70 kmh) will be unambiguous for the transmitted PRF of 2 kHz, and for when processing with a concatenation factor $d = 2$, which will reduce the processing PRF to 1 kHz.

### 4.6.4. TI EXPERIMENTAL SETUP

A mmWave radar is used to investigate the possibility of range-resolution improvement, as discussed in Section 4.5. The radar used is the Texas Instruments (TI) IWR1443/1642 module mounted on the DCA1000EVM data capture card. The radar operates in the band of 76 to 81 GHz. The experiment setup is shown in Fig. 4.11. The radar is mounted on a table, and two corner reflectors are placed at a range of 3.36 m and 3.75 m respectively (39 cm difference). The wall behind the corner reflectors is at a range of around 6.9 m. The radar transmits classical up-chirps with a PRF of 200 kHz (PRI = 50 $\mu s$), and a transient time of 5 $\mu s$,

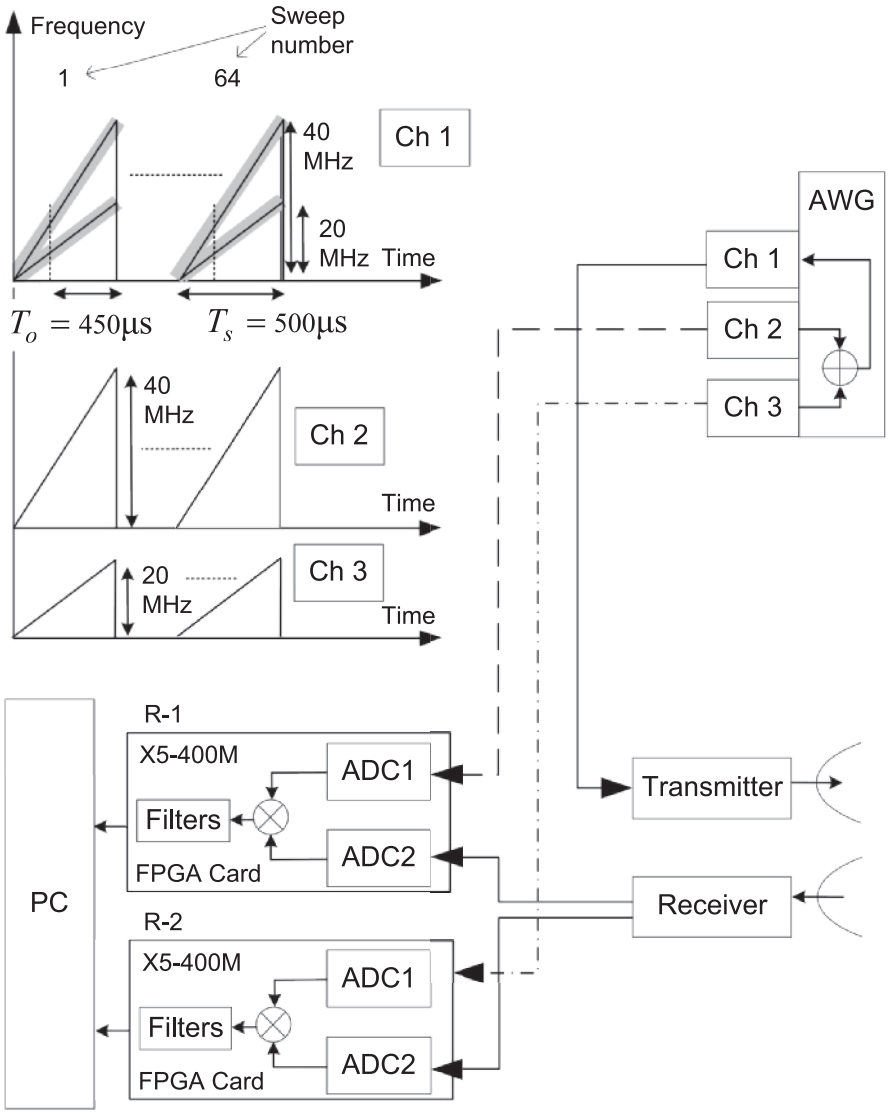



Figure 4.10: Simplified PARSAX radar block diagram with the configuration used for experiments discussed is Section 2.5. A waveform combining a 20 MHz and a 40 MHz sweeps is generated and combined by the Arbitrary Waveform Generator (AWG). Both FPGA receivers R-1 and R-2 are SSB IQ ones, with the ability to reject either positive or negative frequencies. The shaded areas depict the receivers' upper and lower LPF bounds.

resulting in $T_o = 45\ \mu s$.

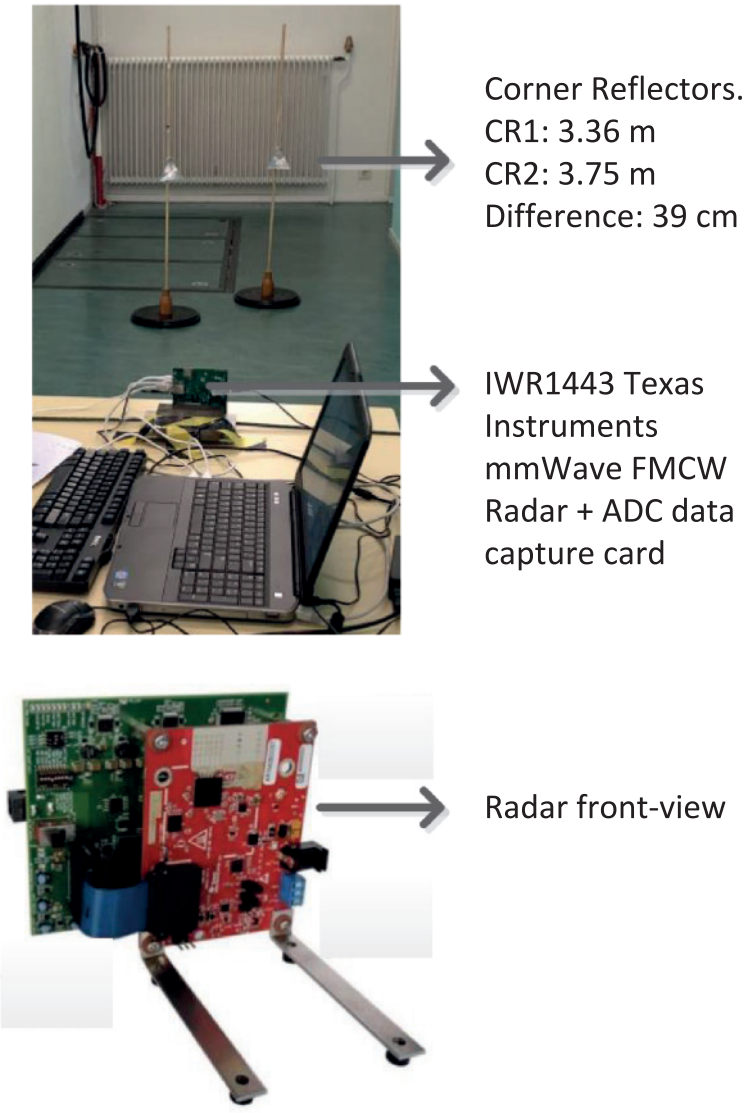



Figure 4.11: Experiment setup using the TI mmWave IWR1443 radar, as described in Section 4.6.4. Two corner reflectors are placed at a range of 3.36 m and 3.75 m respectively (39 cm difference). The wall behind the corner reflectors is at a range of around 6.9 m.

### 4.6.5. TI EXPERIMENT 1: CORNER REFLECTORS

A measurements is first taken with a bandwidth of 3 GHz, yielding an effective bandwidth of 2.7 GHz and a range resolution of 5 cm. A second measurement

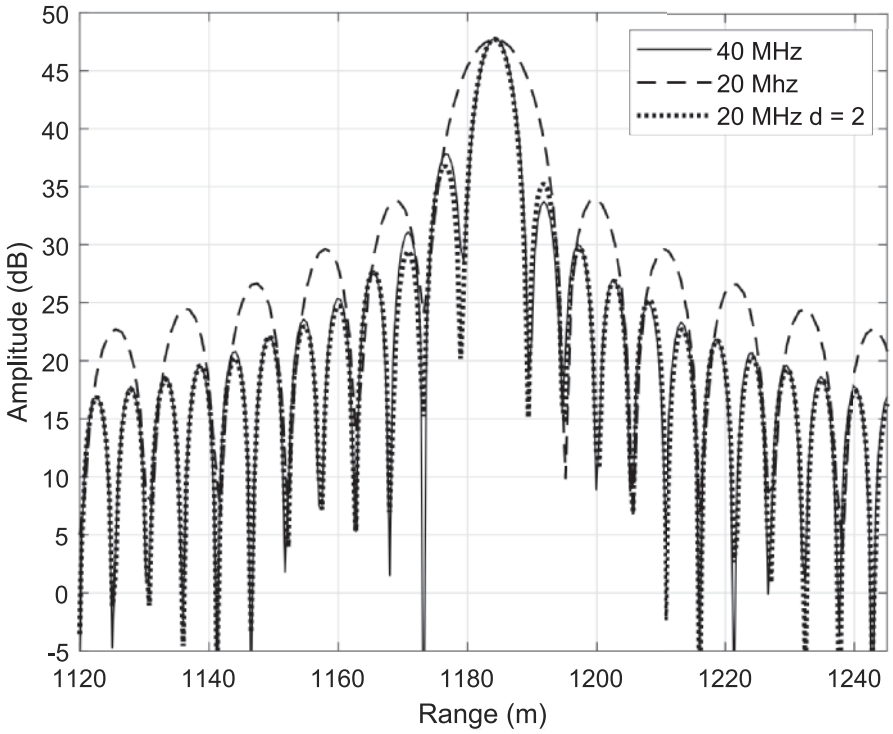



Figure 4.12: Zero-padded Zero-Doppler cut zoom-in on the Chimney shown in Fig. 4.9 (a) and (b). The proposed processing of the 20 MHz channel - with a concatenation factor $d$ =2 - closely matches that of the 40 MHz channel.

is then made with a bandwidth of 325 MHz, yielding an effective bandwidth of 293 MHz, and a range resolution of 51 cm. The aim is to process the data captured using the 293 MHz bandwidth with a concatenation factor $d = 8$, and check if the corner reflectors – separated with 39 cm, which is less than the theoretical 51 cm resolution – can be resolved using the proposed processing method. Note that when $d = 8$, the expected range resolution is 6 cm following (4.16).

### 4.6.6. Results and Discussion

For the first PARSAX experiment, the results are shown in Fig. 4.12. When processing the 20 MHz waveform with a concatenation factor $d = 2$, the target response function width improvement results closely match that of the 40 MHz waveform. For the second PARSAX experiment, the results are shown in Fig. 4.13. The automobile appears to be of around 7 m in length in the 40 MHz channel, which is expected due to the range resolution being 3.74 m, FT leakage, and typical automobile lengths of around 4 m. In the 20 MHz channel, the automobile appears to be of around 14 m in length, which is also expected due to the

range resolution being 7.49 m and the target response function width degradation. When processing with manually discarding every other sweep of the the 20 MHz channel, similarly to what was done in the simulations section, the automobile appears to have the same velocity but with a slight SNR loss and a slight velocity displacement due to the FT leakage. When processing the 20 MHz waveform with a concatenation factor $d = 2$, the automobile's target response function width closely match that of the 40 MHz waveform, in range, velocity and SNR.

For the TI experiment, the results are shown in Fig. 4.14(a) and (b), with and without windowing (Hamming) respectively. Both corner reflectors are resolved. The first corner reflector appears at the correct range of 3.36 m, but the second one has an error of 11 cm and appears at a range of 3.84 m instead of the correct range of 3.76 m. An SNR improvement of around 9 dB was expected for both corner reflectors from a concatenation factor $d = 8$, but only an improvement of 4 and 8 dB was achieved for the first and second corner reflectors respectively. The range error and SNR loss are due to concatenation errors.



## 4.7. CONCLUSION

A reconfigurable range-Doppler processing and target response function width improvement method for FMCW radar was presented. The problem which this chapter offered a solution for was the existence of the transient dead-time region between sweeps in FMCW deramp processing. This region does not allow for longer targets observations, and this limits the maximum target response function width improvement that can be achieved due to the reduced observation time. The solution proposed in this chapter was to coherently concatenate beat-frequency slices in the STFT domain, by applying a phase correction to each frequency slice as appropriate, followed by an Inverse STFT (ISTFT). The method extends the observation time by using returns from more than one sweep at a time, or used returns from multiple densely stacked frequency multiplexed chirps from one sweep, which resulted in an improved target response function width without the need to transmit additional bandwidth. The maximum possible number of chirps to be multiplexed was also discussed. The method also made it possible to decouple the Doppler processing PRF from the transmitted signal PRF. This is in the sense that it became possible to - in parallel and from one CPI - create different lengths fast-time slow-time matrices, without compromising on the total processing gain in any of the created matrices. This therefore also allows for the observation of different unambiguous Doppler velocity intervals from a single CPI. This chapter additionally set the ground for and made hypotheses about possible range resolution improvement due to the target response function width improvement. Simulations and an experiment were presented where such an improvement in range resolution was possible, but left the

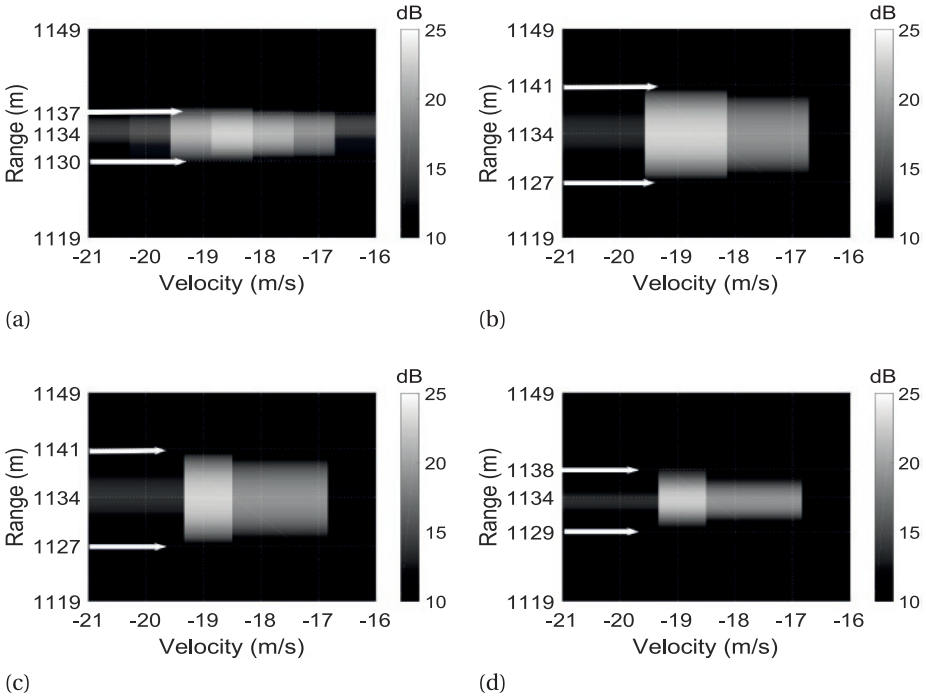
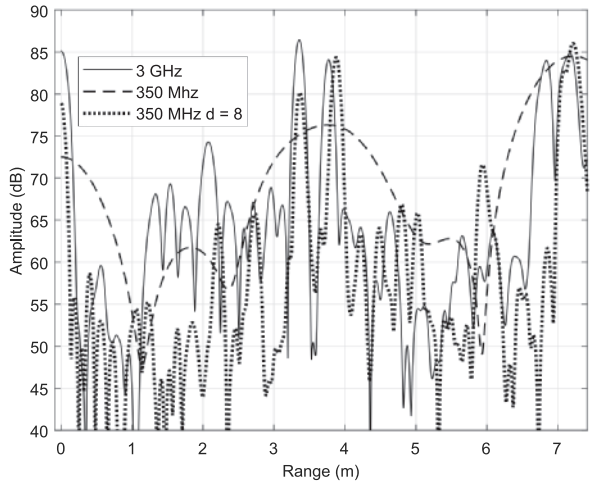
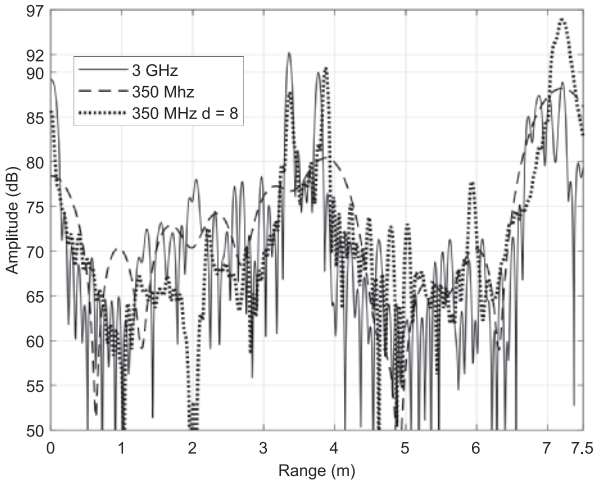



Figure 4.13: Range-Velocity results maps for the automobile in the experiment described in Section. 4.6.3. (a) As seen in the 40 MHz channel. (b) As seen in the 20 MHz channel. (c) Processing with manually discarding every other sweep of the 20 MHz channel. (d) Processing the 20 MHz waveform with a concatenation factor $d = 2$, the automobile's response function width closely match that of the 40 MHz waveform, in range, velocity and SNR.

door open for future research on that aspect.




(a)




(b)

Figure 4.14: Range profiles for the result of the experiment described in Section 4.6.5. (a) Hamming window is used for the range FT. (b) No window used for the range FT. Both corner reflectors are resolved. The first corner reflector appears at the correct range of 3.36 m, but the second one has an error of 11 cm and apeears at a range of 3.88 m, instead of 3.75 m. An SNR improvement of around 9 dB was expected for both corner reflectors from a concatenation factor $d = 8$, but only an improvement of 4 and 8 dB was achieved for the first and second corner reflectors respectively.

## REFERENCES

[1] A. G. Stove, "Linear FMCW radar techniques," *IEE Proc. or Radar and Signal Process.*, 1992. [Online]. Available: http://dx.doi.org/10.1002/andp.19063240204

[2] N. B. Jones and J. D. Watson, *Digital signal processing: principles, devices, and applications*. P. Peregrinus Ltd. on behalf of the Institution of Electrical Engineers, 1990.

[3] D. E. Barrick, "FMCW radar signals and digital processing," *NOAA Technical Report ERL 283-WPL 26*, 1973.

[4] M. A. Richards, *Fundamentals of Radar Signal Processing, Second Edition*. McGraw-Hill, 2014.

[5] E. D. Adler, E. A. Viveiros, T. Ton, J. L. Kurtz, and M. C. Bartlett, "Direct digital synthesis applications for radar development," in *Proc. Intern. Radar Conf.*, May 1995, pp. 224–226.

[6] Y. Li and S. O'Young, "Method of doubling range resolution without increasing bandwidth in FMCW radar," *Electron. Lett.*, vol. 51, no. 12, pp. 933–935, 2015.

[7] V. K. Nguyen and M. D. Turley, "Bandwidth extrapolation of LFM signals for narrowband radar systems," in *Int. Conf. on Radar*, Sep. 2013, pp. 140–145.

[8] K. Suwa and M. Iwamoto, "A bandwidth extrapolation technique of polarimetric radar data and a recursive method of polarimetric linear prediction coefficient estimation," in *IGARSS 2003. 2003 IEEE International Geoscience and Remote Sensing Symposium. Proceedings (IEEE Cat. No.03CH37477)*, vol. 7, July 2003, pp. 4329–4331 vol.7.

[9] M. I. K. Suwa, "A two-dimensional bandwidth extrapolation technique for polarimetric synthetic aperture radar images," *IEEE Transactions on Geoscience and Remote Sensing*, vol. 45, no. 1, pp. 45–54, Jan 2007.

[10] B. G. M. A. Lulu, "Phase matching of coincident pulses for range-doppler estimation of multiple targets," *IEEE Signal Processing Lett.*, vol. 26, no. 1, pp. 199–203, Jan 2019.

[11] W. L. Melvin and J. A. Scheer, *Principles of Modern Radar: Volume 3 : Radar Applications*. SciTech Publishing Inc, 2014.

[12] G. M. Brooker, "Understanding millimetre wave FMCW radars," in *1 st Int. Conf. on Sensing Technol., IEEE, New Zealand*, 2005, pp. 152–157.

[13] S. Neemat, F. Uysal, O. Krasnov, and A. Yarovoy, "Reconfigurable range-doppler processing and range resolution improvement for fmcw radar," *IEEE Sensors Journal*, vol. 19, no. 20, pp. 9294–9303, Oct 2019.

[14] M. Jankiraman, *Design of Multi-Frequency CW Radars.* SciTech, 2007.

[15] S. Kay, *Modern Spectral Estimation: Theory and Application.* Prentice Hall, 1999.

[16] O. A. Krasnov, L. P. Ligthart, Z. Li, G. Babur, Z. Wang, and F. van der Zwan, "PARSAX: High-resolution doppler-polarimetric FMCW radar with dual-orthogonal signals," *18th Int. conf. on Microwave Radar and Wireless Communications (MIKON)*, 2010.

# 5

# CONCLUSIONS AND RECOMMENDATIONS

In this dissertation a number of methods and waveforms for the operational enhancement of deramping FMCW radars have been developed. These methods allows the overcoming of existing state of the art FMCW radar performance limitations, and increase radar resistance to interference. In this Chapter, the main conclusions, societal, scientific and technical implications are summarized and followed by recommendations for future work.

## 5.1. CONCLUSIONS

The main research conclusions presented in this dissertation are as follows: A novel interference mitigation method for FMCW radar using beat-frequencies interpolation and phase matching in the time-frequency domain was developed as an answer to research question 1 (RQ1) in Chapter 2.

After the suppression of interference-contaminated frames of beat-frequencies in a sweep in the STFT domain, useful beat-frequencies are subsequently reconstructed based on a known beat signal model. The beat signal model parameters estimation analysis is done using the STFT. Linear prediction coefficients for the signal parameters are then estimated using auto regression for the current observation scene – for each STFT frequency-slice – from the interference-free parts of each slice, or optionally – in a reconfigurable manner – from a previously known interference-free sweep in the CPI. Suppressed beat-frequency frames are then replaced by the linear-predicted interpolated ones, followed by a phase matching procedure. The proposed technique satisfies the requirement to keep using the FT as the radar's beat-frequency estimation tool. It furthermore

does not require target detection/thresholding – at the strongest target peak – to begin with, nor algorithm convergence. The technique is real-time implementable with a predictable execution delay (latency), based on FT banks and fixed-length extrapolation filters. The technique's performance improvement was demonstrated with respect to the known zeroing and inverse cosine windowing solutions, against interference for a stable targets scenario. Evaluating the technique's performance was done in range-Doppler for a moving targets scenario, where an interference-free reference-data CPI is processed using the zeroing technique and vs inverse cosine windowing in comparison to the proposed method. The proposed method has shown significant improvements in 2-D correlation coefficients (0.42, 0.66 and 0.89 for zeroing, inverse cosine windowing and the proposed method respectively), amplitude average error percentages (44.8, 34.45 and 12.93 for zeroing, inverse cosine windowing and the proposed method respectively), phase average error percentages (116.89, 77.89 and 18.53 for zeroing, inverse cosine windowing and the proposed method respectively) and phase RMSE (0.93, 0.56 and 0.16 for zeroing, inverse cosine windowing and the proposed method respectively). Noting that these numbers pertain to an interference constituting 25% of the entire signal duration. The proposed technique is not applicable to applications where targets might have a considerably high acceleration - causing a frequency change within a single sweep - as in ballistic missile applications, for example. The method was simulated and experimentally validated.



A novel waveform and a processing method to decouple the Doppler ambiguity interval from radar parameters such as the maximum operational range, range-resolution and processing gain in frequency multiplexed FMCW Radar was proposed in Chapter 3 to answer the research question 2 (RQ2). The method allowed the keeping of the radar's operational parameters while increasing the PRF – to unambiguously observe fast(er) moving targets, without having to trade-off these operational parameters. The method proposed exploits the fact that beat-frequency signals have the same baseband frequencies, even if the transmitted and received chirps occupied different RF bands. Such baseband signals can be concatenated in the time-frequency domain to restore any operational parameters' losses due to the PRF increase. The price to be paid was to use more receiver channels in the radar. Usage constraint were discussed, such as the maximum chirp's center-frequency separation. The proposed method allowed for more usage scenarios for standard FMCW radars without the use of unpredictably convergent algorithms, where all operations proposed are mainly Fourier – and inverse Fourier – transform with a predictable latency. The method was simulated and experimentally validated. Limitations for all developed methods were highlighted. The SNR, system non-linearities and accumulating concatenation errors

are the main drawbacks. A poor SNR will result in incorrect phase estimations. Because of non-linearities, even a point-target will have a certain 3 dB spectral width. Any concatenation errors will also result in grating-lobes and spectral width widening. The developed methods are not suitable for targets which have a substantially high acceleration, to the point that a target's beat-frequency changes within one sweep, with a value greater than that of the STFT frequency grid resolution.

Finally, to answer the research question 3 (RQ3), a novel reconfigurable range-Doppler processing and target response function width improvement method for FMCW radar was developed (Chapter 4). The solution extends the observation time by using returns from more than one sweep at a time, or used returns from multiple densely stacked frequency multiplexed chirps from one sweep, which resulted in an improved target response function width without the need to transmit additional bandwidth. To achieve this, beat-frequency slices from multiple sweeps are coherently concatenated in the STFT domain by applying a phase correction to each frequency slice as appropriate and followed by an Inverse STFT (ISTFT). The method proposed also made it possible to have a Doppler processing PRF which is different from the transmitted signal PRF. This is in the sense that it became possible – in parallel and from one CPI – to create different lengths fast-time slow-time matrices without compromising on the total processing gain in any of the created matrices. This therefore also allows for the observation of different unambiguous Doppler velocity intervals from a single CPI. The method was simulated, experimentally validated and showed in the experiments an improvement in target response function width by a factor of eight. The expected gain from using the concatenation method of different sweeps in time is also limited to when range migration can be neglected, or first corrected for. The chapter additionally set the ground for and made hypotheses about possible range resolution improvement due to the target response function width improvement. Simulations and an experiment were presented where such an improvement in range resolution was possible, but left the door open for future research on that aspect.



## 5.2. SOCIETAL, SCIENTIFIC AND TECHNICAL IMPLICATIONS

In the spirit of encouraging academics to seek closer societal links from their work [1], this subsection highlights a few possibilities of these societal links, along with the traditional scientific and technical ones.

For the Interference Mitigation Technique for FMCW Radar Using Beat-Frequencies Interpolation in the STFT Domain in **Chapter 2**: The proposed method does not rely on waveform-diversity – which are bound to relate to system architecture-diversity – can lower radar production costs. The existence of mitigation tech-

niques might allow for more and more radars to cohabit. This would directly benefit consumers. Approaching beat-frequencies in the time-frequency domain has the scientific implication of encouraging the adaptation of acoustic signal processing methods for radar.
For the Decoupling of the Doppler Ambiguity Interval from the Maximum Operational Range and Range-Resolution in FMCW Radars in **Chapter 3**: The ability to extend the Doppler ambiguity interval without compromising on the maximum operational range can allow for faster radar decision making. This might benefit the systems used in industrial automation and increase user safety levels from example. The ability to construct a single fast-time slow-time matrix – with an extended Doppler ambiguity interval and an improved target response function width – in one go, has the scientific implication of the introduction and evaluation of a new waveform.
For the Reconfigurable Range-Doppler Processing and Target Response Function Width Improvement for FMCW Radar in **Chapter 4**: The ability to decouple the target response function width from the transmitted bandwidth allows potentially for considerable cost reductions for radar. Wide bandwidth circuitry is more expensive than narrow ones. Sectors which could benefit from this are numerous. Examples are industrial automation and robotics. In a competitive economic environment, cost reductions directly benefit consumers in the form of the ability to add more product features or simply a direct price reduction.



## 5.3. RECOMMENDATIONS FOR FUTURE WORK

The recommendations for future work are grouped by research-question as defined in the introduction chapter:

**Chapter 2** (**RQ**1): **An Interference Mitigation Technique for FMCW Radar Using Beat-Frequencies Interpolation in the STFT Domain**

Researching different transforms other than the STFT to avoid frequency grid resolution and leakage issues can have promising outcomes. Developing an adaptive way where the radar decides on the STFT window length and hop size based on the current target beat-frequency slice fluctuation in the observation scenario might be interesting. A recommendation is researching combining the interference mitigation method with an interference detection technique, where based on the interference severity (number of affected STFT frames for example). The STFT window length and hop size are selected to emphasize more samples to interpolate from, or to reduce processing power by selecting a bigger hop size.

**Chapter 3** (**RQ**2): **Decoupling the Doppler Ambiguity Interval from the Maxi-**

**mum Operational Range and Range-Resolution in FMCW Radars**
A recommendation is researching the influence of extending the operational maximum range on the different waveforms presented in the chapter, and finding at which point does the proposed method and waveform lose their advantage in comparison to a standard sweep. It would be interesting to research techniques that would allow the method's adoption in systems operating with high chirp-centre-frequency deviations from each other, to a point that it would result in targets' frequency-slices mismatch at the different receivers.

**Chapter 4** (**RQ**3): **Reconfigurable Range-Doppler Processing and Target Response Function Width Improvement for FMCW Radar**
Researching techniques on how to align frequency-slices in the STFT domain before concatenating them –for range migrating targets – can have promising outcomes. The same can be true for researching techniques that would make the proposed method applicable for accelerating targets, where their frequency-slice changes within one sweep.



## REFERENCES

[1] Editorial, "Bridge research and impacts," *Nature*, vol. 553, no. 5, 2018.

# SUMMARY

Deramping Frequency Modulated Continuous Wave (FMCW) radars with chirp-sequence waveforms are widely used in numerous applications. The research objective behind this dissertation was to develop methods and waveforms for the operational enhancement of that class of radars. This is in the sense that there was a desire to take FMCW radars beyond their existing state of the art performance limitations, and increase their resistance to interference. To achieve these objectives, the following research questions were addressed:
Is there a way to mitigate FMCW radar interferences where the developed mitigation method restores any SNR loss due to the interference and/or the mitigation technique itself? Can the method be evaluatable in performance in the range-Doppler domain (as opposed to only in a range-profile)?
Is there a way to decouple the Doppler velocity ambiguity interval – defined by the PRF – from parameters like the maximum operational range, range resolution, all while maintaining the same transmitted chirp-rate? Would it be possible to liberate the radar from the design/operational trade-offs associated with these parameters? Particularly in the scenario in which the PRF is to be increased for the observation of fast(er) moving targets.
Is there a way to overcome the existence of the transient (fly-back) region in deramping FMCW radar beat-signals? This is in the sense that its existence limits the maximum observation time in a single sweep. Would manoeuvring it then allow the coherent chaining of beat-signals – from multiple sweeps – in a way that could improve the target response function width? Could it also improve the SNR? And since the beginning of a sweep and the transient region are related – and therefore the Doppler velocity ambiguity interval is related too in de facto – could overcoming the presence of the transient region then allow for Doppler processing PRFs that are different from the transmitted PRF? The novelty, main results and implications of the research presented are:

- A method was developed to mitigate FMCW radar interferences. The method restored any SNR loss due to the interference, and was evaluatable in performance in the range-Doppler domain (as opposed to only in a range-profile). It was the first ever interference mitigation method for deramping FMCW radar receivers via model-based beat-signals interpolation in the time-frequency domain. It allowed the introduction of an optional linear prediction interpolation coefficients reconfigurable estimation mode

for CPI processing. Coefficients are estimated for the current observation scene using a known single interference-free sweep. These coefficients are then reused for the restoration of subsequent interference-contaminated sweeps in the CPI. It was also suitable for real-time implementation, with a predictable execution delay (latency), based on FT banks and fixed-length extrapolation filters, as opposed to iterative methods relying on algorithm convergence. The evaluation of the method's performance was done in the range-Doppler domain. The aim was to additionally showcase the maintenance of the radar's coherence over a CPI after interference mitigation.

- A method was developed to decouple the Doppler ambiguity interval – defined by the PRF – from parameters like the maximum operational range and range resolution, all while maintaining the same transmitted chirp-rate. It was the first ever processing method for the coherent integration of frequency multiplexed chirps within one sweep/PRI – for deramping FMCW radar in the time-frequency domain. It constructed a single fast-time slow-time matrix – with an extended Doppler ambiguity interval, while maintaining the range resolution and CPI processing gain – in one go. It did not use iterative algorithms with unpredictable latencies, nor requires any detection or a-priori information about the observed scene, and is applicable to very-extended targets like rain/clouds.

- A method was developed to overcome the existence of the transient (fly-back) region in FMCW radar. It was the first ever method for deramping FMCW radar sweeps coherent concatenation in the time-frequency domain. It allowed for target response function width improvement without transmitting additional bandwidth. It offered the ability to – in parallel – generate different size fast-time slow-time matrices, and allowed for Doppler processing PRFs that are different from the transmitted PRF, without compromising on the total CPI processing gain. This offered the ability to observer different unambiguous Doppler velocity intervals in one CPI.

# SAMENVATTING

Compressie frequentie gemoduleerde continue golf (frequency modulated continuous wave, FMCW) radars met frequentie als functie van tijd (chirp)-reeksen golfvormen, worden veelvuldig gebruikt in tal van toepassingen. Het doel van onderzoek achter dit proefschrift is het ontwikkelen van methoden en golfvormen voor de operationele verbetering van deze klasse van radars. Dit wil zeggen dat het gewenst is om FMCW radars te ontdoen van prestatie beperkingen bij de huidige stand der techniek, en meer bestand te maken tegen interferentie. Om deze doelen te verwezenlijken zijn de volgende onderzoeksvragen gesteld:
Is er een methode FMCW radar interferentie te bestrijden waarbij de ontwikkelde methode het verlies in SNR, ten gevolge van de interferentie en/of de herstel techniek zelf, hersteld? Kan de prestatie van de methode geëvalueerd worden in het afstand-Doppler domein (en niet alleen in een afstandsprofiel)?
Is er een manier om het Doppler dubbelzinnigheidsinterval, gedefinieerd door de PRF, te ontkoppelen van parameters als de maximale operationele afstand en de afstandsresolutie, en daarbij een en dezelfde uitgezonden chirp herhalingstijd te behouden? Zou het mogelijk zijn radar te bevrijden van ontwerp/operationele compromissen die verbonden zijn aan deze parameters? Dit met name in het geval dat de PRF dient te worden vergroot ten behoeve van de waarneming van snel(ler) bewegende doelen.
is er een manier om het optreden van het overgangsgebied (terugslag) bij compressie FMCW radarfrequentieverschil (beat) signalen te voorkomen? De aanwezigheid van dit gebied beperkt immers de maximale observatietijd in een enkele frequentiezwaai. Zou deze aanpassing de coherente aaneenschakeling van beatsignalen, van meerdere sweeps, toelaten om de doelrespons functie breedte te verbeteren? Zou het mogelijk zijn om de SNR te verbeteren? Aangezien de start van een sweep en het overgangsgebied gerelateerd zijn, en daarmee in feite eveneens het Doppler snelheid dubbelzinnigheidsinterval, zou het vermijden van de aanwezigheid van het overgangsgebied dan Doppler processing PRFs toelaten die kunnen verschillen van de uitgezonden PRF?
De nieuwheidsapecten, belangrijkste resultaten and implicaties van het gepresenteerde onderzoek zijn:
Een methode is ontwikkeld om FMCW radar interferenties te onderdrukken. Deze methode herstelt het verlies in SNR veroorzaakt door interferentie, en de prestatie hiervan is geëvalueerd in het afstand-Doppler domein. Dit is de eerste

interferentie onderdrukkingstechniek ooit die gebruik maakt van (model gebaseerde) beat-signaal interpolatie in het tijd-frequentie domein. Het introduceert een optionele lineaire voorspellende interpolatie coëfficiënten herconfigureerbare schattingsprocedure voor CPI processing. Coëfficiënten zijn geschat voor het momentele waarnemingsscenario gebruikmakend van een bekende enkelvoudige interferentie-vrije sweep. Deze coëfficiënten zijn vervolgens gebruikt bij de restoratie van opeenvolgende door interferentie verstoorde sweeps in het CPI. Daar de methode niet berust op golfvorm-diversiteit, gebruikelijk gerelateerd aan systeem architectuur-diversiteit, resulteert dit in lagere radar productie kosten en kunnen meer en meer radars naast elkaar bestaan.

Een methode is ontwikkeld om het Doppler dubbelzinnigheidsinterval – gedefinieerd door de PRF – te ontkoppelen van parameters als de maximale operationele afstand en de afstandsresolutie, met behoud van een en dezelfde uitgezonden chirp herhalingstijd, en is dit de eerste processing methode ooit voor de coherente integratie van freqentie multiplex chirps in één sweep in het tijd-frequentie domein. Hiermee kan een enkele 'snelle tijd' 'langzame tijd' matrix – met een vergroot Doppler dubbelzinnigheidsinterval en verfijnde afstandsresolutie – in een keer worden geconstrueerd.

Een methode is ontwikkeld die het bestaan van het (inschakeleffect)overgangsgebied tegengaat, dit is de eerste methode ooit voor coherente samenstelling van sweeps in het tijd-frequentie domein. Deze bemogelijkt doelrespons functie breedte verbetering zonder toevoeging van zendsignaal bandbreedte, tevens is het hiermee mogelijk -eveneens in parallel- 'snelle tijd' 'langzame tijd' matrices van verschillende grootte te genereren, en ook kunnen de Doppler processing PRFs verschillen van de uitgezonden PRF zonder afbreuk aan de totale CPI processing winst. Dit maakt het mogelijk verschillende ondubbelzinnige Doppler snelheidsintervallen in één CPI waar te nemen. Dit resulteert in kosten reductie aangezien radar circuits met grotere bandbreedte duurder zijn.

# ACKNOWLEDGEMENTS

The cats herding is over after around 1800 cups of coffee and 200 hours of discussions. I am now pleased to have the opportunity to express my appreciation to those who facilitated the completion of this research.

I would like to thank my promoter Prof. Alexander Yarovoy for the opportunity to do a PhD at MS3. I would also like to thank Prof. Mike Inggs for putting in a good word for me – about my Cape Town M.Sc. days – when asked for a recommendation by Prof. Yarovoy.

I am grateful to my daily supervisor Dr. Oleg Krasnov for his guidance, knowledge, motivation, humbleness, patience and perseverance. I will always remember him as the man with the "if you have a question, just knock" slogan! What I've learned from him during this study will be a T-slab support for more exciting work that is lying beyond.

Non of this would have been possible without the titanic – minus the sinking association – guidance and support of Dr. Álvaro Blanco-del-Campo during and after his gig at the TU Delft. That ranged from moving beast-size dining tables, basic math, radar, Spanish-food superstitious cooking methods and recipes – sorted ascendingly by importance. Some debts can never be repaid!

I am eternally grateful to Etiënne Goossens during his time at the university for never ever turning down a question I had about life in the Netherlands, from soup to nuts. The DIY know-how I learned from Etiënne has helped me hammer out a great deal of logistical day-to-day problems, which would have had taken days and days to clear up while PhD time was relentlessly pouring through the sandglass. A great example of how an institute's value is by its people, and not the hight of its concrete.

My gratitude for Minke van der Put is everlasting. She is an admin magician, has an open-door policy with a genuine good-will to assist in anything and everything. A small booklet is needed to list the topics I received advice on, from books on Dutch culture to finances demystification!

I would like to thank Dr. Faruk Uysal for stepping in to assist in my supervision when unfortunate circumstances hit out of nowhere. I appreciate the signal processing knowledge, the sleeves rolling up and the diving into Matlab code whenever things didn't go as expected. Faruk's continued enthusiasm and his on-demand consultation policy for me and all students – even when not related to any of his projects – is much appreciated.

I would like to thank Prof. Hatim Behairy for 15 years of unconditional support! Matlab, DSP, FPGA, system engineering, project management, English language, travel tips and fine-dining – just to name a few.

I would also like to recognize the support of Fred van der Zwan and Pascal Aubry in all experimental work during the PhD, and the fresh-doctor Nikita Petrov for always giving constructive feedback and new ideas when attending my seminars.

# ABOUT THE AUTHOR



**Sharef Ahmed NEEMAT**

was born in 1981 in Riyadh, Saudi Arabia. He received his B.S. in computer engineering from King Saud University (KSU) in 2004 and his M.Sc. in electrical engineering from the University of Cape Town (UCT) in 2010. His study focused on Secondary Surveillance Radar (SSR) Identification Friend or Foe (IFF). Before and after receiving his M.Sc., he was involved in airborne radios work in the form of design, development and test of Field Programmable Gate Array (FPGA)/Digital Signal Processor (DSP) drivers and application layer SW for radio housekeeping and scheduling. The DSP designs and code were developed to comply with DO-178B level C (Software Considerations in Airborne Systems and Equipment Certification) and MISRA (Motor Industry Software Reliability Association C standard). He was furthermore responsible for system engineering/project man-

agement of asset-tracking-systems' development. The work had involved writing system engineering management plans and requirements documentation for systems and their sub-systems, complying with MIL-STD-490 and MIL-STD-491.

# List of Publications

## PATENTS

1. **S. Neemat**, F. Uysal, O. Krasnov, A. Yarovoy, "Processing of Radar Signals for FMCW radar" (Octrooiregister-NL2022991, Pending), The Netherlands Patent Office, 2019.

## JOURNAL PAPERS

1. **S. Neemat**, O. Krasnov, A. Yarovoy, "An Interference Mitigation Technique for FMCW Radar Using Beat-Frequencies Interpolation in the STFT Domain", IEEE Transactions on Microwave Theory and Techniques, vol. 67, no. 3, pp. 1207-1220, 2019.

2. **S. Neemat**, O. Krasnov, Fred van der Zwan, A. Yarovoy, "Decoupling the Doppler Ambiguity Interval from the Maximum Operational Range and Range-Resolution in FMCW Radars", IEEE Sensors Journal, to be published, DOI: 10.1109/JSEN.2020.2972152, 2020.

3. **S. Neemat**, F. Uysal, O. Krasnov, A. Yarovoy, "Reconfigurable Range-Doppler Processing and Range Resolution Improvement for FMCW Radar", IEEE Sensors Journal, vol. 19, no. 20, pp. 9294–9303, 2019

## CONFERENCE FULL PAPERS

1. **S. Neemat**, O. Krasnov, A. Yarovoy, "Waveform and receiver parameters design choices for a reconfigurable digital FMCW radar,", in 17th International Radar Symposium (IRS), Krakow, 2016, pp. 1-4.

2. **S. Neemat**, O. Krasnov, A. Yarovoy, "Radar polarimetry with interleaved dual-orthogonal and time-multiplexed signals: The PARSAX radar setup and preliminary results,", in 11th European Conference on Antennas and Propagation (EUCAP), Paris, 2017, pp. 3931-3935.

3. **S. Neemat**, O. Krasnov, A. Yarovoy, "Simultaneous processing of time-shifted orthogonal LFMCW waveforms,", in Signal Processing Symposium (SPSympo), Jachranka, 2017, pp. 1-4.

4. **S. Neemat**, O. Krasnov, A. Yarovoy, "Amplitude, Phase and I/Q Mismatches in Joint-Processing Multichannel FMCW Radars,", submitted to the 17th European Radar Conference (EuRAD 2020).

## CONFERENCE ABSTRACTS

1. **S. Neemat**, O. Krasnov, A. Yarovoy, "Towards a Reconfigurable Radar: Enhanced LFMCW Waveform Processing on Flexible Architectures,", Union Radio-Scientifique Internationale (URSI) BENELUX Forum, 2018, Delft, 2018.